STUDY OF PASSIVE OPTICAL TECHNIQUES FOR DETECTING CLEAR AIR TURBULENCE

By A. J. Montgomery and A. Weigandt

Prepared under Contract No. NAS 12-116 by
IIT RESEARCH INSTITUTE
Chicago, Illinois

for

NATIONAL AERONAUTICS AND SPACE ADMINISTRATION

FOREWORD

This technical report was prepared by IIT Research Institute, Chicago, Illinois 60616 for the National Aeronautics and Space Administration, Electronics Reseach Center, on Contract No. NAS 12-116. The program was under the administrative direction of the Space Optics Laboratory with Dr. Charles Leigh as the project monitor.

Personnel who contributed to this project include J. Ash, A. J. Montgomery and A. Weigandt.

Appendix A represents results of work carried out for the National Aeronautics and Space Administration, George C. Marshall Space Flight Center, both by IIT Research Institute on Contract No. NAS8-20107 and by Colorado State University. The computer programs used in the data reduction and analysis were developed by MSFC personnel. Dr. F. R. Krause is the project monitor for MSFC on the crossed-beam programs.

TABLE OF CONTENTS

TABLE OF CONTENTS

LIST OF FIGURES

LIST OF FIGURES

LIST OF FIGURES

SYMBOLS

A	collector area
A	wave amplitude
B	brightness
C_n	refractive index structure constant
C_T	temperature structure constant
c_n	radiation constants
D_n	refractive index structure function
d	collector diameter
e	electronic charge
e_i	molecular extinction coefficient
Δf	electrical bandwidth
g	gravitational acceleration
H	atmospheric scale height
H_o	incident flux density
h	altitude
h	Planck's constant
I	intensity
i_θ, i_1, i_2	Mie scattering functions
K	coefficient of eddy diffusivity
k	wavenumber
L_o	outer scale of turbulence
ℓ_o	inner scale of turbulence
M	mean vertical refractive index gradient star magnitude
N(r)	number density

SYMBOLS (Cont.)

n	index of refraction
Δn	refractive index fluctuation
P	collected radiation power
p	pressure
R_1	radiance
R	radius of the earth
Ri	Richardson number
S	wave phase
T	temperature
t	atmospheric transmission
u	wave function
$V(K)$	one dimension spectral density function
v	convection speed
α	polarizability of air
$\Delta\alpha$	angle fluctuation
β	vertical gradient of horizontal wind
$\beta(\lambda,\theta)$	Rayleigh scattering function
γ	angular field of view
ε	dissipation of turbulent energy per unit mass
θ	scattering angle
λ	wavelength
ν	coefficient of kinematic viscosity
ρ	density
σ	log amplitude fluctuation of scintillation

SYMBOLS (Cont.)

τ	time delay
$\Phi(K)$	three dimensional power spectrum
φ	solar elevation angle
ψ	wave function
ω	collection solid angle

STUDY OF PASSIVE OPTICAL TECHNIQUES FOR DETECTING CLEAR AIR TURBULENCE

By A. J. Montgomery and A. Weigandt
IIT Research Institute

SUMMARY

Passive optical techniques that could be utilized to provide an aircraft pilot with advanced warning of Clear Air Turbulence (CAT) and inform the pilot of the direction, the distance, the size, and shape of the turbulence region were studied.

The techniques evaluated include:

- Detection of spatial nonuniformities in scattered sunlight
- Relative movement of stellar images
- Stellar scintillation
- Detection of thermal emission to determine temperature variations, gradients, and ozone concentrations
- Schlieren-type system using the earth's horizon as a source.

The lack of detailed information concerning the optical characteristics of CAT prevented complete evaluation of these techniques. Estimates of refractive index, temperature, and density fluctuations associated with CAT are made on the basis of available information and additional calculations.

Two techniques, detection of nonuniformities in scattered sunlight and stellar scintillation, are sufficiently promising for CAT detection to warrant further investigation. Although these techniques may be capable of providing limited angular size and direction information, the capability to provide useful range information is still subject to question.

An airborne program of CAT investigation is described which should provide the information that is required for a decision on the feasibility of these two approaches.

1. INTRODUCTION

Turbulence in clear areas of the sky as a problem to aircraft has been under investigation for a number of years. The altitudes at which direct measurement of vertical and horizontal gust velocities have been made have increased with the altitude performance of aircraft and show that, contrary to the predictions of some early investigators, regions of turbulence are found at altitudes above 12 km (40,000 ft). Aircraft operating at these altitudes can expect to encounter clear air turbulence* some significant fraction of the time. The severity of a CAT encounter is determined by the magnitude and direction of the wind gusts we well as by the characteristics of the aircraft i.e., airspeed, geometry, loading. The buffeting that an aircraft is subjected to in flying through a CAT region generally results in discomfort to the occupants, but, at times, control of the aircraft may be affected seriously and injuries can result. Aside from these effects we must also consider the structural effects. Repeated gust loads can fatigue parts and surfaces thus speeding failure or near-failure, making more frequent inspection and replacement necessary.

Previous investigations, as summarized by Vinnichenko, et al., 1966, of the frequency of occurrence of turbulence with altitude are summarized in Figure 1. A dependence on geographic location also is clearly demonstrated. Additionally, the frequency of occurrence depends on the time of the year for each location.

Atmospheric turbulence has a complex, irregular structure, making experimental investigation and theoretical prediction difficult. Sufficient measurements of several important characteristics of CAT have been made permitting statistical descriptions to be used. The cumulative frequency of the vertical size of turbulent regions is shown in Figure 2. We can see that, generally, we must deal with thicknesses of less than 1 km. This is in contrast to the distributions of horizontal size shown in Figure 3, which shows that we can expect regions of approximately 100 km in horizontal extent with at least intermittent turbulence. The thermal stratification and state of the atmosphere is, of course responsible for these characteristics. Thus,

---

*The phrase clear air turbulence, or its acronym, CAT, was defined by the National Committee for Clear Air Turbulence (U. S. Dept. of Commerce, 1966) as follows: CAT comprises "all turbulence in the free atmosphere of interest in aerospace operations that is not in, or adjacent to, visible convective activity. This includes turbulence found in cirrus clouds not in or adjacent to visible convective activity.

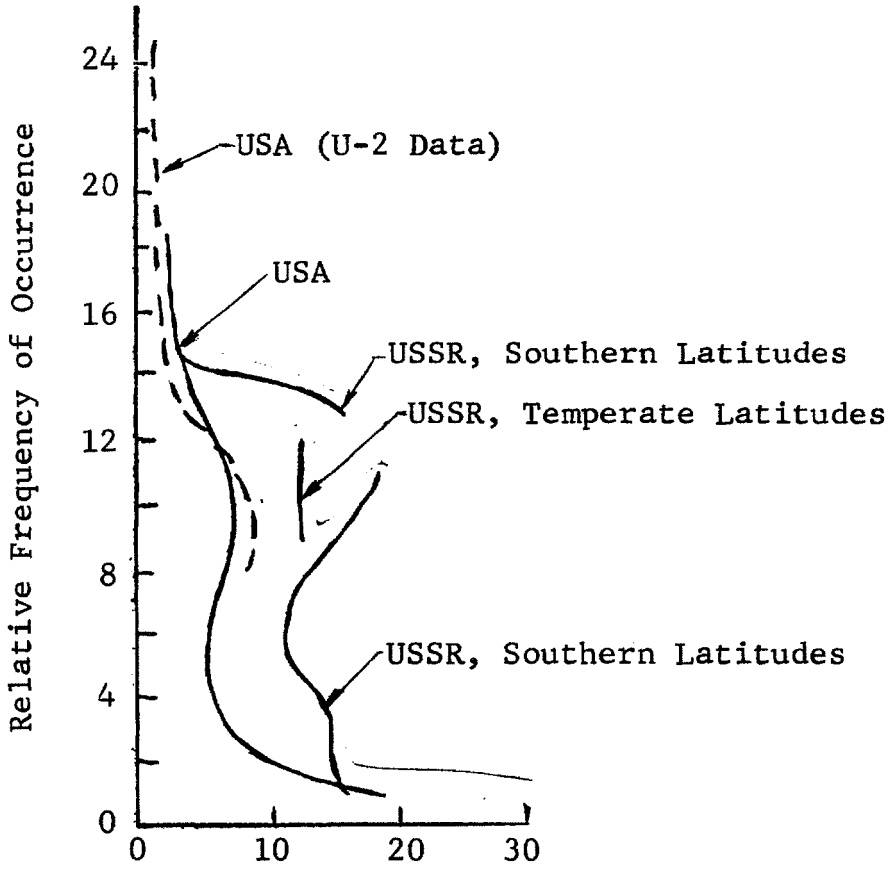

Figure 1 Frequency of Turbulence as a Function of Altitude

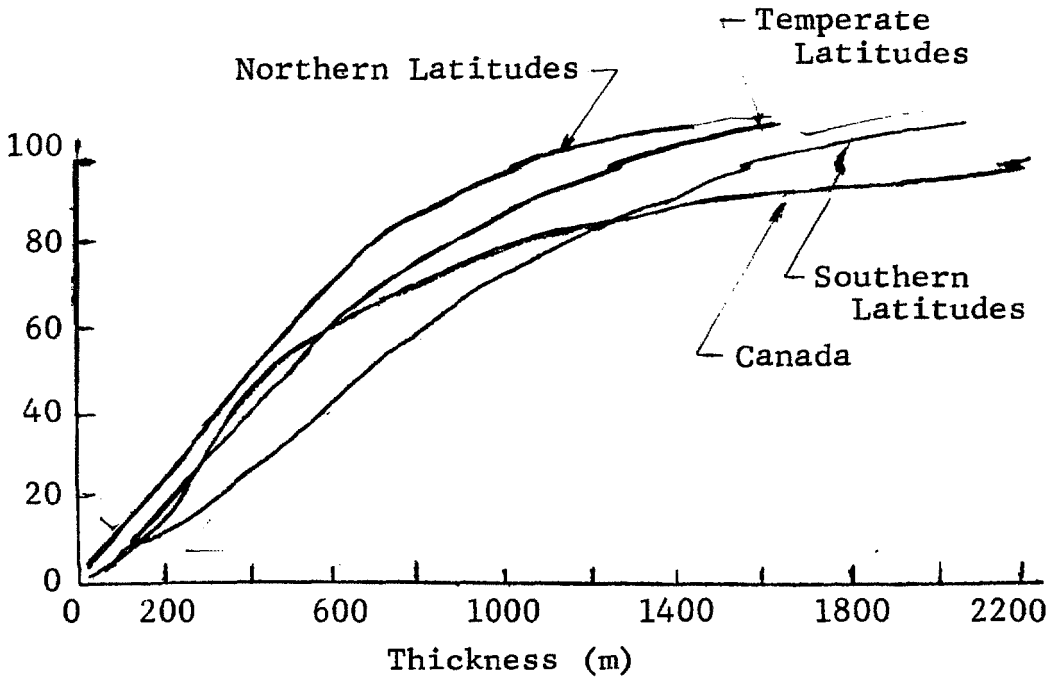

Figure 2 Integral Frequency of the Thickness of Turbulent Layers

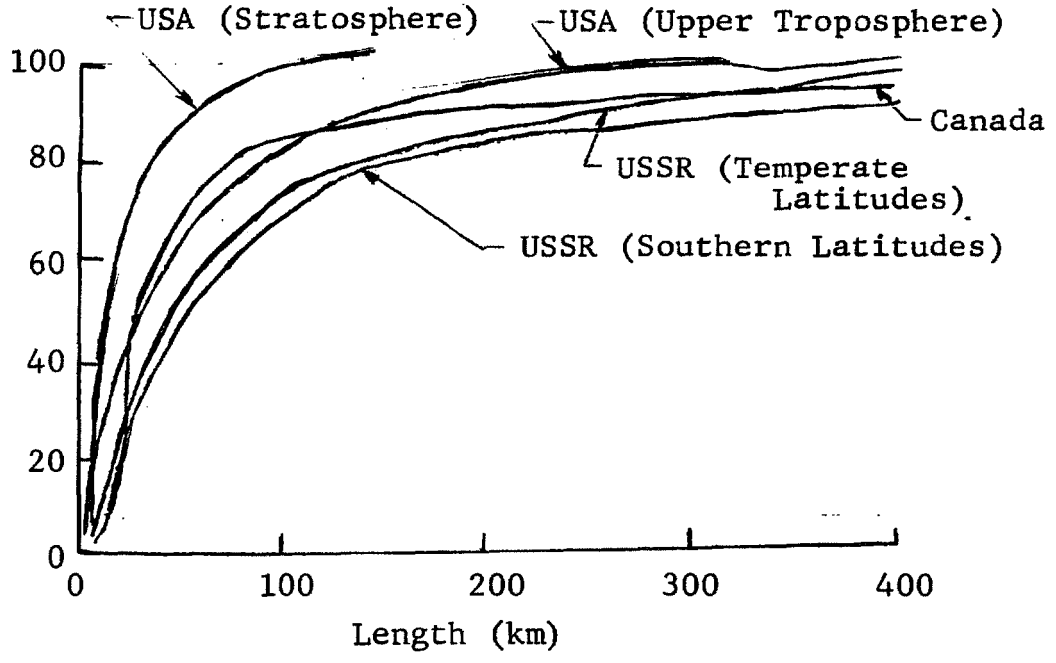

Figure 3 Integral Frequency of the Horizontal Length of Turbulent Layers

an important function of a CAT warning system must be the ability to determine the vertical extent of the turbulence region, since evasion by an altitude change will be simpler than a horizontal maneuver. A point to be emphasized is that, while the horizontal extent of the disturbed volume is of the order of 100 km, turbulent intensities within this volume will vary, and regions of severe turbulences will be of much small horizontal extent. This points out the general weakness of detection methods based on large scale nonuniformities or gradients.

The forecasting of CAT will come about when atmospheric parameters can be measured in detail in time and space, at which time the various mechanisms and characteristics of atmospheric behavior will also be established. Whether this will ever be achieved is a matter for conjecture; it is quite clear that global coverage of the atmosphere with the spatial and temporal resolution needed for accurate forecasting must be relegated to the future. The present practice of large area CAT forecasts coupled with in-flight reports and past experience demonstrates the relatively primitive state of prediction. In addition, the present efforts are mainly directed toward defining areas of possible CAT generation rather than areas of CAT existence.

The different methods of CAT detection may be divided into three groups. The first, and the most direct method, is actual remote measurement of velocity differences. Optical heterodyning methods using a pulsed laser have been studied (Breece, et al., 1966), but implementation must await improvements in laser technology. Doppler radar falls into this category, but an airborne system is impractical (Atlas, et al., 1966a). No passive methods are in this group.

The second group consists of detection of parameters known to be very closely connected to CAT. This group includes refractive index, density, and temperature variations which have spectra, scales, and other properties etc., similar to the velocity fluctuations themselves. The relationship between the magnitude of the velocity fluctuations or the mechanical turbulence and the magnitudes of the fluctuations in refractive index, density, or temperature is less clear. If there are large vertical refractive index gradients, then very light mechanical turbulence can produce large refractive index flucturations Radar reflections from the so-called echo layers associated with sharp inversions of great thermal stability, where such large vertical refractive index gradients exist, have been observed for altitudes of up to 5 km by Hardy, et al.,(1966).

In the region of the tropopause and lower stratosphere, the refractive index gradients are usually quite small, therefore, large refractive index fluctuations are associated with intense mechanical turbulence.

The third group includes methods of detection of CAT based on measurements of some quantity that may often be very indirectly associated with CAT. This group includes measurement of gross temperature changes, as distinct from temperature fluctuations, ozone concentrations, electric fields, particulate matter, and other possible physical properties of CAT.

This grouping is considered to emphasize the distinction between the second and third groups. Frequently this distinction is not made, although it is an important one, because ultimately one would like to know the intensities of turbulent fluctuations as a function of wave number, or simply the turbulent spectrum, so that the effect of the turbulent region on the aircraft itself may be determined from the known aircraft response and air speed. The indirect methods of group three are unlikly to yield this information.

The objectives of this study were to analyze the optical characteristics of the atmosphere in the light of the capabilities of optical detection and imaging instruments, and propose and evaluate passive optical techniques of forming an image of the turbulence, or of providing other visual indications of the presence of turbulence. From these analyses, a detection and imaging system was to be devised. Although a technique that would work both day and night, is clearly preferable, techniques with work only during the day were also to be considered. A number of possible remote detection techniques were to be evaluated which were:

- Rayleigh-scattered sunlight is refracted in the region of turbulence. Rays that come from above the horizon and then are refracted toward the observer will have narrower spectral lines than rays originating near or below the horizon. By using a filter which passes a very narrow spectral region on the edge of an absorption line, rays which travel straight will be made invisible, while those which are refracted rays might be used to form an image.

- If the stars can be made visible day or night (for example, by the use of an appropriate spectral filter), movement of the images relative to each other might be used as an indicator of turbulence.

- The atmospheric thermal emission in particular spectral regions might be utilized to provide a temperature "map" of the atmosphere.

- If an infrared scanning and imaging instrument that detects the infrared emission of the atmosphere is aimed at calm air ahead of an aircraft, it will show intensity gradients from top to bottom, but no gradients from right to left. If the proper spectral region is utilized (for example, a region which includes emission lines of water vapor), it might be discovered that there is a certain elevation angle at which infrared emission decreases sharply, and a definite infrared "horizon" appears in the picture. If a region of turbulence were to come into the field of view, one should expect the refraction to cause a distortion of the pattern seen in calm air. In particular, the "horizon" might appear to become less sharp with an appreciable amount of radiation now appearing to come from above the "horizon."

- A technique of spectral analysis might be utilized to make a comparison between the radiation which has been transmitted through the disturbance and the radiation which has passed through calm air. This is similar to the first possibility except that whole spectral bands might be used instead of the edge of a single line. There might be several aspects of this; for example, one could search for absorption bands of ozone which might be superimposed on the thermal emission of the atmosphere beyond the turbulence, one might compare the emission intensity of water bands in different parts of the field of view, or one might compare the carbon dioxide atmospheric bands which are superimposed on scattered sunlight.

Other techniques, in addition to those suggested in the contract scope of work, which were evaluated were:

- Detection of spatial nonuniformities in scattered sunlight produced by atmospheric density and temperature variations.
- Application of two detector systems with crossed fields of view to the detection of scattered sunlight. Such a system would permit distance information to be obtained.
- Stellar scintillation.

In this study insufficient information was available to completely evaluate several of the passive optical techniques that were considered. In the case of the methods based on turbulent fluctuations, the only reliable data available are from gust velocity measurements. Some information about temperature fluctuations has been published, (Glagolev 1964) but there are generally no complementary gust data. The measured gust spectra have indicated that within certain wavelength limits isotropic turbulence theory applies, and this has, therefore, been used in some of the calculations. However, it is only an approximation of the real case.

Measurement of a parameter having some association or correlation with CAT poses a different problem. Aside from establishing detectability, it is also necessary to delineate the correlation with CAT. Past measurements have not shown an adequate correlation between any measured parameter and occurrence of CAT; on the contrary, they tend to indicate a lack of the correlation which would be required for consistent and reliable remote warning systems.

Since adequate assessment of several of the techniques considered required a knowledge of density and temperature variations associated with clear air turbulence, an important phase of this study was to attempt to predict such variations on the basis of the experimental and theoretical work that has been done in the field of atmospheric turbulence.

2. REFRACTIVE INDEX AND DENSITY FLUCTUATIONS

2.1 Refractive Index Structure Constant

In studying different passive optical methods of detecting CAT, both the transmission of radiation through clear air turbulence regions and radiation directly originating in the CAT region either by scattering or thermal emission must be considered. The latter case requires a knowledge of the actual density or temperature variations associated with CAT. These variations may be calculated directly from the refractive index structure constant C_n (Tatarski, 1961). Before proceeding to discuss actual density and temperature variations, the values of C_n appropriate to CAT will be explored.

The structure constant has been used by numerous investigators in considering the propagation of electromagnetic waves through locally isotropic turbulent flows, which may be described in terms of the structure function of the form:

$$D_n(r) = \begin{cases} C_n^2 r^{2/3} & \text{for } \ell_o \ll r \ll L_o \\ C_n^2 \ell_o^{2/3} \left(\frac{r}{\ell_o}\right)^2 & \text{for } r \ll \ell_o \end{cases}$$

where ℓ_o is the limiting microscale or inner scale of the turbulence and L_o is the outer scale. The general shape of the structure function is shown in Figure 4. The structure function for velocity fluctuations has the same form and, for $r \ll \ell_o$, is controlled by viscous dissipation of energy into heat. Over the region of eddy scales for which the two-thirds law applies, turbulent energy is transferred down a cascade of decreasing eddy sizes. Energy input at large eddy scales, which no longer can be regarded as isotropic and homogeneous, may be caused by the "breaking" of gravitational shearing waves.

The limiting microscale, ℓ_o, is not fixed but depends on the quantity ε, the rate of dissipation of turbulent energy per unit mass. Megaw (1957) defines ℓ_o as

$$\ell_o = 5.9 \, (\nu^3/\varepsilon)^{1/4}$$

where ν is the coefficient of kinematic viscosity. Since ν varies only slowly with altitude, if we take $\nu = 0.335$ cm^2 sec^{-1} corresponding to an altitude of ~9 km and a temperature of -35°C, then

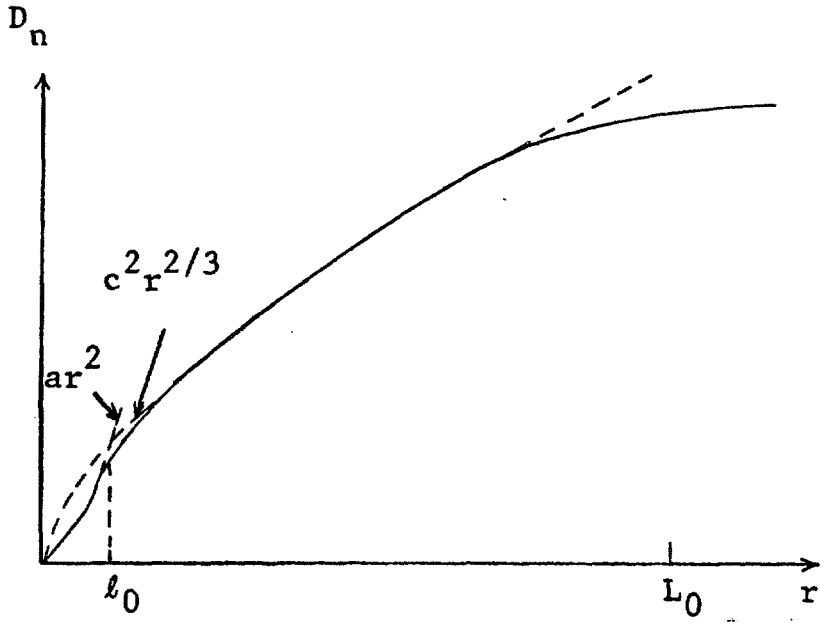

Figure 4 General Shape of the Structure Function D_n

$$\ell_o \sim 2.6\ \varepsilon^{-1/4}.$$

Thus, the greater the degree of turbulence, the smaller the inner scale and, as noted by Atlas, et al (1966), if this inner scale could be measured, we would have an approximate measure of the intensity of the turbulence. For a typical quiet atmosphere at an altitude of 9 km, Wilkins (1963) gives $\varepsilon = 0.035$ cm^{2}sec^{-3}. Extrapolation of measured results on project TOPCAT (Reiter and Burns 1961) gave $\varepsilon = 131$ cm^{2}sec^{-3}, while Panofsky (1965) suggest that ε may be as large as 1000 cm^{2}sec^{-3}. The inner scales corresponding to these values of ε are:

ε (cm^{2}sec^{-3})	ℓ_o (cm)
0.035	6.5
131	0.77
1000	0.56

The outer scale, L_o, is indicated in Figure 4 with respect to the structure function, and spectra measured by Reiter and Burns (1966) are shown in Figure 5. Reiter and Burns found outer scales from approximately 100 to 600 m. Tatarski (1961) defines L_o by

$$L_o = (K/\beta)^{1/2}$$

where K is the coefficient of eddy diffusivity and $\beta = \frac{\overline{du}}{dz}$, the vertical gradient of the mean horizontal wind. Since ε is given by

$$\varepsilon = K\beta^2,$$

we have for the outer scale

$$L_o = (\varepsilon/\beta^3)^{1/2}, \tag{1}$$

which is thus related to the vertical gradient of the wind and the rate of energy dissipation.

For one particular case of project TOPCAT (Figure 5), ε is estimated, from the limiting microscale by extrapolation of the spectrum, to be 131 cm^2sec^{-3}; L_o is known from the point at which the spectrum begins to deviate from the minus-five-thirds power law to be 100 to 600 m; therefore, β can be calculated. The value of $\beta = 0.005$ sec^{-1}, obtained from Eq. (1) for $L_o = 325$ m, corresponds to the average rate of change of horizontal wind velocity with altitude, for an altitude of 9 km. It is of interest to note that, for a nominally "quiet" atmosphere with $\varepsilon = 0.035$, the outer scale of the turbulence $L_o \approx 4$ m.

Now it has been shown by Tatarski (1961) that the structure constant of refractive index fluctuations is given by

$$C_n^2 = a^2 L_o^{4/3} M^2 \tag{2}$$

where a^2 is a nondimensional proportionality parameter of order unity and $M = \overline{(dn/dz)}$. This equation can very easily by shown to physically plausible. The outer scale of the turbulence, L_o, is the maximum vertical distance between two points for which the two-thirds power law for the structure function and, synonymously, the minus-five-thirds power law for spectral density are obeyed. If there is a refractive index gradient between these two points, then there will be a systematic difference in values of n equal to $(\partial n/\partial z)$ z. There will, therefore, be a contribution to the structure function,

$$D_n = \overline{(n(z_1) - n(z_2))}^2$$

which increases as the square of the vertical separation of the two points. This contribution to the structure function will be equal to the contribution caused by fluctuations violating the condition for isotropy when

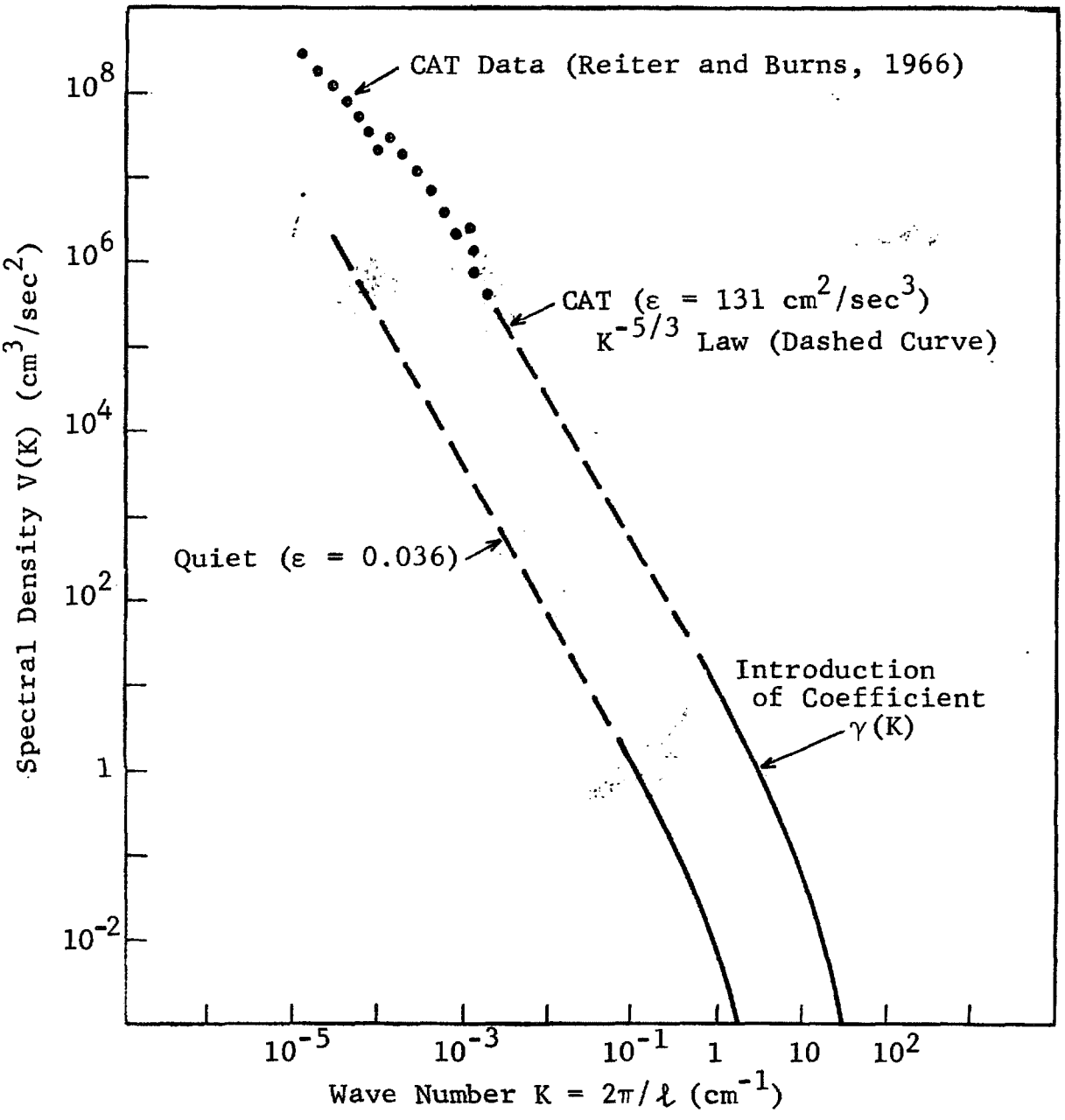

Figure 5 Spectrum for Quiet Atmosphere at 9-km Altitude Compared with Spectrum for CAT Case

$$C_n^2 L_o^{2/3} = L_o^2 \left(\frac{\partial n}{\partial z}\right)^2$$

or

$$C_n^2 \sim L_o^{4/3} M^2.$$

The constant a in Eq. (2) has been determined by Tatarski (1960) to be a function of Richardson's number, as shown in Figure 6. Atlas, et al. (1966) have used Eq. (2) with the following values for the parameters to determine values of C_n^2 appropriate to CAT:

a^2 = 2, corresponding to a Richardson number of 0.05

L_o = 100 - 600 m, based on the CAT spectra of Reiter and Burns (1965)

M = 4.4×10^{-11} cm^{-1} obtained from the equation,

$$M = -79 \times 10^{-6} \, pT^{-2} \frac{d\theta}{dz}$$

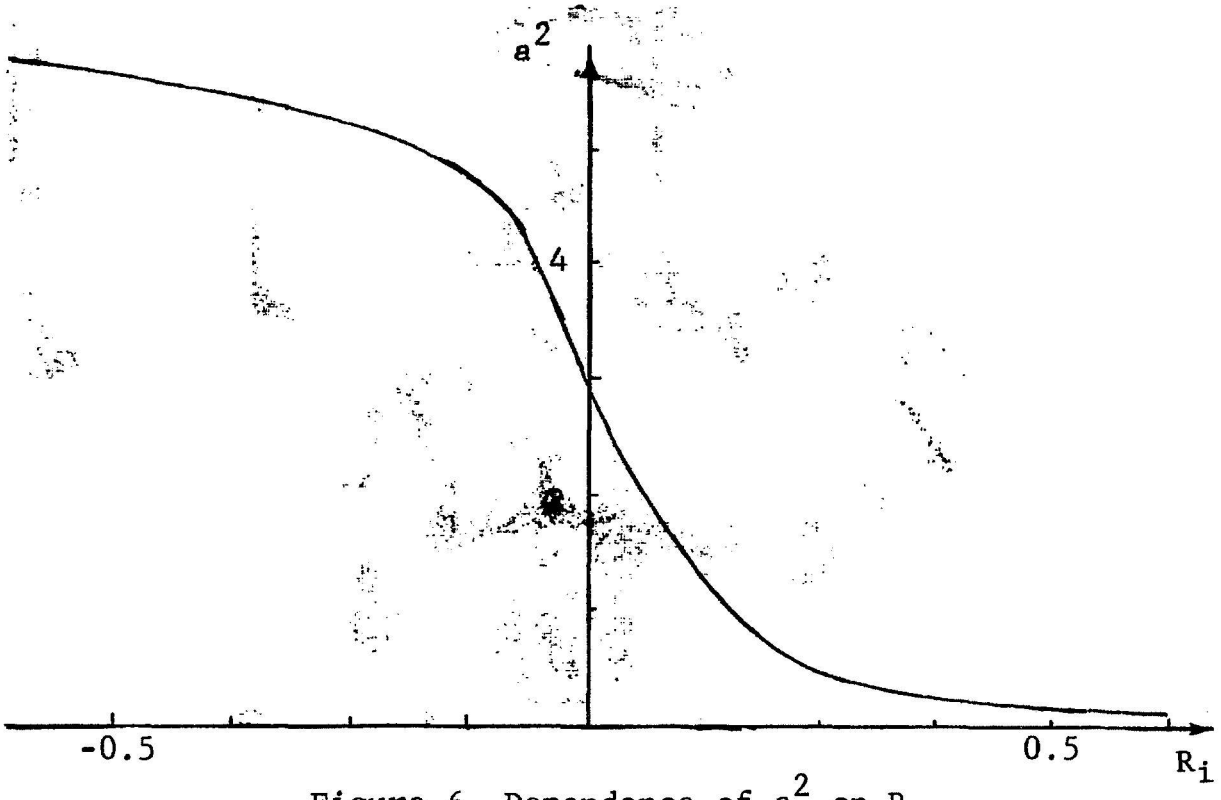

Figure 6 Dependence of a^2 on R_i

where p and T respectively, are the mean pressure (in mb) and absolute temperature and θ is the potential temperature, Again, following Atlas, et al. (1966), we will take p ~ 300 mb and T ~ 233°K, corresponding to an altitude of 9 km. Assuming that CAT occurs preferentially in thermally stable layers (Panofsky, 1965), $d\theta/dz$ is taken as 10^{-4}°K cm^{-1}. We therefore have the following values for C_n^2 :

L_o (m)	C_n^2 $cm^{-2/3}$
100	8.25×10^{-16}
300	3.5×10^{-15}
600	8.95×10^{-4}

Stephens and Reiter (1966) have cast doubt on the validity of these results. The vertical wind shear $\beta = (\partial u/\partial z)$ may be obtained from Eq. (1) and also from the Richardson number

$$R_i = \frac{g}{T} \frac{\partial\theta/\partial z}{\beta^2} . \qquad (3)$$

Substituting the values of the parameters used by Atlas, et al. (1966) in these equations, we obtain conflicting results that differ by a factor of five for the wind shear.

From Eq. (3), we obtain

$$\beta \sim 8 \times 10^{-2} \text{ sec}^{-1};$$

and from Eq. (1), taking a high value for ε of 400 $cm^2 sec^{-3}$ and the minimum L_o = 100 m, we arrive at

$$\beta \sim 1.65 \times 10^{-2}.$$

Stephens and Reiter note that this value of β gives a Richardson's number of 1.2; and they state that Atlas, et al., should have evaluated a^2 to be 1/12, leading to values of C_n^2 that are approximately 25 times smaller than those obtained by Atlas. Stephens and Reiter also conclude that their values of C_n^2 are obtained on the tacit assumption that moderate CAT is occurring everywhere and that, when the energy levels are reduced to nonturbulent levels, C_n^2 will be orders of magnitude smaller than even their results indicate. The resolution of this discrepancy is vitally important in determining the feasibility of the passive optical technique for detecting CAT, making use of Rayleigh scattered sunlight.

Having examined these papers in detail and taking into account experimental results, we find that the results obtained by Atlas appear more nearly correct. The cause of the discrepancy is harder to identify because many of the equations used in turbulence work and in atmospheric turbulence work, in particular, are based on dimensional arguments and include ill-defined constants known only through a very limited number of experimental measurements. The coefficient a is a prime example. This analysis also assumes that both density and temperature effects may be treated as passive additives. Obukhov (1959) has investigated departures from the two-thirds law for a temperature field, which are connected with its lack of passivity. He concludes that in regions small compared with a characteristic dimension, L_K depends on meteorological conditions being related to the outer scale of velocity fluctuations or fluctuations of a passive additive by the equation

$$\frac{L_o}{L_K} = (Ri)^{3/2}$$

This lack of passivity has not been taken directly into account by Atlas or by Stephens and Reiter. Rather than regarding a^2 as a function of the Richardson number, it may be equally appropriate to write

$$\frac{C_n^2}{L_K^{4/3} M^2} = f(Ri)$$

where this function of Ri has to be determined.

2.2 Experimental Evidence for Values of C_n^2

Direct experimental evidence of the correctness of the values of C_n^2 deduced by Atlas, et al. (1966) was obtained by Atlas, et al. (1966) by radar backscatter measurements. Using the measured reflectivity of 10.7-cm wavelength radar waves, they deduced a value of the structure constant of refractive index as

$$C_n^2 = 4.4 \times 10^{-16} \text{ cm}^{-2/3}.$$

This result falls well within the range of 10^{-6} to 10^{-14} $\text{cm}^{-2/3}$ estimated theoretically.

Further evidence of the order of fluctuations in the case of a nominally quiet atmosphere has been deduced by Tatarski (1961) from measurements by Kolchinski (1957) of stellar scintillation. Stellar scintillation effects have been shown by various authors to be a result of refractive index fluctuations at altitudes of the order of 19 km as distinct from poor "seeing," which is produced by fluctuations in the immediate vicinity of the telescope. Depending on precisely how the profile C_n^2 (z) is specified, Tatarski obtained values of C_n^2 from 1.3×10^{-17} to 5×10^{-17} $cm^{-2/3}$. These figures exceed those obtained by Stephens and Reiter for CAT regions.

On the basis of these experiments, we are taking the results of Atlas, et al. (1966) to be correct, and we will now derive the density and temperature fluctuations directly from the structure constant.

2.3 Magnitudes of Refractive Index, Density and Temperature Fluctuations

Hardy, et al. (1966) have shown that

$$\overline{(\Delta n)^2} = 0.19\, L_o^{2/3}\, C_n^2. \tag{4}$$

Approximately the same results may be obtained from the structure function from general considerations. The structure function is given by

$$D_n(\vec{r}_1-\vec{r}_2) = C_n^2\,(\vec{r}_i-\vec{r}_2) = \left[n(\vec{r}_1) - n(\vec{r}_2)\right]^2. \tag{5}$$

Now writing $n(\vec{r}_1)$ and $n(\vec{r}_2)$ in terms of a mean and a fluctuating part, we have:

$$n(\vec{r}_1) = \bar{n}_1 + \Delta n_1$$
$$n(\vec{r}_2) = \bar{n}_2 + \Delta n_2.$$

For isotropic homogeneous turbulence, we may write

$$\bar{n}_1 = \bar{n}_2$$

and

$$\overline{(\Delta n_1)^2} = \overline{(\Delta n_2)^2}.$$

Therefore:

$$D_n = \overline{\left[(\overline{n_1} + \Delta n_1) - (\overline{n_2} + \Delta n_2)\right]^2}$$

$$= \overline{(\Delta n_1 - \Delta n_2)^2}$$

$$= \overline{\Delta n_1^2} + \overline{\Delta n_2^2} - 2\overline{\Delta n_1 \Delta n_2}.$$

If we assume that the structure function flattens out for some length scale L_o, then fluctuations between two points separated by a distance greater than L_o are uncorrelated.

Therefore:

$$\overline{\Delta n_1 \Delta n_2} = 0$$

and $$D_n \sim 2\overline{\Delta n^2}.$$

Thus,

$$2\overline{\Delta n^2} \sim C_n^2 \, L_o^{2/3}$$

or

$$\overline{\Delta n^2} \approx 0.5 \, C_n^2 \, L_o^{2/3}.$$

This equation differs from Eq. (5) by a factor of 2.5. To avoid any possible overestimation of the fluctuation levels, the Table I was derived from Eq. (5).

2.4 Refractive Index Fluctuations as a Function of Bandwidth of Observations

The magnitude of the rms refractive index fluctuations

$$(\overline{\Delta n^2})^{1/2}$$

will depend on the wave number components of the CAT that we are able to measure. Because of the finite field of view, there may be a large number of small eddies, or high-wave-number components, in the field of view at one instant of time. There will, therefore, be an average effect that will

TABLE I

REFRACTIVE INDEX, DENSITY, AND TEMPERATURE FLUCTUATIONS

C_n^2 ($cm^{-2/3}$)	L_o (m)	$\overline{(\Delta n^2)}^{1/2}$	$\overline{(\Delta \rho^2)}^{1/2}/\rho_o$ (%)	$\overline{(\Delta T^2)}^{1/2}$ (°K)
10^{-18}	4	3.2×10^{-9}	0.003	0.007
10^{-18}	100	9.3×10^{-9}	0.009	0.021
10^{-18}	600	1.7×10^{-8}	0.016	0.037
10^{-17}	100	2.9×10^{-8}	0.027	0.063
10^{-17}	600	5×10^{-8}	0.047	0.11
10^{-16}	100	9.3×10^{-8}	0.089	0.21
10^{-16}	600	1.7×10^{-7}	0.16	0.37
10^{-15}	100	2.9×10^{-7}	0.27	0.63
10^{-15}	600	5×10^{-7}	0.47	1.1
10^{-14}	100	9.3×10^{-7}	0.89	2.1
10^{-14}	600	1.7×10^{-6}	0.60	3.7

Altitude: 9 km
Standard U.S. atmospheric temperature and density.

reduce the measured $\overline{\Delta n^2}$. With a photometer which scans in a horizontal plane, there will be a limit to the low-wave-number turbulence components that are detected, which will depend on the amplitude of the angular scan, the distance to the turbulence region, the rate of scan, and the low-frequency characteristics of the detector system. It is important to determine how the measured fluctuation power will vary as a function of detector field-of-view, and the distance to the CAT region.

To investigate this problem, it is necessary to assume some form of turbulence spectrum. The theoretically derived expression for the case of locally homogeneous isotropic turbulence will be used:

$$\Phi(K) = 0.033\ C_n^2\ K^{-11/3} \quad (K_o < K < K_m)$$

where C_n is the refractive index structure constant $K_o \sim \frac{1}{L_o}$, and $K_m = 1/l_o$. Considering the turbulence field along one line in space, we need to know the one-dimensional wave-number spectrum $V(K)$ which is related to the three-dimensional spectrum by the expression

$$\Phi(K) = -\frac{1}{2\pi K}\frac{dV(K)}{dK}.$$

Thus,

$$V(K) = 0.124\ C_n^2\ K^{-5/3}.$$

This spectrum is shown in Figure 7. The power in the refractive index fluctuations for the inertial subrange of turbulent fluctuations from K_o to K_m will be given by

$$\overline{\Delta n^2} = \int_{K_o}^{K_m} V(K)dK = 0.19\ (2\pi)^{-2/3}\ C_n^2\ L_o^{2/3}.$$

This expression differs from that derived by Hardy et al. (1966) by the factor $(2\pi)^{-2/3}$ and the source of this discrepancy is unknown at the present time.

Irrespective of the value of this constant, the proportional decrease in

$$\overline{\Delta n^2}$$

may still be usefully studied in terms of wave-number components that would be detected by a scanning system with a finite field of view.

In calculations made in Section 3.1, where detection of refractive index variations using fluctuations in scattered sunlight is discussed, the field of view of the detecting system is taken to be 2×10^{-3} radian. At a distance of 20 km an eddy 40 m in diameter will just fill the field of view of the detecting system. The response to wave-number components 80 m in wavelength will, therefore, be down by approximately 35 percent, and this will be taken as the maximum wave number component that will contribute to

$$\overline{\Delta n^2}$$

Thus,

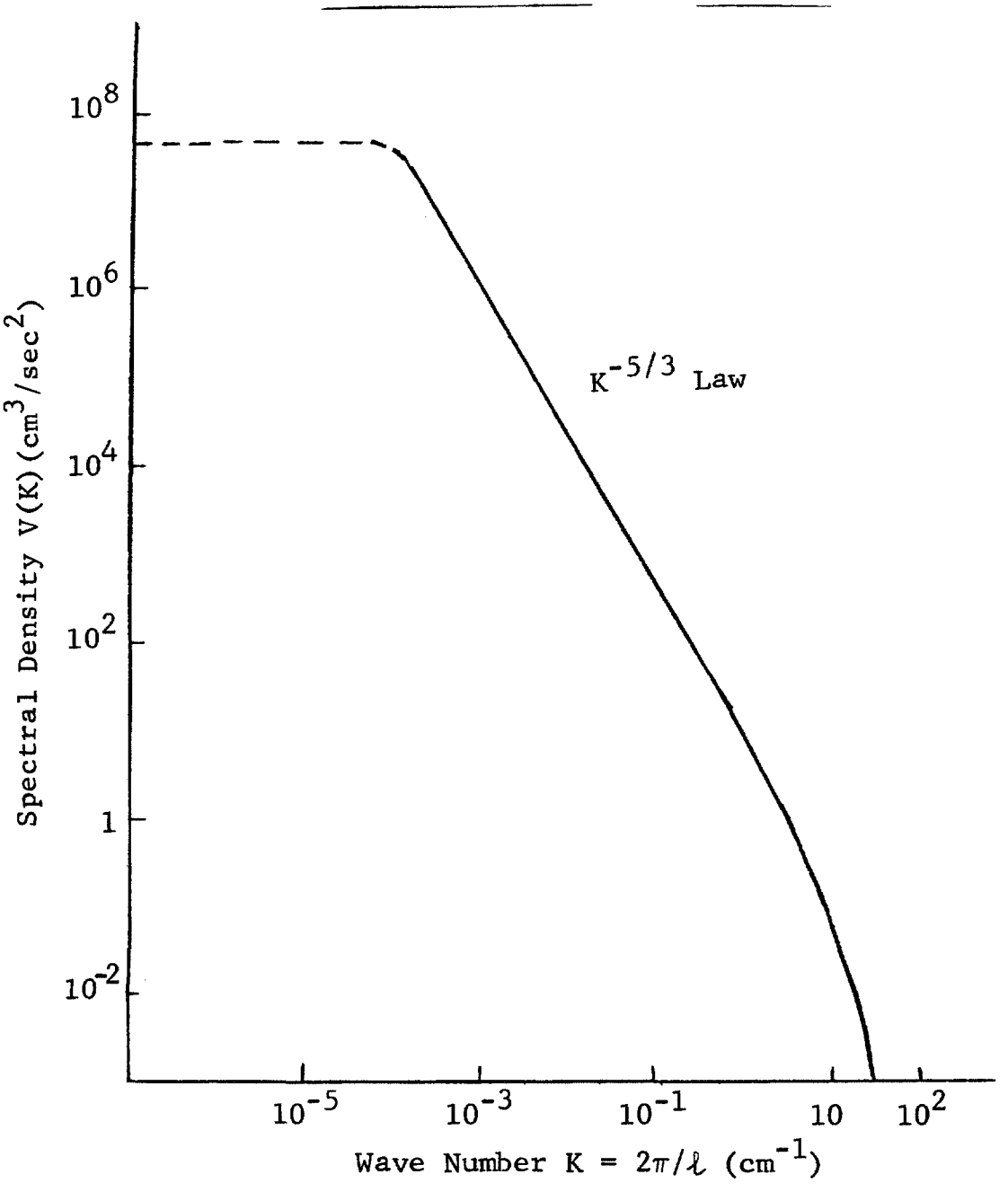

Figure 7 Typical CAT One-Dimensional Refractive Index Spectrum

$$\overline{\Delta n^2} = \int_{K_o}^{K_{max}} V(K)\,dK = 0.19(2\pi)^{-2/3} C_n^2 \left\{ L_o - L_{min} \right\}^{2/3}$$

and the fractional change in $\overline{\Delta n^2}$ will be given by

$$F = \left(\frac{L_o - L_{min}}{L_o} \right)^{2/3} .$$

For $L_o \sim 600$ m and $L_{min} \sim 80$ m, we have $F = 0.9$ and there will be a 10 percent reduction in

$$\overline{\Delta n^2} \quad \text{over the} \quad \overline{\Delta n^2}$$

that would be measured if the complete inertial subrange could be detected.

No account has been taken here of the low wave number components; i.e., $K < K_o$. The shape of the spectrum in this region will depend on the mesoscale structure of the atmosphere; for the purpose of discussion, however, we will assume a flat spectrum from $K = K_o$ to $K = 0$. If we assume that the detecting system scans through an angle of 30° in the horizontal plane, the length of scan at a distance of 20 km is 10 km. If this is taken to be the maximum eddy size, the additional contribution to

$$\overline{\Delta n^2}$$

by this low-wave-number region may be calculated:

$$\overline{\Delta n^2} = 0.124\, C_n^2\, K_o^{-2/3} = 0.124\, (2\pi)^{-2/3} C_n^2\, L_o^{2/3}.$$

The total level of refractive index fluctuations will, therefore, be given by

$$\overline{\Delta n^2} = 0.314\, (2\pi)^{-2/3}\, C_n^2\, L_o^{2/3}$$

of which 40 percent resides in eddies larger than L_o, with the assumed flat spectrum.

It, therefore has been shown that the level of fluctuations will not be appreciably affected by the omission of small scale eddies caused by averaging over the field of view of the detecting system. On the other hand, the shape of the spectral distribution curve for wave numbers less than K_o can appreciably change the measured fluctuation levels.

3. ANALYSIS OF PASSIVE DETECTION METHODS

3.1 Rayleigh Scattering

3.1.1 Detection Sensitivity. If the turbulent region is characterized by an average density different from that of the undisturbed surrounding air or by density variations within the turbulent volume, the information contained in the scattered sunlight can be utilized to detect it. In view of existing knowledge on temperature gradients connected with turbulence (e.g., Endlich and Mancusco (1964), and Fusca (1964)), rather than those associated with the general meteorology of CAT-prone situations (e.g., McLean (1965)), we can reasonably expect density differences arising from temperature differences. The detection of such density differences by scattered radiation measurements may be considered, using either a single detector or two detectors with crossed fields-of-view. The single detector geometry is shown in Figure 8, and the extension to a two-detector correlation method is straightforward.

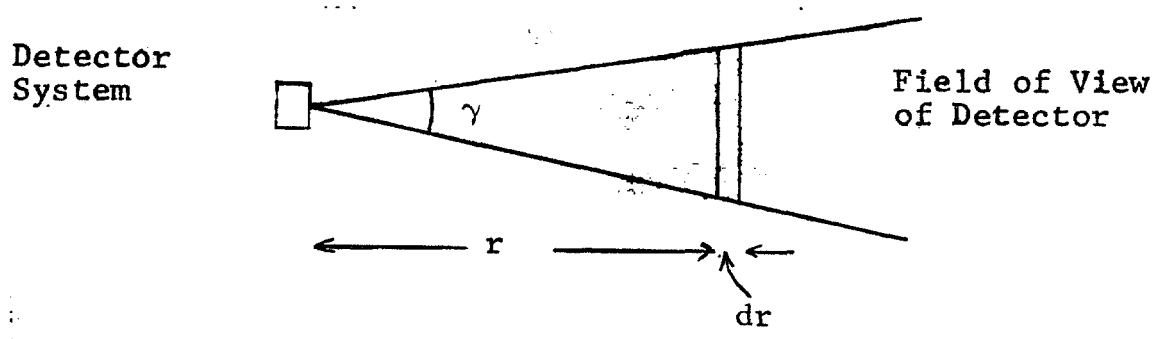

Figure 8 Single Detector Geometry

The detector field-of-view scans in either a horizontal or vertical plane (or both) with some total angular coverage. The intensity of the radiation seen by the detector at one instant in time is given by

$$I = \frac{\pi}{4} A\gamma^2 \beta(\lambda,\theta) H_o \int_o^\infty N(r)\, dr,$$

where

H_o is the flux density at the scattering volume (watts/cm^2)

(λ,θ) is the Rayleigh scattering function for a single molecule for wavelength λ and scattering angle θ

A is the area of the collector, (cm^2)

r is the distance from the detector, (cm)

γ is the angular field-of-view, (radians), and

N(r) is number density at distance r (cm^{-3}).

The scattering function for unpolarized light can be expressed as

$$\beta(\lambda,\theta) = \frac{2\pi}{\lambda}^4 |\alpha|^2 \frac{(\cos^2\theta+1)}{2},$$

where α is the polarizability of air. If the collector diameter is d, then

$$I = \frac{\pi^6 (\cos^2\theta+1) d^2\gamma^2 |\alpha|^2}{2\lambda^4} H_o \int_o^\infty N(r)dr \text{ (watts)}.$$

At a time t later, N(r) will have changed to N'(r), if turbulence is present, owing to the change in the number of scattering centers along the field-of-view of the detector. Changes in elevation angle of the field-of-view would also alter N(r), and this point is discussed when stability requirements are considered. The new received intensity will be written as I'. We can represent N'(r) by

$$N'(r) = N(r) \pm \Delta N(r)$$

i.e., the number density distribution with no turbulence plus a turbulence component (either positive or negative). We consider $\Delta N(r)$ to be zero outside the turbulent region. Turbulence detection, therefore, means measuring $\Delta N(r)$ or, rather, the change in the intensity of the scattered radiation resulting from $\Delta N(r)$. This could be accomplished in the following way. If a single detector on board an aircraft scans a portion of the sky ahead of the aircraft, then spatial variations in scattered intensity could, in theory, be measured. To assess the magnitude of the fluctuations, we will consider the difference signal

$$S = K \left|I'-I\right| \quad \text{at} \quad \lambda = 0.5\mu$$

where K is the radiant sensitivity of the photocathode in amps/watt. The absolute value of the difference is used, since we cannot say a priori what the sign of the temperature fluctuation will be.

Since we are using scattered sunlight for detection of turbulence, photomultipliers are the logical choice for detectors, in view of the predominant scattering in the short wavelength portion of the visible spectrum. For such a photoemissive device, the noise will be that due to I (i.e., the background-induced shot noise will be much greater than the detector dark noise). The rms value of the shot noise is given by

$$N = (2eKI\Delta f)^{1/2}.$$

The resulting signal-to-noise ratio (at the cathode) is then

$$\frac{S}{N} = \frac{K|I'-I|}{(2eKI\Delta f)^{1/2}}.$$

Substituting for I and I', we find that

$$\frac{S}{N} = \left[\frac{CKH_o}{2e\Delta f}\right]^{1/2} \frac{\int \Delta N(r)\,dr}{\left[\int_o^{\infty} N(r)\,dr\right]^{1/2}}$$

where

$$C = \frac{\pi^6}{2}(\cos^2\theta+1)\frac{d^2\gamma^2\alpha^2}{\lambda^4},$$

and the limits on the integral in the numerator are from $R_o-(L_r/2)$ to $R_o+(L_r/2)$ with R_o the distance to the center of the turbulent volume and L_r the extent of the turbulent volume along r.

If we characterize $\Delta N(r)$ and $N(r)$ by some suitable space-averaged values and integrate over appropriate limits, we can evaluate this expression for some reasonable instrumental parameters, We will use

$$\Delta N(r)dr = (\overline{\Delta N})L_r$$

and

$$\int_o^{\infty} N(r)dr = \int_o^{200km} N_o dr = 2 \times 10^7 N_o \text{ cm}$$

with N_o the density at 10 km and $\overline{\Delta N}$ the space average of $\Delta N(r)$ over the turbulent volume viewed at any instant of time. Then,

$$\frac{S}{N} = \left[\frac{CKH_o}{2e\Delta f}\right]^{1/2} \frac{(\overline{\Delta N})\ L_r}{(2 \times 10^7 N_o)^{1/2}}$$

If we assume that

$\theta = 90°$

$d = 15$ cm

$\gamma = 2 \times 10^{-3}$ radian

$\alpha = 3 \times 10^{-24}$ cm^3

$\lambda = 0.5\mu$

$H_o = 5 \times 10^{-3}$ watts/cm^2 $(\Delta\lambda = 0.1\mu)$

$K = 5 \times 10^{-2}$ amps/watt

$e = 1.6 \times 10^{-19}$ coulombs

$N_o = 8.6 \times 10^{18}$ cm^{-3}

$\Delta f = 100$ cps,

then

$$\frac{S}{N} = 5 \times 10^{-3} \frac{(\overline{\Delta N})L_r}{(N_o)^{1/2}} .$$

We can relate $\overline{\Delta N}$ to temperature variations since

$$\frac{\Delta N}{N_o} = \frac{\overline{\Delta T}}{T} .$$

From data obtained by Project Jet Stream Flights, a $\overline{\Delta T}$ of two to three degrees is many times found to extend

over 10 to 40 miles in the horizontal direction (Endlich and Mancusco 1964). While not all such temperature changes can be obviously related to the recorded turbulence, the clear correlations between turbulence and stretches of pronounced temperature variations are sufficient to warrant using the value

$$\frac{\overline{\Delta T}}{T} = 10^{-2}.$$

Glagolev (1964) has published data on vertical temperature gradients of similar magnitude. The vertical scales are quite different though, as is to be expected from considerations of the real atmosphere (Reiter 1966).

With this value for $\overline{\Delta N}/N_o$, we have a signal-to-noise ratio of

$$\frac{S}{N} = 5 \times 10^{-13} L_r (N_o)^{1/2} \times 10^{-2} \text{ cm}$$

$$\frac{S}{N} = 1.45 \times 10^{-5} L_r$$

where L_r is the size of a turbulent module measured in centimeters. When this expression is reversed and the units of L_r changed,

$$L_r = 0.7 \frac{S}{N} \text{ kilometers}$$

Thus, if we take the minimum useful S/N ratio to be two, a turbulence module 1.4 km in diameter may just be detected.

In practice, of course, there will be a CAT ragion, probably 10 to 60 km in extent, involving a wide spectrum of eddy sizes. Although the relative importance of eddy size has not been clearly established, it has been suggested that the range 30 to 600 m in the horizontal plane is most significant for subsonic aircraft (Cobson 1966). For supersonic aircraft we may expect an appropriate increase in the size of eddies that are significant. The signal received by the detector is the integration along the line-of-sight of the detector and will include a large number of eddies. If a mean size in the middle of the range of interest e.g., 300 m is used, there will be of the order of 120 eddies in the field-of-view of the detector. Contributions from each of these eddies will add up in a random fashion; therefore, the fluctuating signal produced when the detector is scanning will be approximately an order of magnitude greater than the signal produced by movement of a single eddy in or out of the detector field-of-view.

When a 300-m eddy size is used, the S/N ratio obtained with a single eddy is ~0.5. Thus, considering the integrated effect through the CAT region, the signal fluctuations due to the presence of CAT should be five times greater than the rms noise fluctuations.

Considering the contribution of larger eddies, the S/N ratio for a single eddy is directly proportional to eddy size, whereas the fluctuating signal is increased as the square root of the number of eddies along the detector line-of-sight. Thus, doubling the eddy size increases the relative value of the fluctuations by 1.4, relative to the rms noise which will remain constant. In the other direction, it should be possible to detect eddies down to sizes of 60 m with a S/N ratio of 2.

It should be noted that with a field-of-view of 2×10^{-3} radian, a 60-m eddy will not fill the field-of-view at 60 km. This will also decrease the contribution of the smaller eddy sizes to the fluctuating signal measured by the detector. The size of the turbulence module measured for a given S/N is then

$$L_r = 0.7 \frac{S}{N} \text{ (km)}.$$

The minimum value of L_r can be decreased (for a fixed S/N) by changing some instrumental and geometrical parameters. Since the scattering angle will vary, a decrease in L_r of $\sqrt{2}$ is possible for certain flights. The aperture of 15 cm could, of course, be increased, but it is doubtful if it is practical to make it much larger. This leaves only the field-of-view as a variable. The field angle can certainly be increased over the 2×10^{-3} radian used in the calculation. Such an increase, however, will result in a decrease of the signal contribution from the smaller eddies ($<$60 m) since they will not fill the field-of-view.

In establishing the eddy size to be avoided or for which, at least, precautions are to be taken prior to penetration, one must consider passenger comfort and structural fatigue, as well as aircraft control and safety. On the basis of pilot reports of CAT penetrations (Ragland, et al., 1964) at typical subsonic jet speeds, eddy scales in the range 30 to 600 m caused the most discomfort to passengers, and led to the greatest aircraft control problems. It is not at all clear at this point what effect eddy size has on structural fatigue caused by repeated turbulence encounters (MacReady, et al., 1965, Hardrath 1965).

3.1.2 Atmospheric Scattering. The preceding calculations have shown that the use of spatial inhomogeneities in scattered sunlight is a possible method for CAT detection in the daytime.

In analyzing this approach, we have been concerned only with an idealized situation for which turbulence detectability was computed. We have used the concept of molecular scattering only, since inclusion of Mie scattering makes the mathematical treatment much more difficult. A more realistic atmosphere is now examined to determine the validity of the model used.

The radiance of a unit volume of the atmosphere is determined by the angular volume-scattering coefficient to which both molecular and particulate matter contribute. At altitudes of ~10 km, the integrated coefficients are roughly the same so that we must consider both types of processes. Molecular scattering can be treated in a straightforward fashion in its angular and altitude dependencies. Mie scattering by aerosols is quite complicated; therefore, we have used measured values of sky radiance.

The degree of departure from a molecular atmosphere depends on altitude. From the work of Volz and Goody (1962), it appears that, at altitudes of ~10 km, the volume cross sections for molecular and aerosol total scattering are about equal. Doubling the intensity computed from molecular scattering would, therefore, appear to be sufficient for taking aerosol scattering into account. An examination of scattering theory, however, shows that this equation must be used with caution. The reason for this can be seen from Figures 9 and 10, which depict the scattered intensity as a function of scattering angle for the two types of scattering. Since we are dealing with unpolarized incident light, the curves for the two polarizations are not shown. Rayleigh scattering leads to an angular dependence with minima at 90° angles, but with symmetry about both the 90 to 290° and 0 to 180° axes. Aerosol scattering, on the other hand, exhibits a very strong forward lobe with a ratio of 100 possible for forward-to back-scattered light.

3.1.3 Molecular Scattering Theory. For a volume of atmospheric molecules, the solution to the generalized scattering equations are size-independent (see, e.g., Van de Hulst, 1957). This region, where the diameter of the scatterer is much less than the wavelength, is commonly called the Rayleigh region. For incident unpolarized light, the brightness of a scattering volume is given by

$$dB = \left(\frac{2\pi}{\lambda}\right)^4 |\alpha|^2 \frac{(1 + \cos^2\theta)}{2} N I_o \, d\ell \left(\frac{\text{watts}}{\text{cm}^2 \text{ sterad}}\right)$$

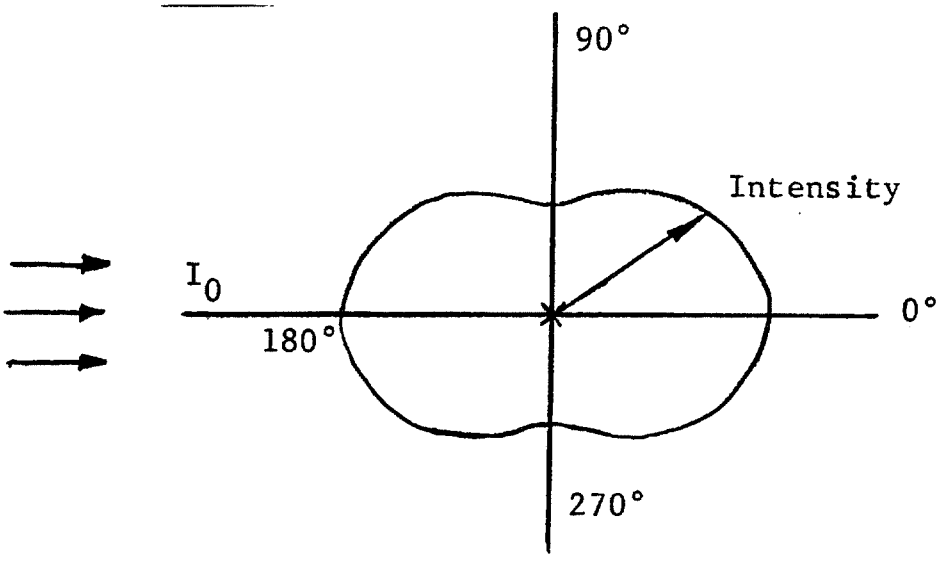

Figure 9 Rayleigh Angular Function

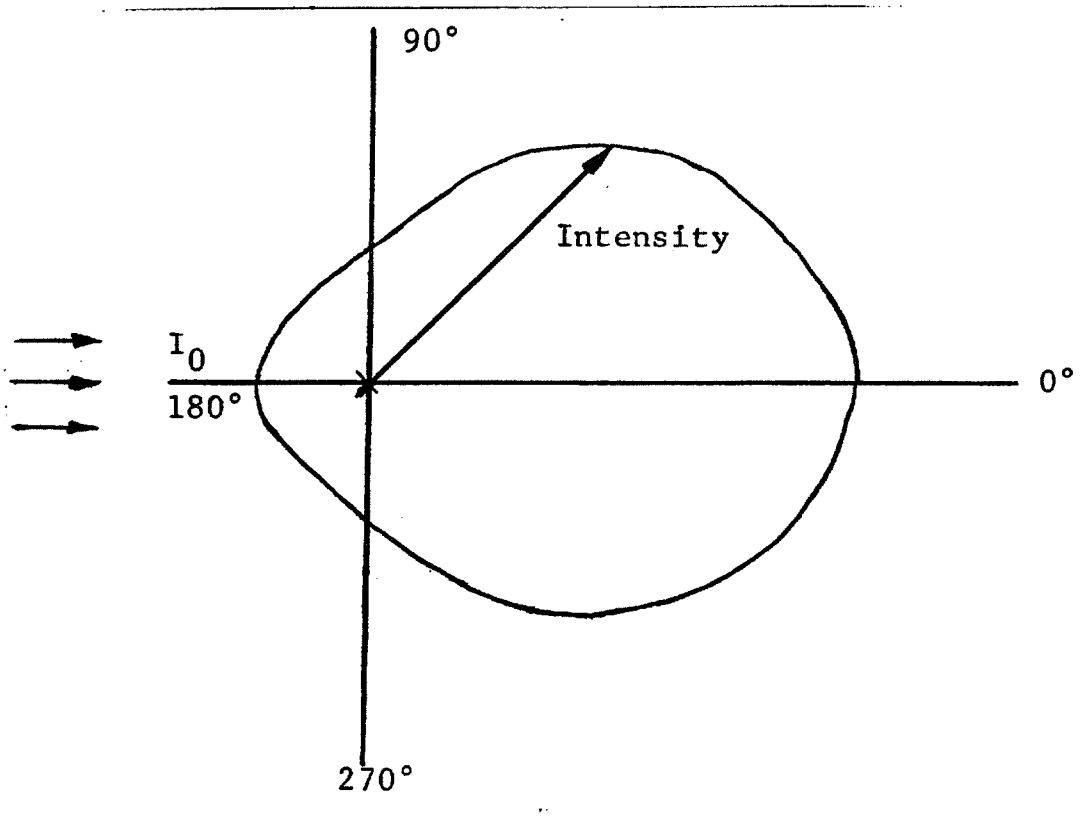

Figure 10 Typical Mie Angular Function

Here,

α is the molecular polarizabilities (cm^3),

θ is the scattering angle (deg),

λ is the wavelength (cm),

N is the number density in the volume (cm^{-3}),

I_o is the incident flux density ($watts/cm^2$), and

$d\ell$ is the length of the volume along the line-of-sight, (cm).

The path brightness is simply

$$\int_P dB = \left(\frac{2\pi}{\lambda}\right)^4 |\alpha|^2 \left(\frac{1 + \cos^2\theta}{2}\right) I_o \int_P N(\ell)\, d\ell,$$

where the integral is over the path. The resulting irradiance at the collecting surface of an optical system is, thus,

$$I = \omega \int_P dB = \left(\frac{2\pi}{\lambda}\right)^4 |\alpha|^2 \left(\frac{1 + \cos^2\theta}{2}\right) \omega I_o \int_P N(\ell)\, d\ell$$

where ω is the solid angle of collection. The number density will be a function of the path although, excluding CAT effects, we can assume that it depends only the elevation angle and, because of spherical symmetry, not on azimuth.

The number density, as a function of altitude, can be approximated by an exponential dependence of the form (Valley 1965).

$$N(h) = N_o e^{-h/H},$$

where N_o is the sea-level density and H is the scale height. In terms of the number density at some altitude h_o this can be written

$$N(h) = N(h_o) \exp -(h-h_o/H).$$

In general, the relation between h and ℓ involves the path-elevation angle, and the path integral may be difficult to evaluate. The detection of CAT will have to be accomplished with a near-horizontal path. Figure 11 illustrates the geometry of a horizontal path for which

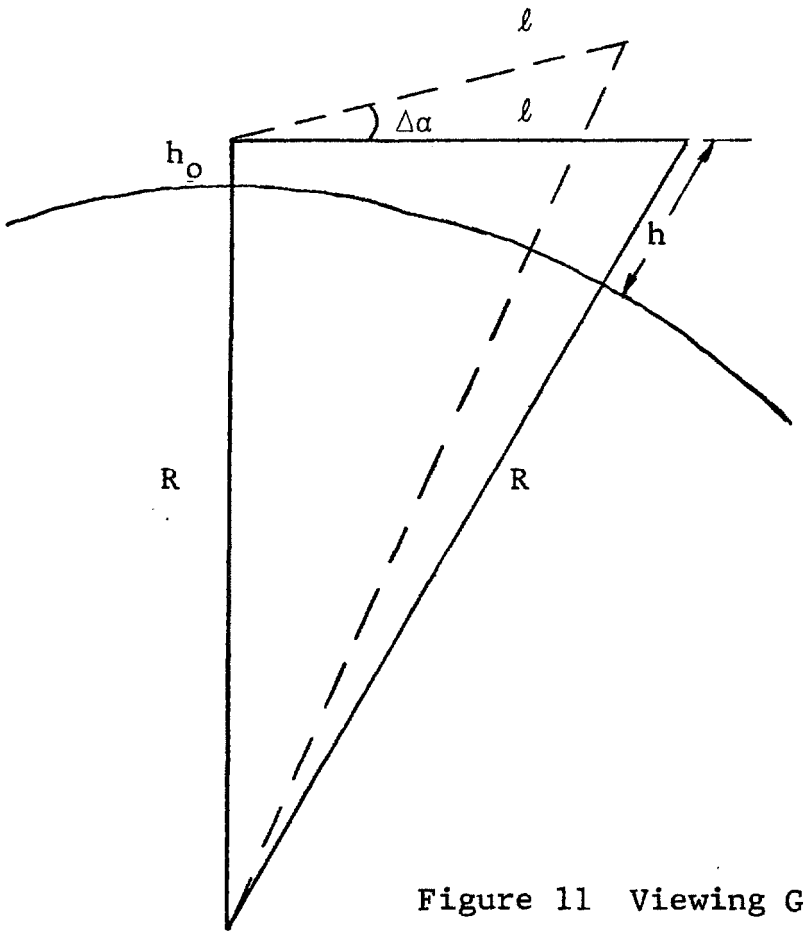

Figure 11 Viewing Geometry

$$\ell^2 = (h - h_o)(2R + h + h_o)$$

where R is the radius of the earth ($\approx$6370 km). Neglecting $h + h_o$ relative to 2R and rewriting, we have

$$h - h_o = \frac{\ell^2}{2R} .$$

Substitution into the density equation then gives

$$N(h) = N(h_o) \exp(-\ell^2/2RH)$$

The irradiance then becomes

$$I = A(1 + \cos^2\theta) \int_o^w N(h_o) \exp(-\ell^2/2RH)\, d\ell .$$

After a simple integration, we obtain

$$I = A\ (1 + \cos^2\theta)\ N(h_o)(\pi RH/2)^{1/2}.$$

For viewing along the local horizontal, the scattering angle θ is related to the azimuth angle ψ relative to the sun and the solar elevation angle φ by

$$\cos\ \theta = \cos\ \varphi\ \cos\ \psi.$$

The spatial brightness distribution in the horizontal plane is thus determined by the intersection of the plane and the surface of revolution generated by rotation of the cross section in Figure 9 about its long axis.

3.1.4 Aerosol Scattering. Small particles up to sizes of ~0.03 μ can be treated according to the theory of molecular scattering. Diffraction effects become important for larger particles, and Maxwell's equations then need to be solved for the individual case. Exact solutions can be found only for simple geometric surfaces: Approximate solutions must be accepted for more complicated boundaries of discontinuity. A number of excellent reviews are available so that we will indicate only briefly the formulation and the difficulties in applying even approximations to atmospheric aerosol scattering. We will then describe some of the experimental results that are available.

The case of isotropic spheres of radius r is the simplest and was solved by Mie (1908). An incident-plane monochromatic wave falls on the sphere. At a distance large compared to the particle radius (far field) the intensity is given as

$$I = I_o\ f\ (\lambda, r, n, \theta),$$

where

I_o is the incident intensity,

λ is the wavelength,

r is the sphere radius,

n is the index of refraction relative to the dispersion medium, and

θ is the scattering angle.

For incident unpolarized light, the intensity at an angle θ and a distance d from the particle can be written as

$$I(\theta,n) = I_1 2k^2 d^2 \left[i_1(\alpha,n,\theta) + i_2(\alpha,n,\theta) \right].$$

Here, $\alpha = 2\pi r/\lambda$, $k = 2\pi/\lambda$. Alpha is called the size parameter. The angular scattering coefficient is

$$i_\theta = (2\pi k^2)^{-k} (i_1 + i_2),$$

where the parametric dependencies have been dropped. We can interpret i_θ as the flux scattered by one particle per unit solid angle in the direction θ for unit flux incident on the geometric particle cross section. For computations of atmospheric scattering, the angular-volume scattering coefficient given by

$$\beta_\theta = \pi r^2 N i_\theta = \frac{N}{2k^2} (i_1 + i_2)$$

is more helpful. Here, β_θ is the ratio of the flux scattered by a unit volume of homogeneous aerosol, with number density N into unit solid angle in direction θ, to the flux incident on the unit cross section of this volume.

The atmosphere contains different size particles so that i_θ must be expressed as an integral over the size distribution. In addition, the particles are not all spherical, thus necessitating further approximations and complex numerical evaluations. The complexity of this procedure can be seen in the review by Bullrich (1964).

The intensity functions i_1 and i_2 are the sums of the partial wave solutions from the diffraction theory and have the form

$$i_1 = \left| \sum_1^\infty \frac{2n+1}{n(n+1)} (a_n \pi_n + b_n \tau_n) \right|^2$$

$$i_2 = \left| \sum_1^\infty \frac{2n+1}{n(n+1)} (a_n \tau_n + b_n \pi_n) \right|^2 .$$

The coefficients a_n and b_n depend on the size parameter and the refractive index n, and can be obtained in terms of spherical Bessel functions. The angle-dependent functions π_n

and τ_n are first and second derivatives of Legendre polynomials of order n and argument cos θ. The detailed relations are discussed by Van de Hulst (1957) and Bullrich (1964), among others.

It is clear that any attempt to include a reasonably accurate description of particulate scattering at aircraft altitudes would involve a large computational effort. In addition, it is uncertain that the results would be sufficiently meaningful when atmospheric variability is considered. We will, therefore, use experimental results to develop a description of expected scattered intensities.

3.1.5 Measurements on Scattering. In the selection of a suitable detection system it is necessary to know the mean signal expected, as well as the variations of the mean signal with time. We have pointed out that the total coefficients for molecular and aerosol scattering are roughly the same at altitudes of ~10 km. The angular scattering function for particle scattering is, however, heavily peaked in the forward lobe so that aerosol scattering must certainly be considered in the analysis for certain cases. The difficulties encountered in applying the theory of large-particle scattering can be seen from the preceding brief discussion. We can benefit much more by considering some of the data obtained from airborne measurements.

A comprehensive series of measurements was made by Clark (1964). In these flights, sky brightness and polarization were measured at altitudes from 6 to 21 km. Clark also measured the spectral distribution but the data were not reduced. The brightness is given in photometric units so that it cannot be used in absolute terms. The spatial distribution is quite important, however, and the graphs given by Clark are quite illustrative. Figure 11 is a typical isolume presentation in an almucantor coordinate system. Any two-dimensional representation of the spherical coordinate system raises problems of interpretation. In the chosen graphical approach, the isolume curves have to be compared to curves representing the intersection of a surface defined by the scattering angles, and the surface described by the angular scattering functions. In a molecular atmosphere, the observed scattering will be symmetrical about 90° and 180° scattering angles. That reasonable symmetry around the 180° direction exists can be seen. Symmetry around 90° is also present, but the influence of forward scattering from particles becomes large in the quadrant centered on the sun. Figure 12 illustrates this behavior quite well. With the sun at the horizon, the shape of the isolume curves is that expected for a molecular atmosphere with the Mie forward lobe added to increase the forward- to back-scattered ratio to 10:1. Figure 13 is for 50,000 ft.

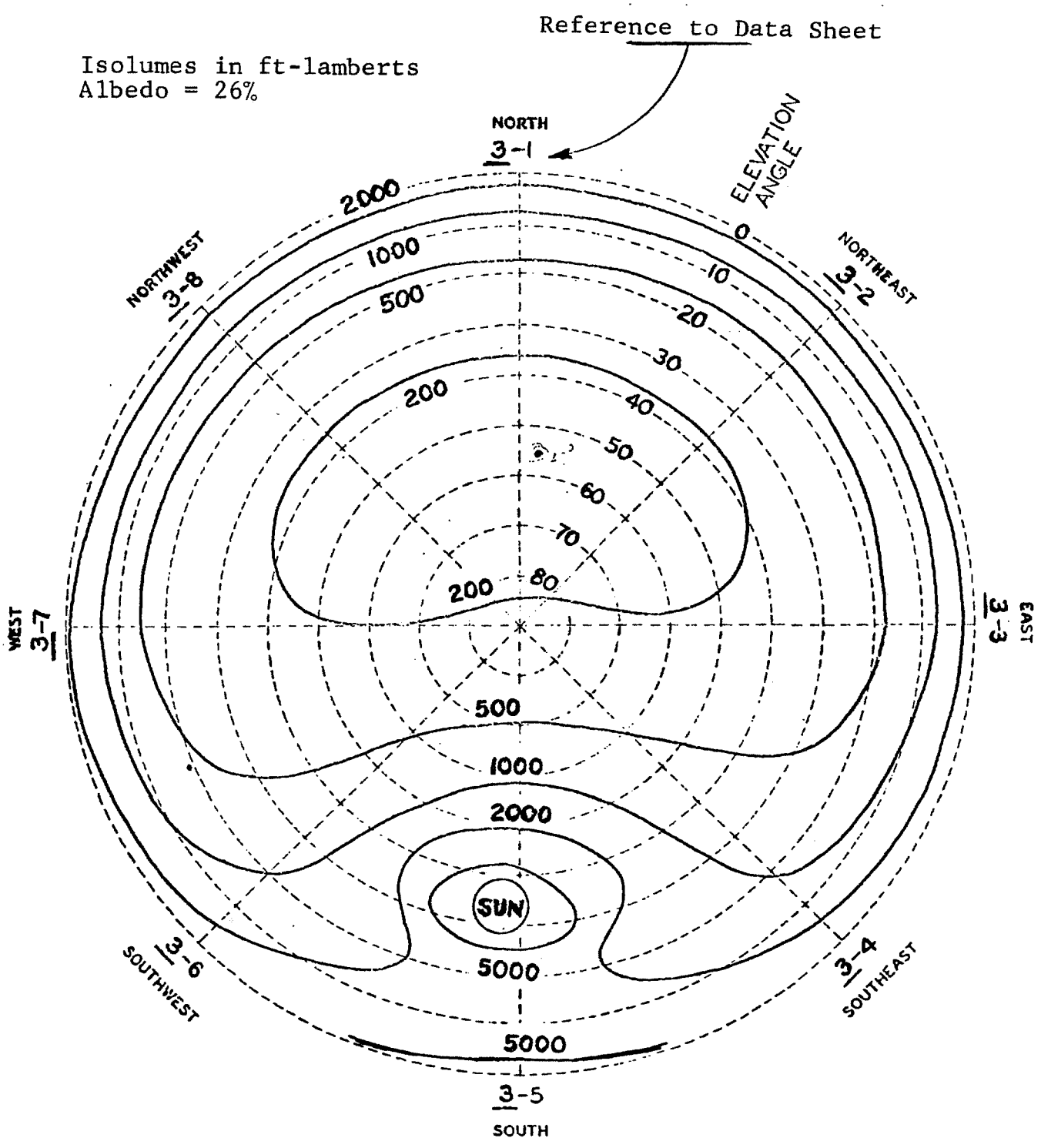

Figure 12 Isolume Plot Showing Brightness of Sky at 30,000-ft Altitude (Flight Number 1-23-64-1)

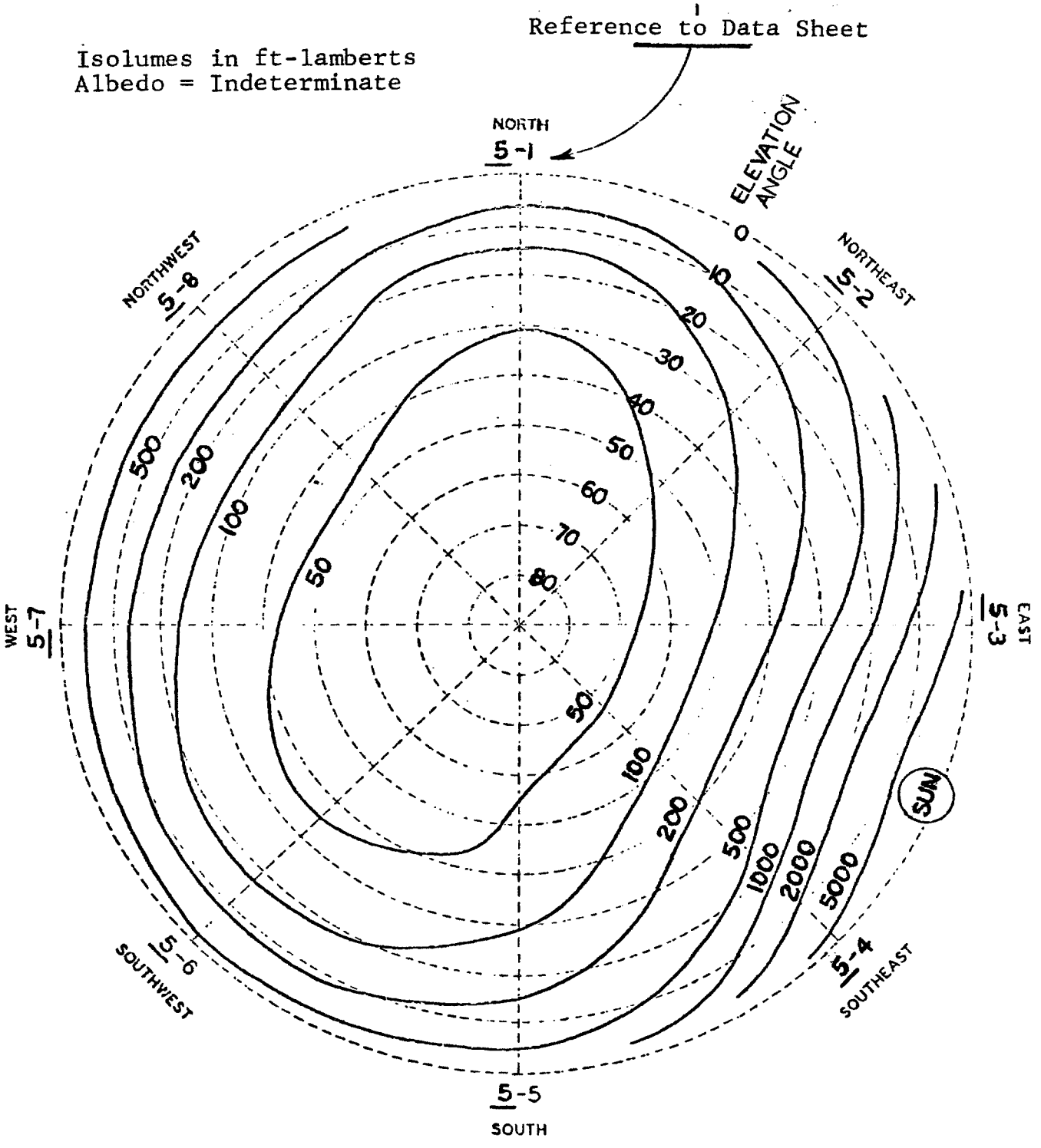

Figure 13 Isolume Plot Showing Brightness of Sky at 50,000-ft Altitude (Flight Number 1-23-64)

At 30,000 ft the effect of aerosol scattering appears to be somewhat stronger and the departures from Rayleigh symmetry are more pronounced. Figure 14 illustrates this point.

We are concerned mainly with the brightness near the horizon. On the basis of Clark's measurements, we can expect a variation of two to three in going from a 180° azimuth relative to the sun, to a zero relative azimuth in most cases. Only when the sun is near the horizon is the ratio of forward- to back-scattered radiation larger, reaching values near 10. In this low-sun-angle situation, the glare correction for Clark's instrument becomes very large, approaching the measured brightness at times. A question, therefore, exists about the reliability of the data at low-scattering angles. Restricting the line-of-sight to angles of more than ~15° from the sun will keep the brightness changes to no more than a factor of five.

3.1.6 Signal Fluctuations Due to Angular Changes. The measurement of fluctuations in scattered light can be influenced by, among other things, changes in the line-of-sight of the photometer. Because of the proportionality of the measured intensity and the total number of scatters in the field, tilting the optical axis from the horizontal will introduce changes in the detected signal at the frequency of the angular changes. The reasonable assumption that any pitching of the aircraft gives rise to much lower frequencies in the signal than are achieved by scanning the volume ahead of the aircraft allows electronic suppression of aircraft-induced fluctuations.

Consider the geometry of Figure 11. The normal line-of-sight is taken along the local horizontal and the line-of-sight after an angular change is shown, at some angle $\Delta\alpha$ to the horizontal. Admittedly, one should consider both Rayleigh and Mie scattering; at the altitudes we are considering, however, molecular scattering normally precominates (except at small scattering angles), and the mathematical treatment using only molecular scattering is quite simple.

The range ℓ to any elemental volume at altitude h is given by

$$\ell^2 = (h - h_o)(2R + h + h_o),$$

where h_o is the altitude of the aircraft and R is the radius of the earth. Since R = 6370 km $\gg$ h or h_o, we have

$$\ell^2 \simeq (113)^2(h - h_o) \text{ km}.$$

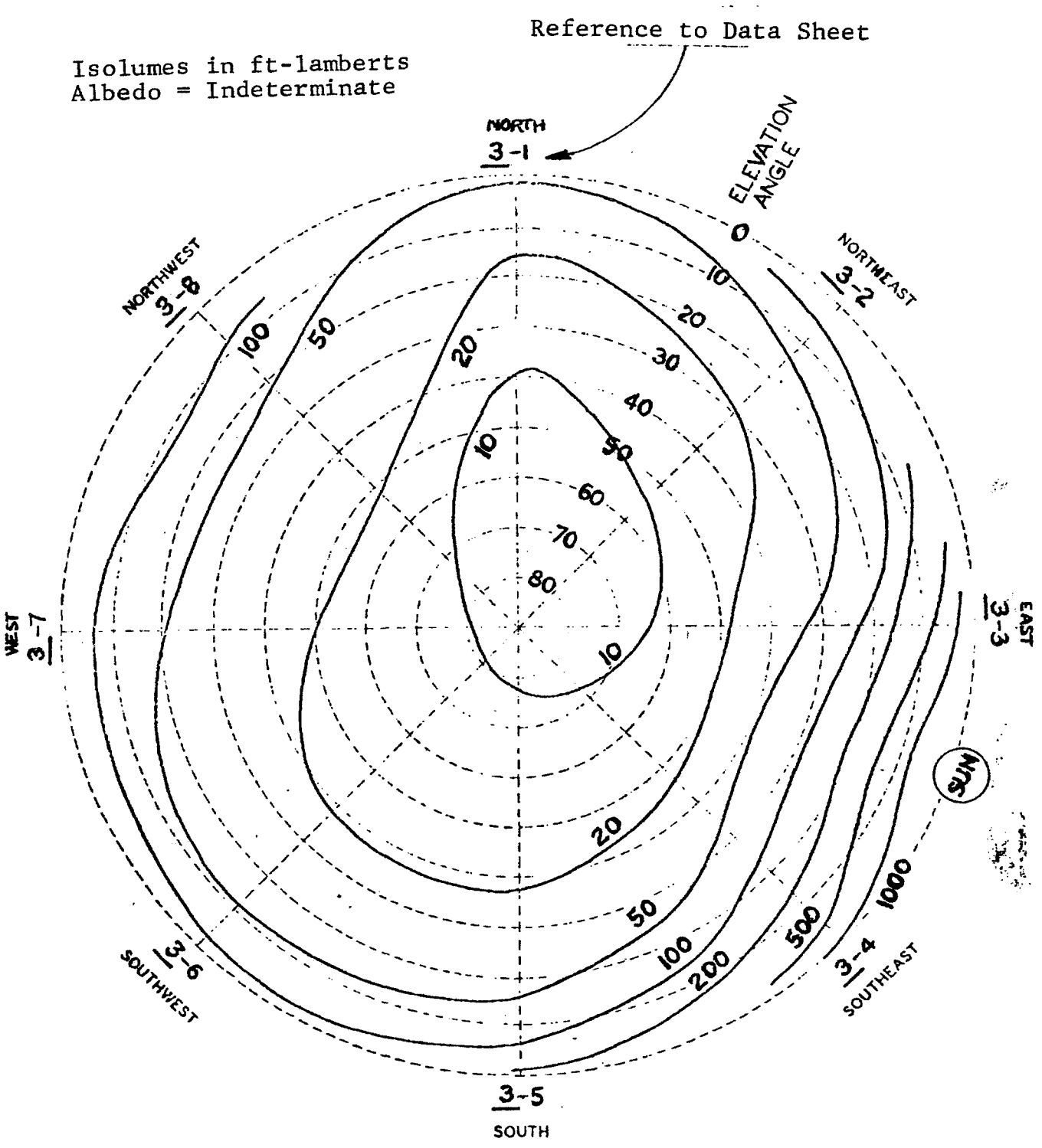

Figure 14 Isolume Plot Showing Brightness of Sky at 30,000-ft Altitude (Flight Number 1-23-64-1)

For small angular change $\Delta\alpha$, we have

$$\Delta h = \ell \Delta\alpha .$$

This approximation is good to 0.5 percent at $\Delta\alpha = 1$ degree. We will assume the same density distribution,

$$N(h) = N_o \exp(-h/H),$$

for the atmosphere used previously (Valley, 1965), where N_o is the number density at sea level and H is the scale height at altitude h. Because of the angular change, each elemental volume will have a number density differing from the horizontal path. The difference is given by

$$\Delta N(h) = -N \frac{\Delta h}{H}$$

$$\Delta N(\ell) = -N \frac{\ell}{H} \Delta\alpha .$$

The difference in the signal will, therefore, be proportional to

$$\int_o^\infty \Delta N(\ell) d\ell = - \int_o^\infty N(\ell) \frac{\ell}{H} \Delta\alpha \, d\ell .$$

In terms of the number density at altitude $h_o(\ell = 0)$, we have

$$\int_o^\infty \frac{\Delta N(\ell)}{N(0)} d\ell = - \frac{\Delta\alpha}{H} \int_o^\infty \ell \frac{N(\ell)}{N(0)} d\ell .$$

The fractional change in signal, after substitution for $(h - h_o)$, is

$$\frac{\int_o^\infty \Delta N(\ell) d\ell}{\int_o^\infty N(\ell) d\ell} = \frac{\frac{-\Delta\alpha}{H} \int_o^\infty \ell \exp(-a\ell^2) d\ell}{\int_o^\infty \exp(-a\ell^2) d\ell} ,$$

where $a = (2RH)^{-1}$.

After integration, we have

$$\frac{\Delta S}{S} = \frac{-\Delta\alpha}{H} \frac{1}{2a} \frac{2\sqrt{a}}{\sqrt{\pi}} = -\Delta\alpha \sqrt{\frac{2R}{H}} .$$

With R = 6370 km and H = 8 km, we have

$$\frac{\Delta S}{S} = -22.6\ \Delta\alpha .$$

For a one-degree angle change ($\Delta\alpha = 1.745 \times 10^{-2}$ rad),

$$\frac{\Delta S}{S} = 0.39.$$

This result is consistent with Figures 12, 13, and 14. Therefore, if we require fluctuations because of changes in the line-of-sight of the photometer to be less than 1/10 percent, it would be necessary to mount the photometer on a stabilized platform good to 10 arc-seconds. In fact, if, as mentioned, a horizontal scan is used, then with electronic discrimination against the low frequencies associated with the piloting of the aircraft, the platform stability requirements may be reduced considerably.

3.1.7 Absolute Intensity Levels. Only molecular scattering has been considered in the S/N calculations given in previous sections of this report. From this treatment we obtain, for sky brightness,

$$B = \left(\frac{2\pi}{\lambda}\right)^4 |\alpha|^2 \left(\frac{1 + \cos^2\theta}{2}\right) i_o\, N(h_o) \left[\frac{\pi RH}{2}\right]^{1/2} .$$

Evaluation of this equation for

$\lambda = 5000A$

$\alpha = 3 \times 10^{-24} cm^3$

$\theta = 90°$

$I_o = 5 \times 10^{-3}$ watts/cm^2

$N(h_o) = 8.6 \times 10^{18} cm^{-3}$

$R = 6370$ km

$H = 8$ km

gives

$$B \approx 1.5 \times 10^{-6} \frac{\text{watt}}{\text{cm}^2 \text{ sterad A}} .$$

Extrapolation of Lloyd's data (Lloyd, et al., 1965) from a rocket flight gives, for the zenith brightness at the same altitude,

$$B \approx 5 \times 10^{-8} \frac{\text{watt}}{\text{cm}^2 \text{ sterad A}} .$$

For a molecular atmosphere, the ratio of horizon to zenith brightness is about 70, so that

$$B \approx 3.5 \times 10^{-6} \frac{\text{watt}}{\text{cm}^2 \text{ sterad A}} .$$

In view of the influence of particulate scattering, the areeement is quite good.

Sandomirskii, et al., (1964) have reported on their high-altitude measurements in some detail. Even though their reported work was performed at only one zenith angle (60°), comparison of their absolute brightness values with the given values is a good check. At an altitude of 10 km they find a brightness

$$B \approx 8 \times 10^{-8} \frac{\text{watt}}{\text{cm}^2 \text{ sterad A}}$$

for a zenith angle of 60° and a scattering angle of 90°. From Clark (1964), the ratio of horizon to 30° elevation is ~10 so that a horizon brightness of

$$B_h \approx 1 \times 10^{-6} \frac{\text{watt}}{\text{cm}^2 \text{ sterad A}}$$

can be inferred from the results of Sandomirskii. A number of other measurements exist. Hughes (1964) has shown that there is quite reasonable agreement among the various measurements.

Variations in the mean sky brightness due to scattering angle and aerosol content have been discussed qualitatively. Sandomirskii, et al., (1964) measured the seasonal variation of the sky brightness at a zenith angle of 60° and a scattering angle of 90°. Some of their curves are reproduced as Figure 15.

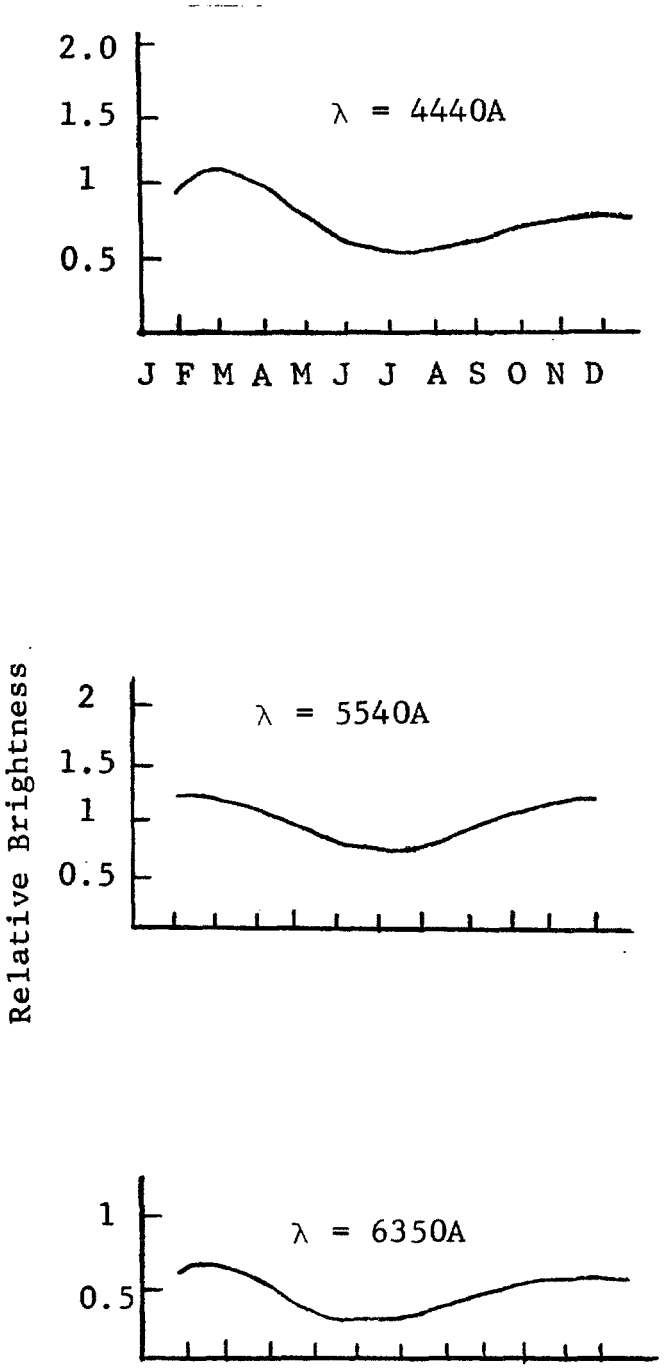

Figure 15 Seasonal Variation of Sky Brightness in 1961

The brightness varied by a factor of 1.5 in the blue and the green, and by up to 2.5 in the red end of the visible. They also found that similar variations occurred from year to year. At 10 km, the decrease in the summer is also found. These authors computed the rms day-to-day variation as ± 14.5 percent after taking the measurement error into account. On the basis of these various measurements, an assumed sky brightness at the horizon and altitude of 10 km of $\sim 2 \times 10^{-6}$ watts/cm^{2}A should be of the correct order of magnitude. Viewing angles close to the sun can give much higher values.

3.1.8 Implementation. From the preceding discussion it is clear that variations of the scattered light intensity contain information about turbulent regions ahead of the aircraft. The next step is to determine how this information can be processed and utilized. Here, we can consider a system using a single detector or one using two detectors.

A single detector combined with a two-dimensional scan will provide information on the angular extent of the disturbed volume. If we now utilize the velocity of the aircraft, in that we compare the angular extent at two times, we can use the relation between range and angle subtended by the turbulent area, $\alpha = L/r$. The change in the angular extent is, therefore, given by $\Delta\alpha/\alpha = -\Delta r/r$. Since all variables but r are known, we can obtain range from $r = V\Delta t(\alpha/\Delta\alpha)$, where $V\Delta t$ is the distance traversed by the aircraft toward the turbulent area.

It is apparent, however, that the uncertainty in the distance to the turbulent region is large, since r is the distance to the largest cross section orthogonal to the flight direction. Because of the large horizontal extent (scale) of the turbulent region (Endlich and Mancusco 1964), a large uncertainty about the distance to the onset of turbulence will exist. The approach would, therefore, seem inappropriate at close range (e.g., 20 miles), but looks promising at large distances (e.g., 100 miles). In such a long-range detection scheme, it will be important to ensure that the turbulence is located along the intended flight path. This need arises because of the generally small vertical extent of atmospheric turbulence.

Instead of relying on angular changes in cross section as a means of identification, we can take advantage of one particular characteristic of CAT, i.e., CAT generally extends over 10 - 60 km horizontally. At large distances, individual small eddies will not be resolved since they are smaller than the instantaneous field-of-view. As the aircraft approaches the turbulent volume, successively smaller eddies will be resolved. Since eddies of all sizes are present (Burns and

Rider 1965), the angular subtense of the smallest resolved detail will not change in time. Another way of looking at this is in terms of spatial frequency. Because of the continuity in eddy size, the highest frequency contained is determined by the angular field of the detector optics system and will, therefore, be fixed (this assumes that the time scale of changes in the turbulence is much greater than those of the detector scan). Nonturbulent regions having density gradients (associated with jet streams or front, for example) will not have this continuity of scales and the signal frequencies will not have this behavior.

The two detector correlation techniques are illustrated in Figure 16. One detecting system is mounted in each wing tip of the aircraft, the wing span of which has been taken to be 30 m. If the fields-of-view of these detecting systems are approximately 2 milliradians and are orientated as shown, then a portion of the atmosphere ahead of the aircraft will be common to both beams. If the covariance is measured between the two detector signals, then fluctuations which are uncorrelated between the two signals can be eliminated. The correlated fluctuations must come from a region surrounding the volume of intersection of the two detector fields-of-view. Expressing this mathematically; if the two detector signals are given by $I_1(t)$ and $I_2(t)$, then each can be considered to be made up of a mean level and fluctuating component. Hence,

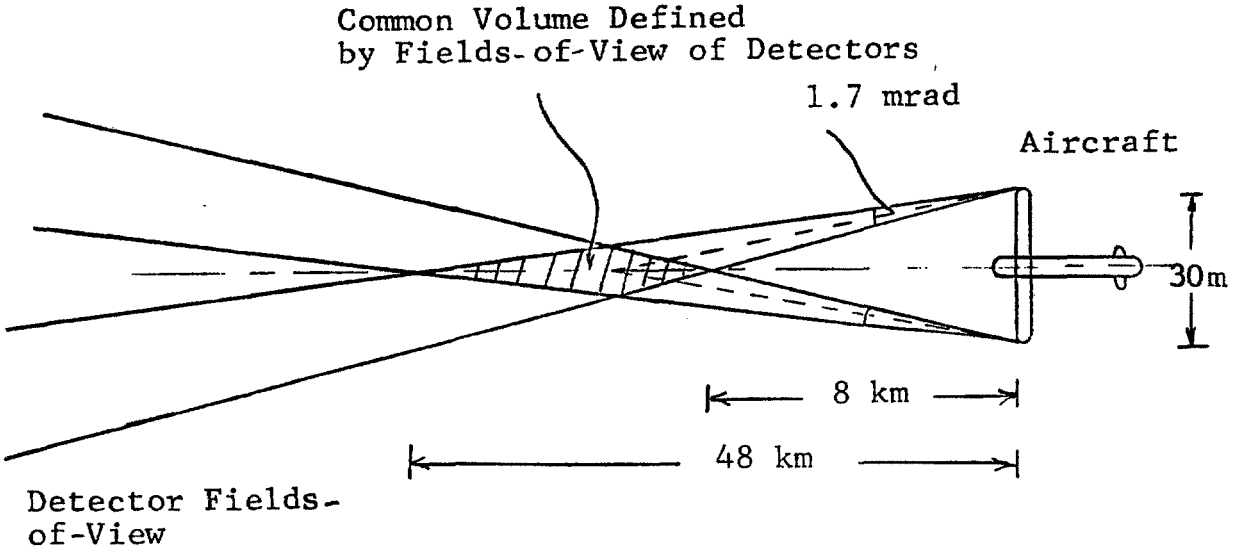

Figure 16 Illustration of Cross-Correlation Technique Applied to Detector of CAT

$$I_1(t) = \overline{I_1(t)} + i_1(t).$$

Then the cross-correlation between the two signals will be given by

$$G = \frac{\overline{i_1(t)i_2(t)}}{\sqrt{i_1^2(t)\ i_2^{\ 2}(t)}}\ .$$

If the signals received by the two detectors are uncorrelated, then G will be zero. Any finite value of G will be related to both the magnitude and scale of the fluctuations common to both detectors.

As the system has been described, the fluctuations would be of inconveniently low frequency. This deficiency can be overcome by having the detectors scan together in a horizontal plane, as illustrated in Figure 17. If the oscillating scan

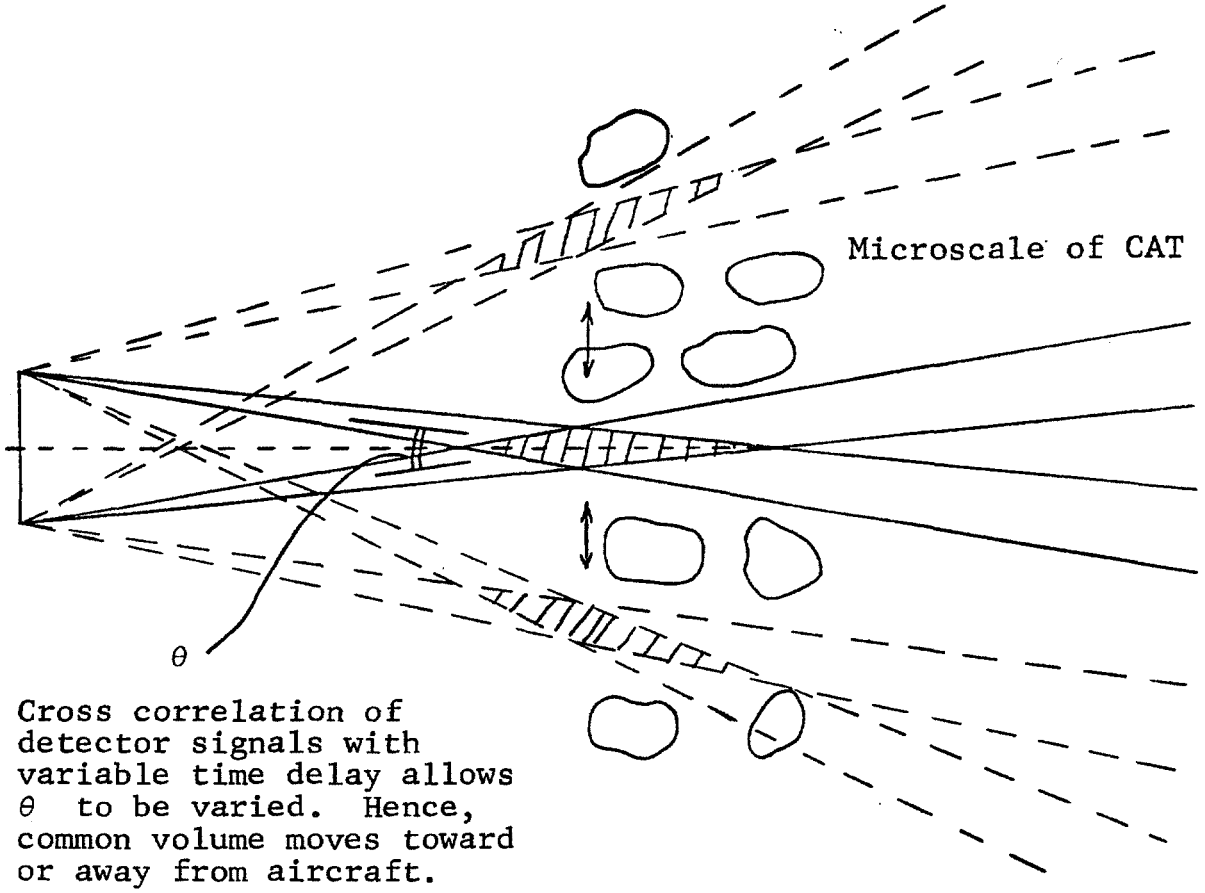

Figure 17 Horizontal Scanning of Detectors (not to scale)

rate is high relative to changes in turbulence pattern, then, by introducing a time delay between the two detector signals before cross-correlating, the portion of the atmosphere seen by both detectors can effectively be made to move toward or away from the aircraft (Figure 16). Successful application of this technique assumes that the angular flexing of the wings of the aircraft will not "uncross" the fields-of-view of the two detector systems, and elimination by electronic filtering of frequencies associated with the scanning would be necessary.

Letters requesting information on the differential angular flexing of aircraft wings were written to Boeing and Douglas Aircraft Companies, but apparently this information is not available. Both companies were able to give us information about the change in angle-of-attack of the wing tips relative to the rest of the wing for different flight and fuel conditions, but only differential twists between the two wing tips will affect the operation of the crossed-beam system. However, since the wing-tip twists range over several degrees, it is highly probable that differential wing twists will be produced, which exceed the field-of-view of the detector systems that is limited, for the crossed-beam system, to ~7 arc-minutes. In fact, we would require the differential twisting not to exceed ~1 arc-minute for satisfactory application of the technique.

The alternative is, of course, to mount the two detector systems on inertial platforms. A comparatively low-frequency response, ~10 cps, is required, and such platforms are available. This would, of course, very much complicate the system, and before further considering the crossed-beam system, it is desirable to see experimentally what a single system will accomplish.

Although not directly related to CAT, IITRI has a contract with NASA-Marshall Space Flight Center to measure wind shears above rocket launch sites. A cross-correlation technique is to be employed and fluctuations in scattered sunlight will be measured. This contract will give some information as to the general feasibility of applying such techniques to the measurement of atmospheric turbulence. Consideration should be given to the application of this same technique at some high-altitude site near to regions where CAT is known to be a frequent occurrence.

Alternatively, much information could be gained by instrumenting an aircraft with a single detector system and measuring both mean levels and fluctuations. A possible problem would be fluctuations introduced by oscillation of field-of-view in a vertical plane, but horizontal scanning of the system could be used to increase the frequencies of the fluctuations caused by CAT, and thereby discriminate against these other effects.

3.1.9 Evaluation. The most obvious drawback of the scattering technique is that its use is restricted to the daytime. Nighttime illumination, even with a full moon, in impractical. This can be seen in the equation for S/N ratio; decreasing the irradiance H_o by four orders magnitude results in a ratio substantially less than one. To improve this, a radical change in the collection system parameters would be necessary. Integration over longer periods could also be employed, but at the cost of much slower response of the system (since the improvement is proportional to the square root of integration time). It is appropriate to point out that the photomultipliers available have such low dark-noise figures that, even in this case, the limiting noise is shot noise due to the scattered-light intensity.

Extensive cloud cover along the line-of-sight can be expected to render the single detector method useless while restricting the information obtainable with the correlation system. The extent of this restriction will, of course, depend on the amount of cloud coverage, the location, and the effect of large uncorrelated fluctuations on measuring smaller correlated fluctuations. Above 20,000 ft, clouds are encountered approximately 13 percent of the time; above 25,000 ft, 7 percent; and above 30,000 ft only 2 percent of the time (Handbook of Geophysics, 1961). Isolated clouds are much less of a problem than extensive cloud cover. Even though a cloud may be indicated as turbulence, the pilot should, in most cases, be able to identify the presence of the cloud.

In any turbulence-detection scheme, one would like to obtain not only the location but also the intensity of the turbulence. If we make the assumption that the intensity of turbulence is reflected in the magnitude of the temperature fluctuations, then the desired information is contained in the signal fluctuations. This information cannot be extracted directly, however, unless both the length of the turbulent region along the line-of-sight of the detector and the spectrum of eddy sizes is known. If future extensive experimental measurements of CAT (such as Project HICAT) indicate that the turbulence spectrum does not vary widely, then some estimate of the intensity of the turbulence can be made. Since there is a square-root relationship between the

amplitude of the fluctuations and the extent of the turbulent region, taking a figure of, for example, 20 miles for the latter would not lead to very large errors.

The single-detector system will be affected by fluctuations in the electronics, and any contemplated instrument would have to be designed with this in mind. Since uncorrelated fluctuations of this nature will not affect the correlation technique, it would only be necessary to ensure isolation of the two systems.

The correlation technique is based on the assumption that only the portion of the signals originating in the common volume is correlated and that all other signal components are uncorrelated. One can easily see that it is possible for both beams to be affected by a large eddy, which is not in the common volume. This can give rise to a correlation for the common volume, thus, indicating turbulence at a distance where turbulence does not necessarily exist. If this "disturbing" eddy is close to the aircraft, turbulence could be indicated for the entire region behind the eddy. If this "disturbing" eddy is farther from the aircraft than the common volume, then turbulence would be indicated for some ranges, depending on the scale of correlation. These scales in the latter case would have to be very large to give a significant correlation, since the included volume would be very large at distances beyond the common volume.

The basic soundness of turbulence detection using the fluctuations in Rayleigh scattered sunlight has been established (Montgomery, 1968). The possible problems associated with extracting usable information are described with the result that we can see that the technique appears feasible except, of course, at night or with extensive cloudiness along the line-of-sight. The concept of "obscuring eddy" has been discussed, since this could be the limiting factor in using any correlation method.

The effectiveness of correlation in extensive volumes of very large eddies cannot be determined, since available data are rather scarce. Hopefully, this lack will be eliminated with future measurements.

3.2 Absorption-Line Shape Method

A filter that passes a very narrow spectral region on the edge of an absorption line may be used to distinguish between radiation originating above the horizon and that originating at or below the horizon in denser air. This method suggested in the Contract Work Statement is illustrated in Figure 18. Since the absorption line is

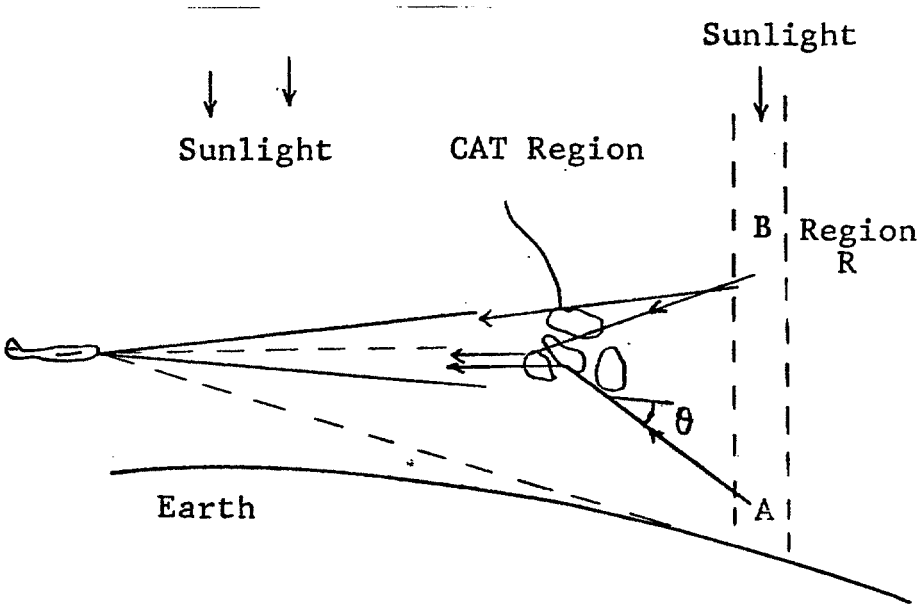

(a) Pictorial Presentation of Method

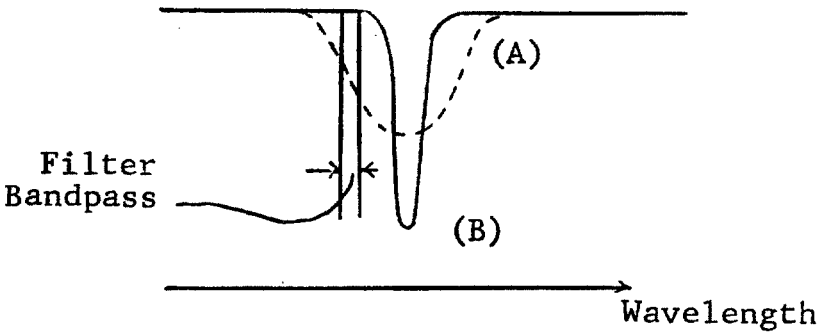

(b) Absorption Lines

Figure 18 Near-Infrared Line-Shape Modification

required, the wavelength would probably be in the near-infrared, and one of the lines in carbon dioxide or water vapor bands might be considered. Radiation scattered out of region R could reach the detector both directly and after refraction in the CAT region. The radiation originating near or below the horizon would have been partially absorbed in the air in the denser regions of the atmosphere and the shape of the absorption line might be as shown on Curve A of Figure 18. Light originating from B would have been partially absorbed in air at low pressures and temperatures (smaller optical depth) and the absorption line would be narrower for scattering and absorption. In addition, radiation from region A would have to pass through the denser regions (relative to region B radiation) of the atmosphere, to reach the detector. This would further broaden the absorption line for radiation from A as compared with B. The source A and B at short infrared wavelengths is assumed to be a result of scattering or fluorescence.

These effects in absorption, together with refraction in the region of clear air turbulence, do not appear to permit an image of the CAT region to be obtained, however. With the filter bandpass as shown, relatively less light from the region A will reach the detecting system than if the absorption-line effects were absent. The arrangement would appear to be more appropriate if applied to broad- and narrow-emission lines instead of absorption lines. In this case, there would be no radiation from high altitudes that would be detected with the filter bandpass setting as shown, and the radiation detected would have to originate from A and be scattered into the field-of-view of the detector by refraction or scattering effects.

Using the formulation of Munick (1965), we find the ratio of turbulent to Rayleigh (molecular) scattering to be

$$R \leq AN \frac{C_T^2}{T^2} \left[\frac{(4\pi)}{\lambda} \sin \theta/2 \right]^{11/3}$$

and we can obtain an estimate of the range of angles for which turbulent and Rayleigh scattering are of the same order. Here

A is a constant,

N is the molecular number density,

C_T is the temperature structure constant associated with the turbulence, and

T is the temperature.

With the values

$$A = 2.6\pi$$

$$N = 8.6 \times 10^{18}\ \text{cm}^{-3}\ \text{(10-km altitude)}$$

$$C_T = 4 \times 10^{-2}\ \text{cm}^{-2/3}\ \text{deg}^2$$

$$T = 220°\text{K}$$

$$\lambda \approx 1\mu,$$

we get R of the order of one for $\theta \approx 5°$. Thus, for angles less than 5°, scattering due to refractive-index inhomogenities will exceed Rayleigh scattering. The rms angle through which light rays passing through the turbulent region are refracted will, on the basis of work reported by Tatarski, be less than a few minutes of arc, however. Therefore, radiation reaching the detector after refraction in the CAT region cannot originate from near or below the horizon unless the CAT region is below the aircraft altitude and the detector system points just above the horizon. At the horizon, an angle of 5 arc-minutes corresponds to a vertical height difference of 520 m, over which there will be a very small change in absorption line shape. As pointed out, the application of the suggested technique using absorption lines is impractical because of the background radiation level and suitable emission lines are not available. In fact, if such lines were available the approach would still be very questionable and would depend on how rapidly the shape of the emission line changed with altitude. A very rapid rate of change would be necessary for the technique to have any potential application.

There is a degree of similarity between the emission line approach and another technique using the infrared schlieren-type system which is also discussed in this report. In the first, a filter is used to limit the radiation detected to that originating in the denser regions of the atmosphere, and in the second, the radiation source is thermal emission of the earth itself. In both cases the sensitivity of the technique depends on the rate of change of radiance with altitude. The absorption-line technique is so unpromising that it is not further considered.

3.3 Stellar Scintillation

The inhomogeneities of the refractive index that are due to atmospheric motions give rise to the phenomenon of scintillation. This is manifested in the twinkling of point sources, such as stars, when viewed through the intervening atmosphere.

The refractive index inhomogeneities scatter some of the radiation out of the incident beam and thus gives rise to the "shadowbands" of Keller (1955). Since atmospheric turbulence can lead to refractive-index variations we can logically consider stellar scintillation as a method for detecting CAT.

3.3.1 Scintillation Theory. A large number of papers have been published on experimental and theoretical studies on scintillation phenomena. It is important to distinguish between "seeing" and scintillation effects. Poor seeing is associated with distortion of the wavefront accepted by a telescope system or with variations in angle of the wavefront. To a first approximation, it does not matter whether the turbulent region is near or distant from the detecting system. Scintillation, on the other hand, is caused by the variation in intensity over the wave and is analogous to the so-called shadowgraph method of flow visualization used in fluid dynamics. The intensity variation over the shadow pattern, increases with distance from the turbulent zone until the point is reached when the average lateral displacement of a light ray, as a result of its passage through the turbulent region, is comparable with the scale of the turbulence itself.

In ground-based measurements, scintillation effects have been shown by Protheroe (1955) and others to result from turbulence in the region of the tropopause. The scintillation frequencies observed can be ascribed in large part to translation of a fixed shadow pattern across the telescope aperture. This motion can be correlated with wind speeds aloft, at altitudes of 10 to 12 km in the case of Protheroe's measurements.

Seeing in ground-based measurements is largely dependent upon refractive-index fluctuations in the air within a few hundred feet of the receiving telescope. This is due to the air density near the ground.

For scintillation measurements to be effective in CAT detection, the presence of a CAT region in the field-of-view of the detection system has to result in an increase in the fluctuation level or change in frequency spectrum over that normally present. Figure 19 illustrates this problem. Tatarski (1961) has shown that the log amplitude fluctuation is,

$$\sigma^2 = 2.24\, k^{7/6} \int_0^\infty C_n^2\,(x)\, x^{5/6}\, dx,$$

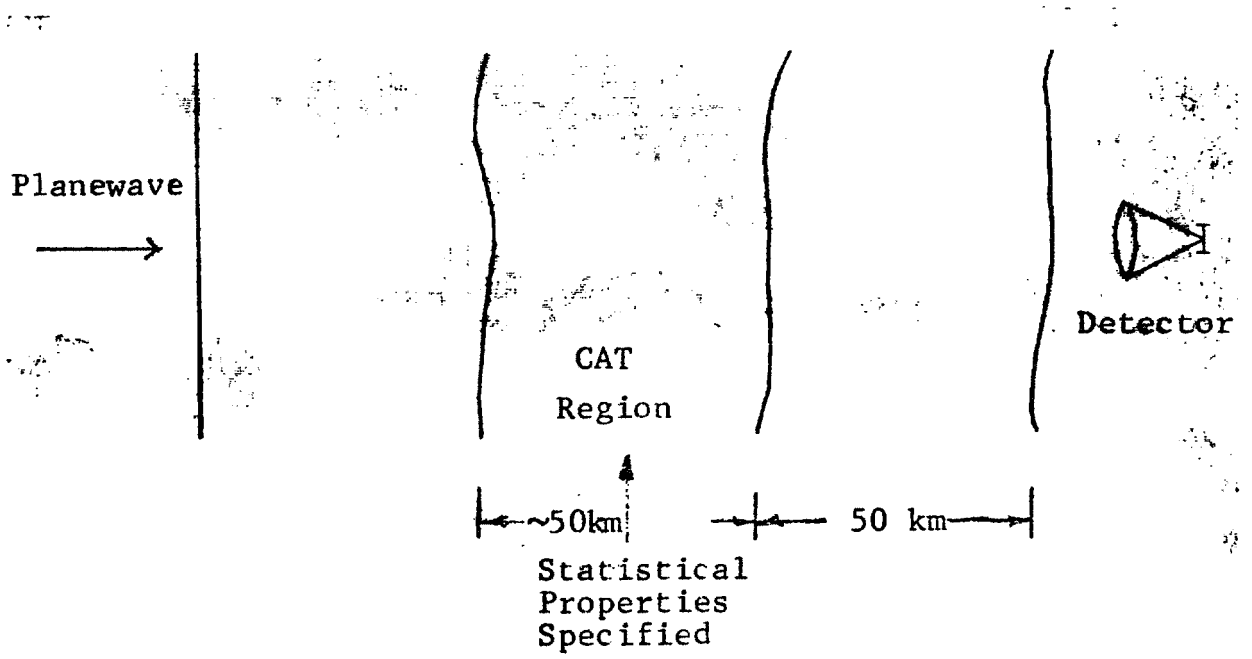

Figure 19 Illustration of Scintillation Problem

where the integration is carried out along a line directed toward the light source, in this case a star. This equation gives the mean-square fluctuation in light intensity since

$$\sigma^2 = \overline{\left(\log \frac{I}{I_o}\right)^2} \approx \frac{\overline{(I - I_o)^2}}{(I_o)^2} .$$

The intensity I_o may be set equal to $\bar{I}$, the mean intensity at the point considered; k is $2\pi/\lambda$. To obtain the mean-square fluctuation of the light flux P received by a telescope of diameter D, the averaging effect of the aperture has to be taken into account. This requires a knowledge of the correlation function in the plane of the aperture. Before considering the fluctuations in power, however, let us consider the fluctuations in amplitude for two different cases. First, we will compute the value of σ^2 which would be measured in the case of an aircraft at 10-km altitude observing a star looking horizontally through a nominally quiet atmosphere. Second, the value of σ^2 will be computed assuming a region of CAT is ahead of the aircraft extending from a distance of 5 to 100 km.

To compute σ^2 for the quiet atmosphere, the results of C_n^2 obtained by Hufnagel and Stanley (1964) will be used. These results are shown in Figure 20. To evaluate the integral

$$\int_o^\infty C_n^2(x)\, x^{5/6}\, dx,$$

the product $C_n^2(x) \cdot x^{5/6}$ has been plotted in Figure 21, and the area under this curve measured. The decrease for long ranges is due to the rapid decrease in C_n^2 with altitude as the line-of-sight to a star directly ahead of the aircraft passes through higher altitude regions. No allowance has been made for the refractive bending of light rays passing through the atmosphere, but, for the present purpose, such effects may be ignored.

To compare the magnitude of the fluctuations for the quiet atmosphere and CAT case, we will assume that a region of CAT exists, beginning 50 km ahead of the aircraft and extending for 50 km. It is assumed that $C_n^2 \sim 5 \times 10^{-15}$ cm$^{-2/3}$ throughout this CAT region. Evaluating the integral, we have:

$$\int_o^\infty C_n^2(x) x^{5/6} = \begin{array}{l|l} \text{Quiet Atmosphere} & \text{CAT} \\ 3.3 \times 10^{-4} & 1.3 \times 10^{-2}\ \text{cm}^{7/6}. \end{array}$$

The contribution to the integral by a region of CAT will, therefore, be large, and a correspondingly large increase in the fluctuating levels observed would be expected. However, computing σ^2, we have for

$$k = \frac{2\pi}{\lambda} = 1.26 \times 10^5 \quad (\lambda = 5000\text{A}),$$

$$\sigma^2 = 6.6 \times 10^2 \quad \text{Quiet Atmosphere}$$

$$= 2.5 \times 10^4 \quad \text{CAT}.$$

These levels are impossibly high although, apparently, Tatarski (1961) notes no restriction that is implicit in the method of solution of the wave equation, which is not satisfied for these cases. The method of solution of the wave equation used to give the above expression for σ^2 was originally due to Rytov (1937) and, thus, takes account of both scintillation and diffraction effects. It is not restricted to small fluctuations; however, Hufnagel and Stanley (1964)

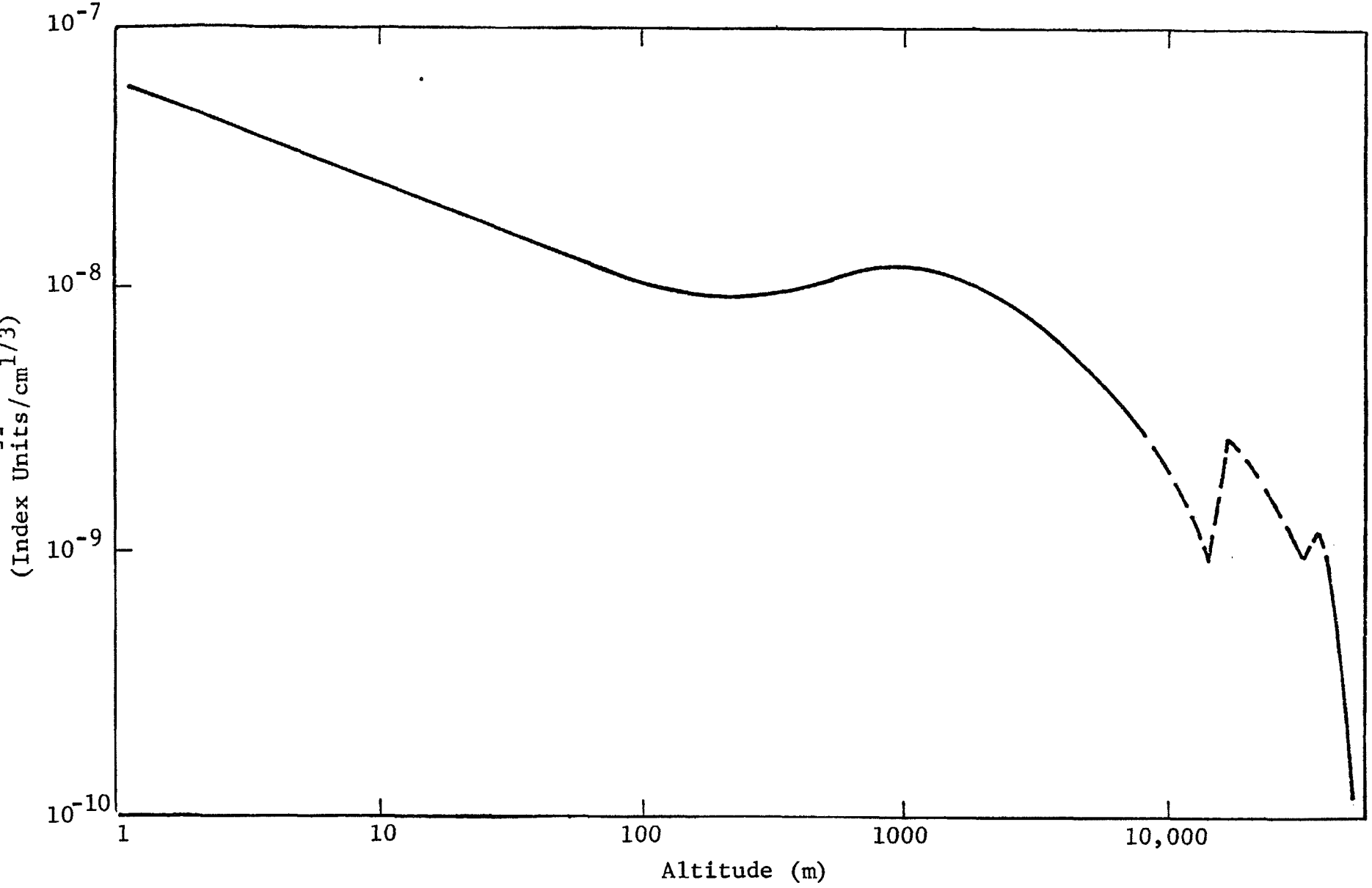

Figure 20 Index of Refraction Structure Constant as a Function of Altitude

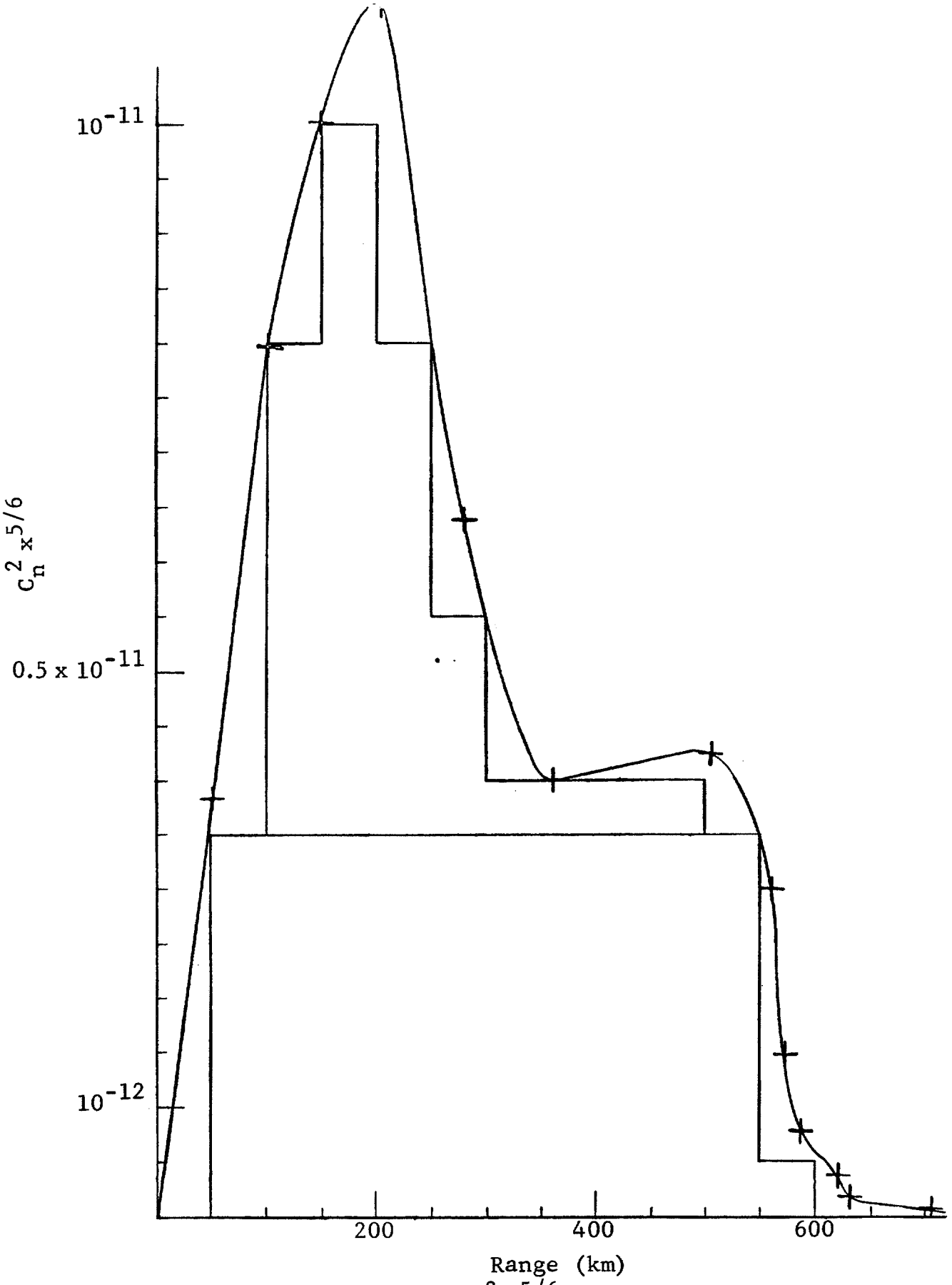

Figure 21 The Function $C_n^2 x^{5/6}$ as a Function of Range

have noted a serious drawback to this approach, which was not discussed by Rytov or by subsequent authors who used the same method. In Tatarski's notation, the wave equation may be written

$$\Delta u + k^2 n^2(\vec{r}) u = 0$$

where $u = Ae^{iS}$, A being the amplitude and S the phase of the wave. By dividing through by u, we can rewrite this equation in the form

$$\Delta\psi + (\nabla\psi)^2 + k^2 n^2(\vec{r}) = 0$$

where $\psi = \log u$. Substituting $\psi = \psi_o + \psi_1$ (ψ_o being the wave in the absence of refractive index variations, i.e., $n^2(\vec{r}) \sim 1$) we see that this equation reduces to

$$\psi_1 + \nabla\psi_1 \ (2\nabla\psi_o + \nabla\psi_1) + 2k^2 \ n_1(\vec{r}) + k^2 \ n_1^2(\vec{r}) = 0.$$

Here, $n_1(\vec{r})$ is the fluctuating part of the refractive index, $n(\vec{r}) \approx 1 + n_1(\vec{r})$; and since $n_1(\vec{r})$ is very small, the last term of the equation may be omitted, leaving,

$$\Delta\psi_1 + (\nabla\psi_1)^2 + 2\nabla\psi_o \cdot\nabla\psi_1 + 2k^2 \ n_1(\vec{r}) = 0.$$

In Rytov's solution of this equation the term $(\nabla\psi_1)^2$ is omitted since it will be small relative to the term $2\nabla\psi_o \cdot\nabla\psi_1$. However, as pointed out by Hufnagel and Stanley $(\nabla\psi_1)^2$ may typically be of the same order as $\Delta\psi_1$, thus there is no more reason for dropping one than the other. Dropping both results in the geometrical optics solution with no account taken of diffraction.

For Rytov's method of solution to be valid, we must impose the condition that

$$(\psi_1) = |(\psi - \psi_o)| = \left|\log \frac{A}{A_o} + i \ (S - S_o)\right| \ll 1.$$

This condition is slightly less restrictive than the assumption $u_1/u_o \ll 1$ used in the method of solution of the wave equation, which assumes small perturbations.

In the particular case we are considering, looking horizontally through the atmosphere at an altitude of 10 km, the results obtained using Rytov's solution both for the quiet atmosphere and with CAT present are

$$\sigma^2 = 4\overline{\left(\log \frac{A}{A_o}\right)^2} = 6.6 \times 10^2 \quad \text{Quiet Atmosphere}$$

$$= 2.5 \times 10^4 \quad \text{CAT.}$$

Thus, $\log A/A_o$ cannot be much smaller than 1 and the method of solution of the wave solution was not applicable.

This is an unfortunate conclusion since no rigorous solution of the complete wave equation exists and it points to the need of further experimental work on scintillation effects over very long paths.

Intuitively, it is to be expected that although, for small fluctuations, their level is directly proportional to C_n^2 if the amplitude fluctuations are already large (20 to 30 percent of the mean level) an increase in C_n^2 by an order of magnitude will not produce a similar increase in the fluctuation level. Therefore, although the contribution to the integral

$$\int_o^\infty C_n^2 (x) x^{5/6} dx$$

is more than an order of magnitude larger when a region of moderate CAT is present, as compared with the quiet atmosphere case, this does not necessarily mean that there will be a measurable increase in the scintillation over the already high fluctuation levels expected for the quiet atmosphere.

Tatarski (1966) examined the limitations of the Rytov method of solution and demonstrated theoretically how a saturation effect occurs. Experimental work by Gracheva and Gurvich (see Tatarski 1966) showed that, for measurements of intensity fluctuations over horizontal paths through the atmosphere, satisfactory agreement was obtained with calculations using the Rytov approximation provided the rms fluctuations of the logarithm of the amplitude die not exceed 0.8.

The method of solution of the wave equation used by Tatarski is briefly as follows. Again, we may arrive, by simple manipulation, at the form of the wave equation given, which has to be solved to give the complete answer to the problem:

$$\Delta\psi + (\nabla\psi)^2 + 2ik\nabla\psi + 2k^2 n_1(r) = 0.$$

We assume an inhomogeneous medium in the region $x > 0$ with an incident plane wave given by $A_o \exp(ikx)$. The wave for $x > 0$ may be written as

$$U(r) = A_o \exp(ikr) + \psi(r)$$

where $\psi(r)$ is the solution to the wave equation whose real and imaginary parts give, respectively, the fluctuations in the log amplitude and the phase fluctuations. Thus,

$$\psi = \ln \frac{A}{A_o} + i\,(S - \underline{k} \cdot \underline{r}).$$

In the Rytov approximation, the wave equation is made linear by dropping the term $(\nabla\psi)^2$, which permits a solution of the equation to be written directly. However, if this term is not omitted there is no direct method of solution. Tatarski uses the result obtained omitting the term $(\nabla\psi)^2$ as a first-order solution, then performs successive iterations by reduction to a nonlinear integral equation that is solved numerically. Because of other approximations made in this method of solution, it is not possible to determine the saturation level, although the solution does predict the saturation effect. The saturation level is, therefore, predicted from the experimental results of Gracheva and Gurvich to occur for log amplitude fluctuations given by

$$\sigma_\infty^2 = 0.8^2.$$

Figure 22 shows the way in which the log-amplitude fluctuations saturate where the form of the curve is determined from the theory and the saturation level, from experimental results.

This discussion bears out the previous conclusion but is on a stronger theoretical basis. If we are already operating in a condition in which the log amplitude fluctuations have reached their maximum value, then the presence of a region of CAT of much higher C_n^2 ahead of the aircraft will not change the fluctuation level.

In contrast to this theoretical result, Mikesell (private communication, April 1967) of the United States Naval Observatory reports that in-flight tests of a portable scintillometer, typical scintillation levels were ~10 percent of the mean intensity. A number of measurements have been made, under different flight

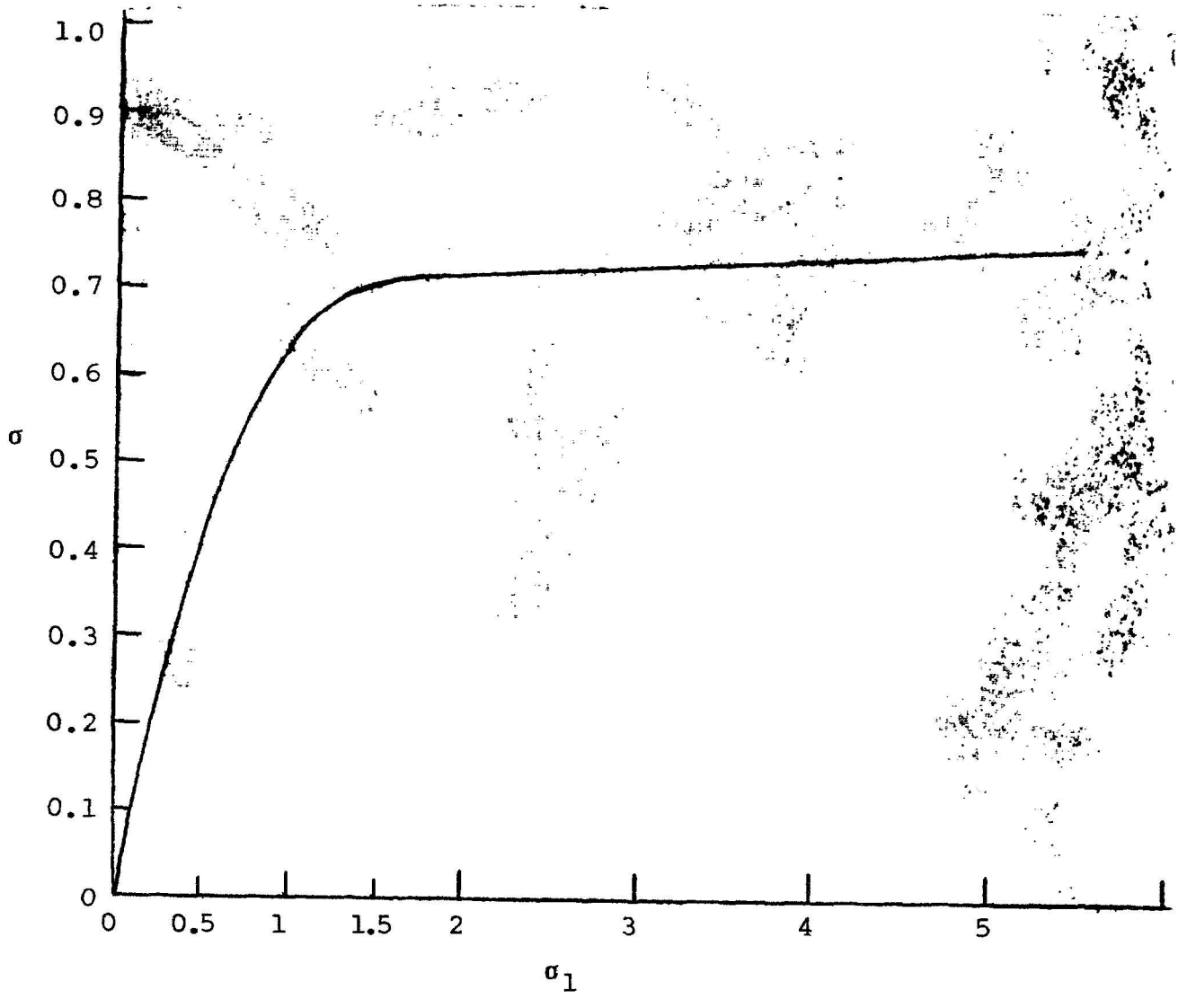

Figure 22 Saturation Effect in Log Amplitude Fluctuations

conditions, with the scintillometer, which has a 2-in.-diameter aperture. There will, of course, be some aperture averaging, but not sufficient to explain (or resolve) the discrepancy between the theoretical and experimental results. We may estimate the degree of aperture averaging from the theoretical work of Tatarski, who introduces the quantity to characterize the decrease in scintillation due to the averaging action of the objective. This quantity G has the form shown in Figure 23, where $D/\sqrt{\lambda L}$ is a nondimensional relative aperture size. Thus, when the diameter of the collecting aperture exceeds the correlation distance, $\sqrt{\lambda L}$, there will be a marked reduction in the recorded fluctuation levels.

With reference to the Figure 21, we can see that the major contribution to the fluctuation level is produced by that region of the atmosphere more than 50 km from the receiver; $\sqrt{\lambda L}$ will, therefore, exceed 16 cm. In the case of stellar scintillation looking vertically upward from the ground, the turbulent region producing the scintillation effects is located at an altitude of the order of 10 km and the experimental results of Keller (1955) gave $\sqrt{\lambda L} \sim 8$ cm. Discussions with Mikesell did not resolve the discrepancy between the theoretical and measured values of the scintillation levels.

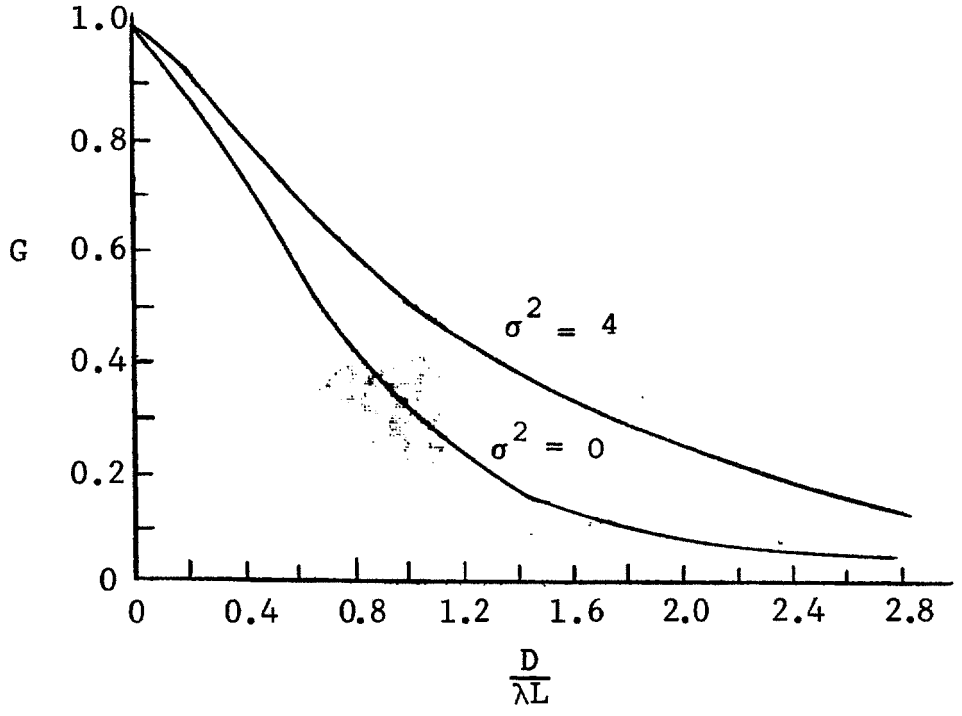

Figure 23 Theoretical Dependence of the Relative Decrease in Fluctuations Due to Aperture Averaging

It should be noted that, in the theoretical approach, we used the variation of C_n^2 with altitude deduced by Hufnagel and Stanley from experimental data on the rate of energy per unit mass dissipated by viscous friction, and average wind shear, both as a function of altitude. The values of C_n^2 obtained do not disagree with the levels expected from ground-based measurements of stellar scintillation.

Ucinsky (private communication, July, 1967) has developed a theory for large fluctuations. When his results are published, it may be possible to come to a conclusion about the usefulness of stellar scintillation as a method of CAT detection.

3.3.2 Star Availability and Detection Sensitivity. An instrument for the remote detection of CAT by stellar scintillation measurements would function approximately as follows. A star is acquired by an on-board tracker with the star essentially along the flight direction. If turbulence exists along this viewing path, the light intensity will fluctuate in a manner related to refractive index variations associated with the turbulent region, the turbulent scales, and the distance of the region from the detecting system. Analysis of the fluctuating signal in terms of its frequency and amplitude content should then reveal the characteristics of the turbulence.

To evaluate this method, three aspects must be examined: (1) the availability and detectability of stars; (2) the existence of perturbations due to turbulence and the magnitude of these perturbations relative to the noise fluctuations and (3) the information that can be obtained from the fluctuations.

The density of stars brighter than seventh magnitude (photographic) varies from 0.36 per square degree at the galactic equator to 0.10 at the galactic poles. For sixth magnitude, the corresponding values are 0.13 and 0.04 (Duncan, 1930). A turbulence cross section of 40 miles by 1 mile subtends about 15 square degrees at 100 miles. Tracking stars brighter than seventh magnitude will, therefore, ensure star availability essentially all the time. Since it is desirable to have the turbulence detection system in operation both day and night, we have to consider the detection of the radiation from sixth to seventh magnitude stars in high backgrounds. Operation of such a device at night presents fewer problems, since no appreciable background will be present.

On the basis of ground-based scintillation measurements, the presence of turbulence along the optical path gives rise to fluctuations in the index of refraction which, in turn, cause fluctuations in the intensity measured in the detector plane. The frequency behavior of the intensity fluctuations is determined by the eddy spectrum and by the eddy motion orthogonal to the viewing axis. The high-frequency cutoff will usually be determined by the telescope aperture size. The mean-square-intensity fluctuation depends on both refractive index fluctuation scales (eddy sizes) and telescope aperture. These relationships were well summarized by Reiger (1963), who compared these conclusions with ground-based experiments. He found good agreement, particularly with the results of Keller (1955) and Protheroe (1955). The predicted temperature fluctiations are compatible with the data of Glagolev (1964) as well as with Project Jet Stream as given by Endlich and Mancuso (1964).

Although, the spectral composition of radiation from different stars varies considerably, in this study, we will assume a spectral distribution similar to that of the sun. For this case, Gebel (1962) has derived an equation for the flux gathered by a telescope with diameter d. In terms of available power, the equation is

$$P = \frac{0.68\ Ch\nu d^2 T}{2.512^M} \text{ (watts)}$$

where P is the power (watts),

d is the diameter of the objective (cm)

T is the transmission of the optical system,

h is Planck's constant (6.626×10^{-27} erg-sec),

ν is some mean frequency of the radiation (cps)

M is the star magnitude, and

C is the fraction of the total number of photons collected by the optical system which fall within the spectral bandpass of the detector.

The background radiation, which in daytime will be predominantly scattered sunlight, will be about a factor of 10 less in the 6000 - 9000A spectral region compared to the 4000 - 7000A region. A factor of five is attributable to the scattering function while the additional factor of two comes from

the greater solar flux density in the shorter wavelength band. However, photomultipliers are of the order of ten times more sensitive in the shorter wavelength region and hence the signal/noise performance will be unchanged. A gain in using the longer wavelength region of the two will be obtained only for stars with temperatures below that of the sun. Except for these red stars, the star energy available will be about the same for both regions. The reasons for choosing these two regions are high detector sensitivity and favorable spectral distribution of radiation. We can, therefore, choose 4000 to 7000A for detection, since the detector noise for uncooled trialkali multiplers is much lower than for either uncooled S-1 tubes or silicon photodiodes. Detector noise is important at night.

Calculations based on a solar spectral distribution yield a value of C = 0.38.

Using $\nu = 5.5 \times 10^{-14}$ (5500A)

$M = 7$

$T = 1$,

we obtain

$$P = 1.5 \times 10^{-5} \, d^2 \text{ watts.}$$

Using Willstrop's (1960) value of approximately 10^{-14} watts cm^{-2} $(100A)^{-1}$ for the irradiance outside the earth's atmosphere from a zero-magnitude star in the visible, we obtain the power collected from a seventh magnitude star as $P \approx 2 \times 10^{-15} \, d^2$ watts in a 3000A band.

Since the radiation received by the detector will be prodominantly scattered sunlight, then, assuming the detector noise may be neglected, the noise fluctuations will be rms shot noise given by the usual equation,

$$N = \left[2eIK\Delta f\right]^{1/2},$$

where N is the rms fluctuations in the cathode current,

K is the cathode radiant sensitivity (amps/watt),

Δf is the electronic bandwidth (cps),

e is the electronic charge,

and (See Section 5.1.1) $I = \frac{\pi^6}{2} \frac{(\cos^2\theta+1)\, d^2\gamma|\alpha|^2}{\lambda^4} H_o \int_o^\infty N(r)dr.$

With

$\lambda = 5500A$

$\cos^2\theta = 1$ (worst case)

$\gamma = 3 \times 10^{-4}$ rad (1 minute of arc)

$H_o = 1.5 \times 10^{-2}$ watt/cm^2 ($\Delta\lambda = 3000A$)

$\alpha = 3 \times 10^{-24}$ cm^3

$\int_o^\infty N(r)dr = 1.7 \times 10^{26}$ cm^{-2}

we obtain

$$I = 2.2 \times 10^{-10} d^2 \text{ (watts)}.$$

If we now take $K = 2 \times 10^{-2}$ amp/watt and $\Delta f = 100$ cps, then from the shot-noise formula, the rms noise is given by

$$N = 1.2 \times 10^{-14}\, d \text{ (amp)}.$$

To successfully track a star, the difference between the mean-signal level when the star is in the field-of-view of the detecting system and the mean-signal level when the star is not present has to exceed the rms noise fluctuations. For the assumed conditions defined, the ratio between this difference signal and the rms noise is given by

$$\frac{PK}{N} = 2.5 \times 10^{-3}\, d.$$

If d = 40 cm is taken as a practical upper limit for an airborne telescope, we will need to gain a factor of 20 or more to track a seventh magnitude star. A factor of 2.5 is obtained for each decrease of one unit in magnitude. It may be possible to gain in the fraction of star energy (for a given magnitude) between 4000 and 7000 A since many stars are hotter than the sun. Any such gain will be small, however as can be seen immediately on a radiation slide rule. Some improvement in the S/N ratio of the system may be obtained by reducing the field angle. A factor of

two decrease to 30 arc-seconds seems to be all that is practical. Tracking with narrow field on an aircraft requires rather well stabilized mounts, and 30 seconds is the best one might expect (Greene, et al., 1966).

3.3.3 Evaluation. We have shown that tracking sixth and seventh magnitude stars from an aircraft is, at best, a marginal proposition in the daytime. Even if we assume that a S/N ratio of five can be achieved (i.e., 40-cm telescope, 1 cps bandwidth and a field angle of 30 arc-seconds), we are still left with detecting the scintillations that may be a few percent of the star intensity (Reiger 1963). Clearly detecting is not even marginal.

At night, the situation is quite different. With the drastically reduced background, the noise equivalent input of the detector can be used to estimate feasibility. For a 100-cps bandwidth, a typical figure for trialkali cathode tubes is 1-5 x 10^{-15} watt. Comparing this with the power available from a seventh magnitude star, we see that with a 15-cm aperture diameter, the S/N ratio is of the order of 100 for tracking, and fluctuations in signal of a few percent can be detected with confidence.

Turbulence detection using a star-tracking system appears feasible only at night. Daytime tracking, even with a large-aperture narrow-field telescope and slow time response, is, at best, marginal, while detection of fluctuations is at least one magnitude removed from tracking.

3.4 Relative Movements of Stellar Images

This technique, whereby the movement of stellar images relative to one another would be measured, has been considered but it possesses so many practical disadvantages that it has been eliminated from further consideration. The reasons are as follows:

- It would be necessary to acquire the "track" at least two stars simultaneously with accuracies of the order of a few arc-seconds.
- An extremely accurate and fast-responding inertial platform would be required to take account of aircraft motions; rolling, pitching, or yawing. This would have to operate with an accuracy of a few arc-seconds.
- To ensure star availability, stars down to the seventh magnitude would have to be used,

necessitating telescope apertures of the order of 6 in. There would, therefore, be some averaging over the aperture that would reduce the dancing of a star, but increase the image blur.

- From ground-based seeing observations, the image is not of uniform shape and changes continuously with time.

- Because of scintillation, the amount of energy in the image would vary in a random fashion. This would make instantaneous (times $\simeq$ 1/300 sec) determination of the position of the star extremely difficult.

These reasons are considered to be sufficiently discouraging to preclude further study of this technique.

3.5 Detection of Temperature Characteristics

Evidence from as early as the Project Jet Stream Flights (Endlich & Mancuso 1964) has shown that many turbulence encounters are associated with horizontal temperature gradients and fluctuations. This information has resulted in a number of suggestions for detection or warning of imminent turbulence encounters. Kadlec (1965) investigated a direct temperature-sensing technique that involves measuring the temperature at the aircraft and then, using established but questionable gradient criteria, determining when an encounter is probable. While extensive tests are still being made, it seems that the objections raised by McLean (1965) are valid and the approach is susceptible not only to a high false-alarm rate but also to a low prediction accuracy.

McLean's major objection is that such a method is utterly dependent on the geometrical relation of aircraft pthh to turbulence. It would appear, that an equally strong criticism is that only turbulence in the front between two air masses of different temperatures can be predicted at all. This is much too restrictive since turbulence is found elsewhere, particularly in regions of mountain wave activity.

Remote sensing of atmospheric temperature has been suggested and examined by several investigators although, as a method of CAT detection, this technique still requires the association of large horizontal temperature gradients with occurrence of CAT. Radiometric detection was analyzed by Merrit and Wexler (1964), who concluded that the 6.3-μ water

vaporband is the best available choice for making such remote temperature measurements and that the detection of a 2°C spike with a 3-km depth is marginally feasible. The single radiometer is not capable of providing range information, but the effect of temperature variations beyond 30-km will be much less than that of variations closer than 30-km. One can, therefore, envision an alarm system of some sort. At best, however, all the pilot will know is that some form of temperature variation is ahead but the system cannot provide more than that since range and magnitude of the variation are complementary.

To increase the amount of information, Astheimer (1964) and others suggested a technique in which the short wavelength wing of the 15-μ carbon dioxide band is scanned spectrally. Their calculations showed that detection of large scale temperature discontinuities is feasible on the basis of the S/N ratio, although the assumption that the turbulence region has dimensions of the order of 80 to 160 km was made.

3.5.1 Sensitivity. The case of a single detecting system pointing approximately ahead of the aircraft and operating at a fixed wavelength will be considered first.

The sensitivity with which horizontal temperature gradients ahead of the aircraft may be detected will depend on the design of the radiometer, the sensitivity of the detector and the stability of the radiometer mounting platform. Quite clearly, for a radiometer looking ahead of the aircraft, changes in the pointing direction in a vertical plane will cause pronounced changes in the temperature along the radiometer line of sight because of normal temperature structure of the atmosphere. The magnitude of this effect would depend on the vertical temperature gradient ahead of the aircraft.

A radiometer controlled to point horizontally ahead of the aircraft would be able to detect horizontal temperature gradients by virtue of the motion of the aircraft. If the aircraft is approaching a region of warmer air then the signal relative to some absolute value will increase. Spatial scanning can also be utilized. The radiometer output signal would normally be constant for an angular scan in the horizontal plane, but would increase as the point down angle increased for scans in a vertical plane. Deviations from this behavior could be used to infer the atmospheric temperature structure ahead of the aircraft which might then be related to occurrence of CAT.

To treat this problem analytically the field of view is divided into elements along the line of sight. The radiometer signal may then be considered to be the sum of the radiance of all the elements multiplied by the transmission of the atmosphere between the detector and the individual element. This total radiance can be written as

$$R = \sum_{1}^{n} t_i R_i .$$

A number of wavelength regions, particularly the 15μ carbon dioxide, 9.6μ ozone and 6.3μ water absorption bands are suitable. The carbon dioxide band appears to be the most advantageous because it is broad enough to allow spectral scanning of the short-wave wing without using a very high spectral resolution, so that both radiometric and spectro-radiometric approaches can be evaluated and compared. The carbon dioxide mixing ratio is essentially constant throughout the atmosphere in contrast to the water vapor variability and the complex behavior of the ozone mixing ratios.

For the values of λT with which we are concerned, the radiance of any element is given by the Wien approximation to Planck's law, multiplied by the thin gas approximation

$$R_i = c_1 \lambda^{-5} \exp\left[\frac{-c_2}{\lambda T_i}\right] \times e_i N_i \ell_i$$

where $c_1 = 3.74 \times 10^{-12}$ watts cm^2

$c_2 = 1.443 \times 10^4$ μ deg

λ is the wavelength (microns),

T_i is the temperature of the element (K°),

e_i is the molecular extinction coefficient (cm^2),

N_i is the molecular number density (cm^{-3}), and

ℓ_i is the length of the element.

To determine the sensitivity of detection of temperature characteristics we have to be able to calculate the effect on the radiometer signal of different forms of atmospheric temperature distribution ahead of the aircraft. Since we are concerned with temperature differences the difference in radiance of any element if the temperature of that element changes from T_i to T_i' is given by

$$\Delta R_i = c_1 \lambda^{-5} e_i \ell_i \left[N_i \exp \frac{-c_2}{\lambda T_1} - N_i' \exp \frac{-c_2}{\lambda T_i'} \right],$$

Now assuming that the mixing ratio of CO_2 is constant and that the density will vary inversely with the temperature then

$$N_i' = N_i \frac{T_i}{T_i'},$$

$$\Delta R_i = c_1 \lambda^{-5} e_i \ell_i N_i \left[\exp \frac{-c_2}{\lambda T_i} - \frac{T_i}{T_i'} \exp \frac{-c_2}{\lambda T_i'} \right].$$

For the wavelength 15μ and the temperature value $\approx 230°K$, the spectral radiance difference is a linear function of temperature difference; i.e.,

$$c_1 \lambda^{-5} \left[\exp \frac{-c_2}{\lambda T_i} - \exp \frac{-c_2}{\lambda T_i'} \right] = \alpha (T_i - T_i').$$

Upon substitution and rearrangement,

$$\Delta R_i = c_1 \lambda^{-5} e_i \ell_i N_i (T_i - T_i') \left[\frac{\alpha \lambda^5}{c_1} - \frac{1}{T_i} \exp \frac{-c_2}{\lambda T_i} \right].$$

Since we are considering an altitude of 10 km, T_i will be $230°K$ and the quantity in the square brackets is then

$$\frac{\alpha \lambda^5}{c_1} - \frac{1}{T_i} \exp \frac{-c_2}{\lambda T_i} \approx 2 \times 10^{-4} \text{ deg}^{-1}.$$

The differential radiance is, therefore, given by

$$\Delta R_i = 1 \times 10^{-5} \Delta T e_i \ell_i N_i \text{ watt/cm}^2\mu \text{ °K sterad.}$$

The difference in the detected signal between the case in which a uniform temperature distribution exists haead of the aircraft and that in which a temperature gradient is present is therefore given by

$$\Delta R = \Sigma t_i \Delta R_i$$

where t is again the transmission of the portion of the atmosphere between the i th region and the radiometer.

To obtain an estimate of the ability of the radiometer to sense temperature gradients or other nonuniformities ahead of the aircraft it is necessary to first substitute into the equation for ΔR_i the appropriate values of e_i, N_i, ℓ_i, and ΔT. The combination of e_i, N_i, and ℓ_i will be the emissivity of the slab of atmosphere being considered and we will assume that the wavelength is chosen so that the $\ell_i \approx 30$ km, the slab emissivity is 0.5. Although actual temperature records are considered later, we will assume here a temperature well ahead of the aircraft as shown in Figure 26 with a depth of $\Delta T = 5°$ extending over the distance ℓ_i. The differential radiance for the slab will therefore be given by

$$\Delta R_i \approx 2.5 \times 10^{-5} \text{ watts/cm}^2\mu \text{ sterad.}$$

If a uniform temperature is assumed along the line of sight of the radiometer with the exception of the temperature well then the change in radiometer output due to the presence of the well will be given by

$$\Delta R = t\Delta R_i .$$

For this preliminary estimate, we will take $t \approx 0.6$ which gives an effective differential radiance of $\Delta R = 1 \times 10^{-5}$ watt/cm$^2\mu$ sterad. This choice of t determines the range of the temperature well from the aircraft since the wavelength was fixed when the slab emissivity was chosen to be 0.5. A spectral bandpass of 0.5μ will, therefore, give rise to a differential radiance of $\Delta R = 5 \times 10^{-6}$ watt/cm^2 sterad. The characteristics of the radiometer will determine the S/N ratio with which this differential radiance may

be detected. If we take the following figures, which would be appropriate for an airborne radiometer,

Area of Collector	300 cm^2
Field of View	$1° = 2.4 \times 10^{-4}$ ster.
Detector Size	1 mm^2
Transmission Factor	0.3
Electronic Bandwidth	1 cps

the S/N ratio with thermistor bolometer detector having a detectivity of 5×10^8 cm $(Hz)^{1/2}$/watt would be 500.

It may be deduced from Figures 24 and 25 that for the slab of atmosphere 30 kms thick the transmission would be equal to 0.5 for a wavelength of 13.2 microns. At this wavelength the emissivity of the slab would also be equal to 0.5. The assumed transmission from the slab to the detecting system of 0.6 would therefore correspond from Figure 25 to the slab being centered a distance of 30 kilometers from the radiometer.

It is clear from the way in which the transmission curves change with wavelength that the spectral bandpass of the radiometer should be made as narrow as possible, preferably less than 0.1 micron, to avoid the signal being smoothed out. A narrow spectral bandpass will reduce the S/N ratio, and so a compromise will usually be necessary.

The approximate difference in radiance between an undisturbed field and one which includes a temperature well 30 kms long, 5° in depth, centered 3 km from the detecting system has been found to be 5×10^{-6} watts/cm^2 -sterad. if the spectral bandpass is a relatively large 0.5 micron. This agrees with the results of Norman and Macoy for a 5° temperature discontinuity starting at 20 km. Since in our case the differential radiance is defined as the difference in signal between the ambient condition and the condition in which temperature gradients occur in the flight path of the aircraft, then the comparison with the Norman and Macoy result from Figure 26 has to be made by taking the difference between curves A and B_{20} km at 13.2 microns. This difference is equal to 9.5×10^{-6} watts/cm^2-ster-micron and with an 0.5μ bandpass the differential radiance would be

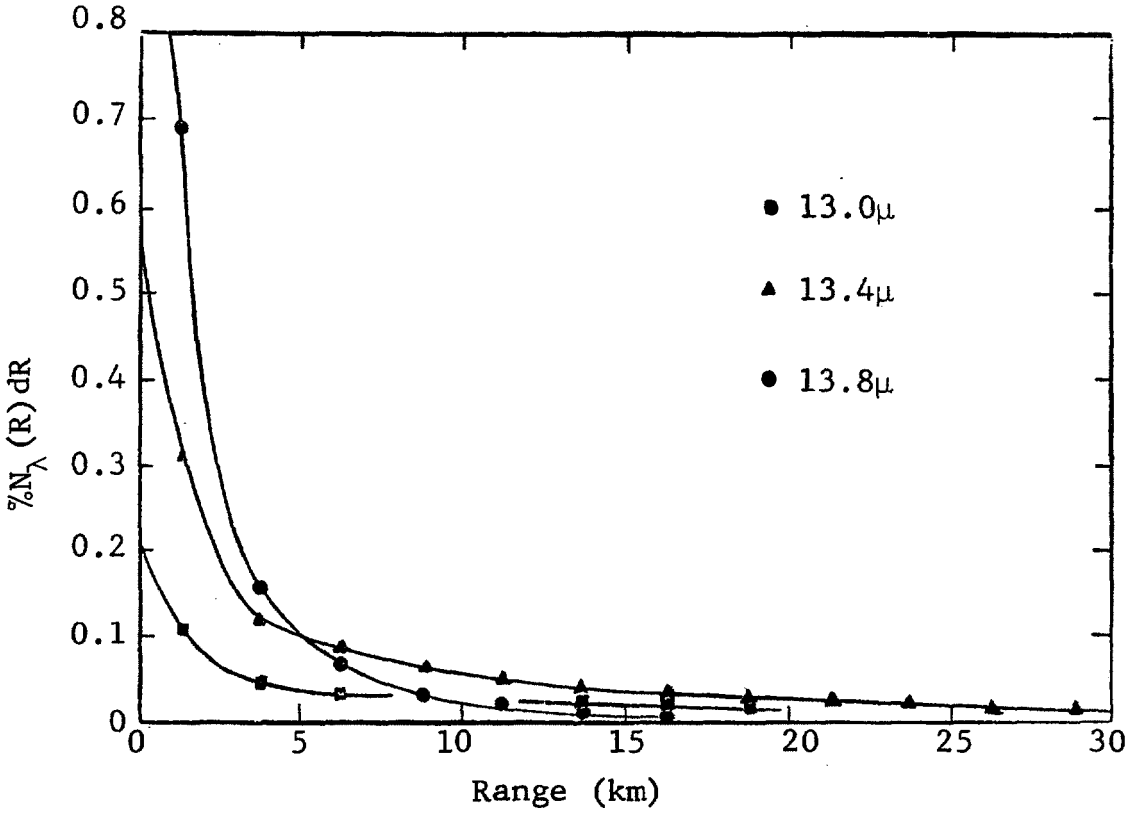

Figure 24 Distribution of Spectral Contribution with Incremental Range (Norman and Macoy, 1965)

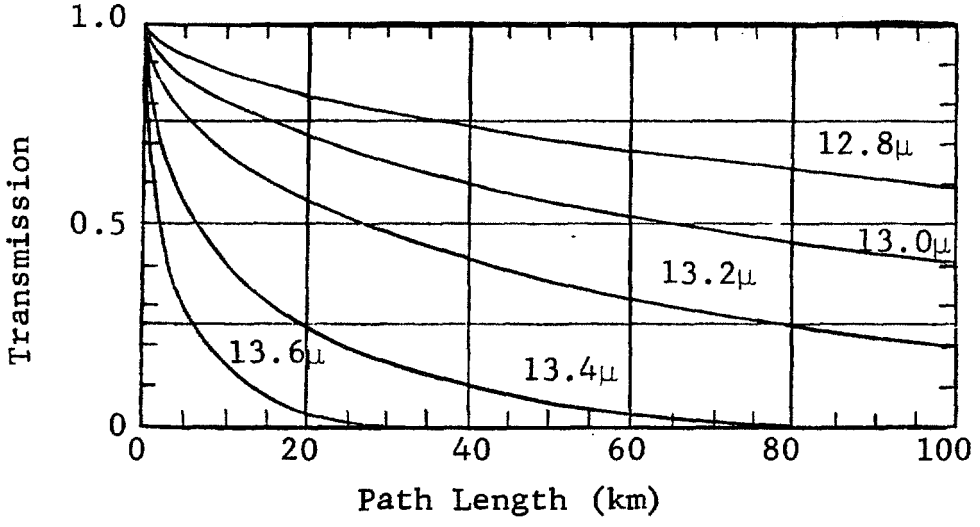

Figure 25 Transmission of Atmosphere at 30,000-ft Altitude (Norman and Macoy, 1965)

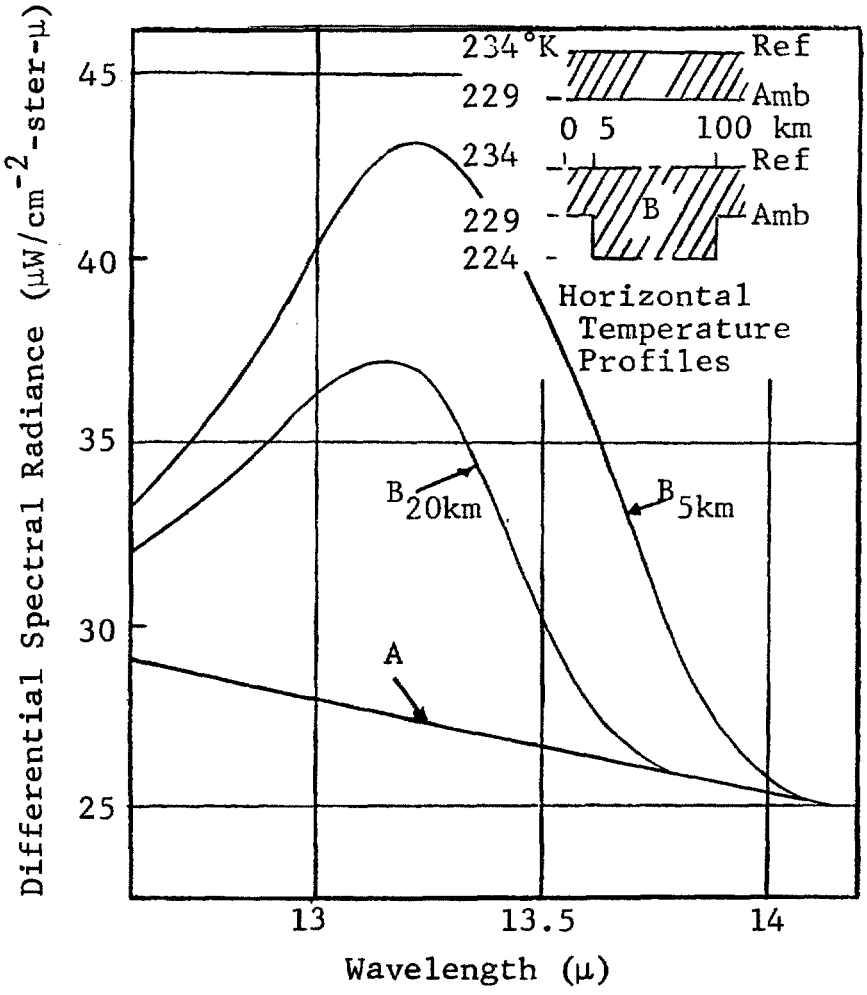

Figure 26 Radiometric Instrument Output for Idealized Horizontal Temperature Profiles (Norman and Macoy, 1965)

4.8×10^{-6} watts/cm^2-ster. Although they extend the temperature well to 100 km, whereas we have considered the well to be between 15 and 45 km, no substantial difference in radiance between the two situations should be expected since the 15- to 20-km portion contributes heavily and will substantially balance the 45- to 100-km region.

According to the results of Norman and Macoy shown in Figure 26, a radiometric system (i.e., operating at a fixed wavelength) would give the largest change with the center wavelength near 13.2 microns irrespective of the range of the temperature well. In case A the ambient temperature, assumed to be uniform, is different to the reference temperature and the differential radiance therefore represents the difference between the blackbody radiances at the two temperatures. There is no peak in the spectral distribution curve. In case B a temperature "well" is assumed to be located ahead of the aircraft and extending out to 100 kilometers. The two curves correspond as marked to the temperature well at a range of 5 km and 20 km respectively. The peak in these curves at 13.2 microns results from the way in which the transmission and the emission are combined. At wavelengths shorter than 13.2 microns the emission from the slab of atmosphere coincident with the temperature well will be less but the transmission through the intervening atmosphere to the radiometer will be greater. At larger wavelengths although the emission is greater, the transmission is less in such a way that a peak is obtained in the spectrum function.

A major problem in the case of a radiometer operating at a single wavelength is that there is no direct way of distinguishing between a horizontal temperature gradient ahead of the aircraft and a change in ambient temperature. By monitoring the air temperature at the aircraft these cases could possibly be distinguished or alternatively spatial scanning could be employed.

However, an alternative approach is to use a spectro-radiometer and to measure the radiative input as a function of wavelength. On the basis of the calculated spectral radiance curves of Norman and Macoy such a technique would appear to be very promising. However, in a practical case the temperature distributions will be considerably different to the idealized temperature wells considered above and therefore, to determine how well this technique will work in practice, actual measured temperatures will be used.

It should again be noted that this discussion relates to the remote dectection of temperature gradients ahead of the aircraft. As we pointed out initially, the correlation between CAT and such temperature gradients is far from clearly established. In fact the evidence indicates that the technique would be susceptible to a high false alarm rate and an inability to give information of turbulent intensities.

3.5.2 Case Analysis. Endlich and McLean (1964) have provided graphs of temperature and espected signal functions from several Project Jet Stream flights. These records involve only temperature changes of fairly large spatial extent and do not include the type of singular temperature spike shown by Merritt and Wexler (1964) and by Fusco (1964). Radiometric detection of such spikes does not appear feasible may be detected.

To calculate the form of the radiometer signals from actual temperature records the atmosphere was divided into 10-km-thick slabs perpendicular to the line-of-sight and the irradiance at the aircraft computed (for each wavelength) from the expression:

$$\Delta I = \omega A \Delta\lambda t_i e_i \Delta B_i$$

where t_i is the transmission of the atmosphere between the aircraft and slab i,

e_i is the slab emissivity (assumed to be constant over the temperature involved and identical for all slabs),

ΔB_i is the difference in the Planck function for turbulent and ambient volumes and is proportional to the temperature difference,

ω is the field of view (solid angle),

A is the collector optics area, and

$\Delta\lambda$ is the spectral bandwidth used.

In terms of the temperature difference,

$$\Delta I = 10^{-5} A\omega\Delta\lambda e t_i \Delta T_i .$$

The summation is only over those slabs which have a temperature different from the ambient. Since the graphs do not specify the ambient temperature, we made a

reasonable estimate of this quantity. We have made no substitution for $A\omega\Delta\lambda$; therefore, the ΔI values thus obtained should not be considered absolute, but only indicative of the form of the signal. The Project Jet Stream records include vertical gust velocities and the turbulent intensities (following Endlich and McLean) may be interpreted as follows:

1. Gusts less than 5 fps; nonturbulent
2. Gusts between 5 and 9 fps; light turbulence
3. Gusts between 10 and 19 fps; moderate turbulence
4. Gusts greater than 20 fps; severe turbulence.

These values are intended only as guides and not as precise definitions. In fact, Colson (1966) notes that derived gust velocities of 5 to 20 fps are (frequently) defined as light turbulence, 20 to 35 fps as moderate, and 35 to 50 fps as severe.

We can examine one case as an example. The records of Figure 27 show a rapid decrease of the temperature from -59° to -62°C just after the onset of turbulence. Since 10 minutes represents about 50 to 60 miles, we see that the temperature drop occurs about 20 miles after turbulence onset and that light-to-moderate turbulence is found for the rest of the record. The signal reflects this temperature step in that the signal becomes more negative as the wavelength decreases and the radiation from larger distances ahead of the aircraft becomes important. Because the temperature record does not indicate the behavior beyond 130 miles, two signal curves were calculated, one for a temperature of -62°C throughout the atmosphere and the other for a -62°C temperature extending over 60 miles (1940 GMT). The signal function clearly depends on the temperature structure at large distances; the imminent turbulence tends to be masked by this.

Figures 27 - 31 represent situations ranging from no turbulence to severe turbulence and should, therefore, be indicative of the interpretability of the signal functions. Examination of the individual graphs and particularly the comparison curves in Figure 31 leads to the conclusion that the spectral scanning of the wing of the carbon dioxide 15μ band does not provide signals that can be used to reliably predict either turbulence or its severity ahead of an aircraft. The signals in Figure 28 and 29 show no significant and useful differences,

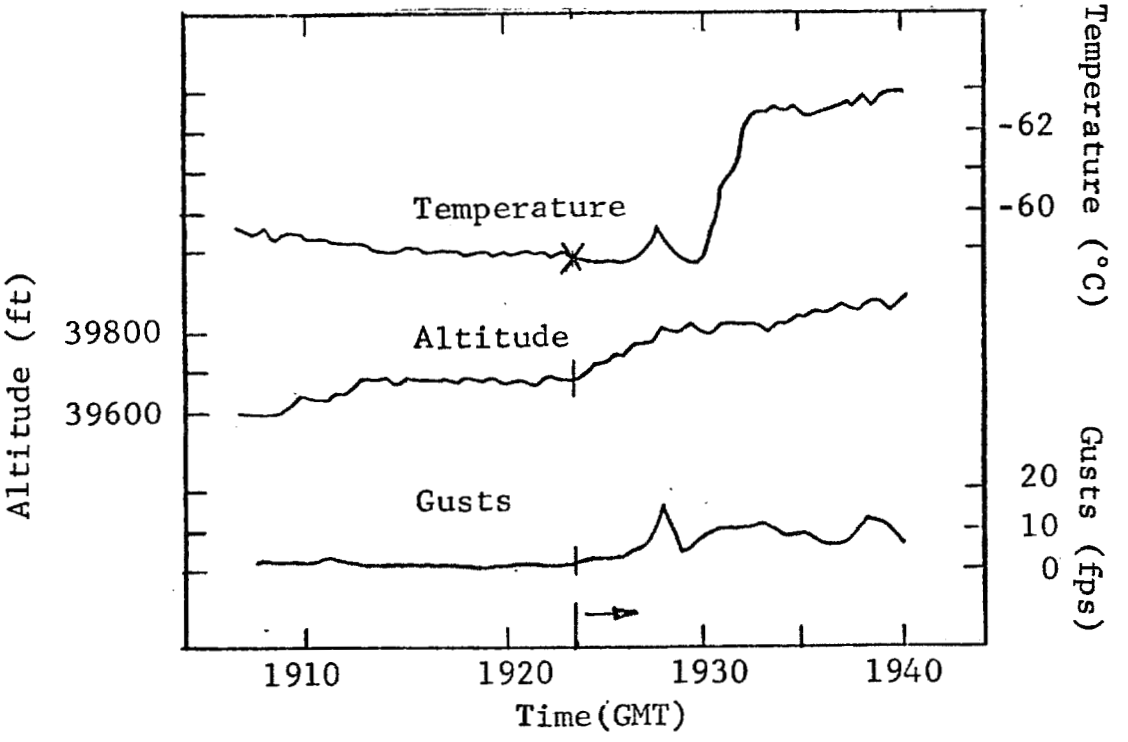

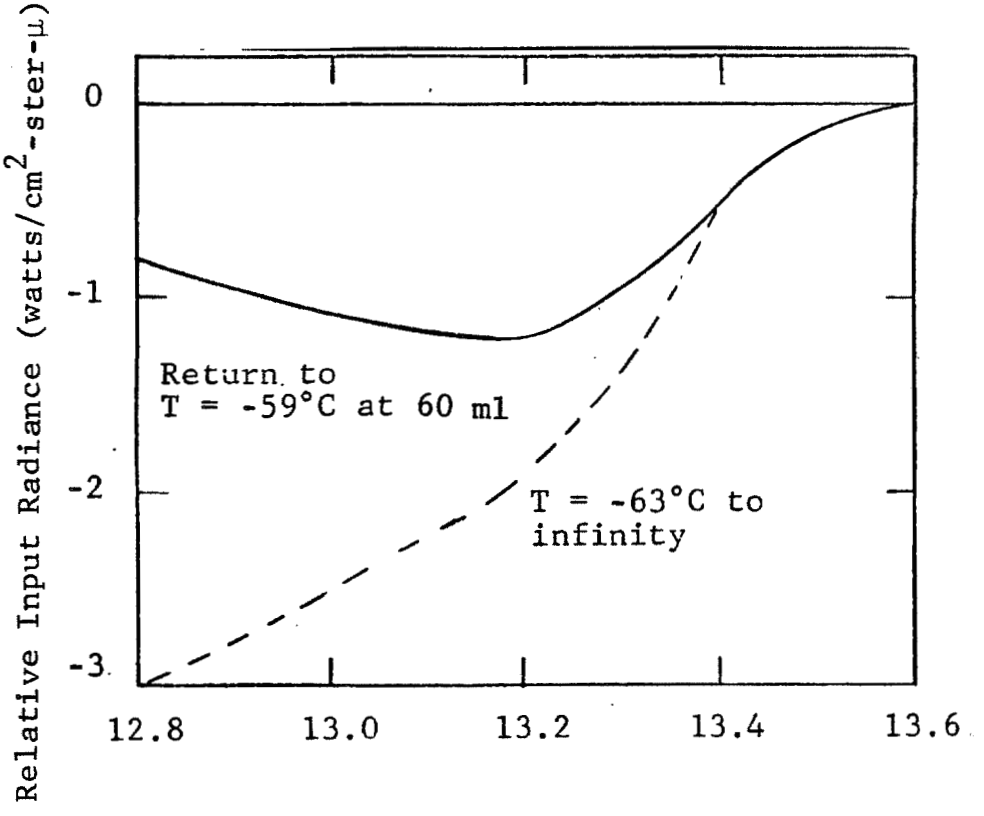

Figure 27 Temperature, Altitude, and Gust Records and Radiometric Instrument Output, Flight 29

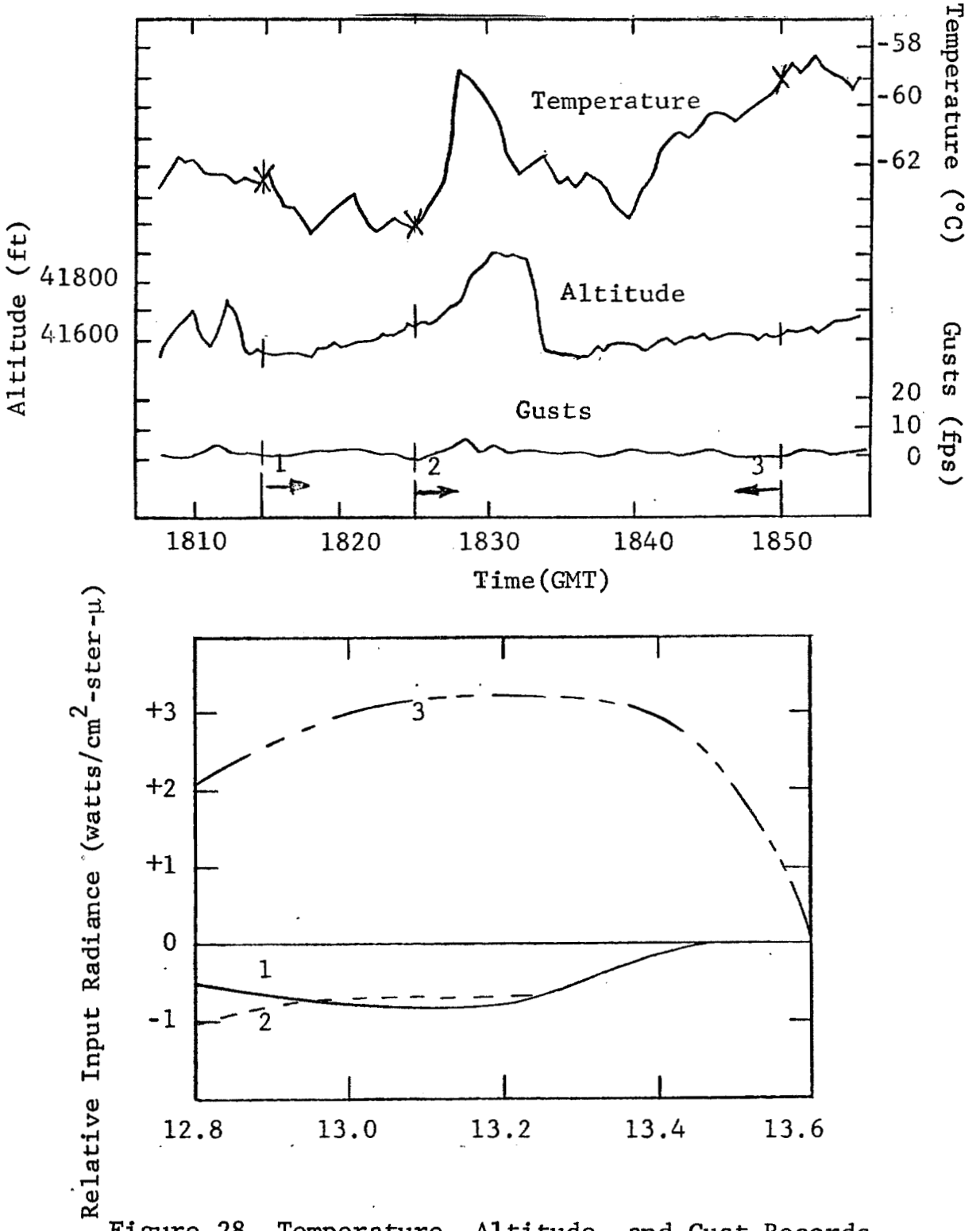

Figure 28 Temperature, Altitude, and Gust Records and Radiometric Instrument Output, Flight 27a

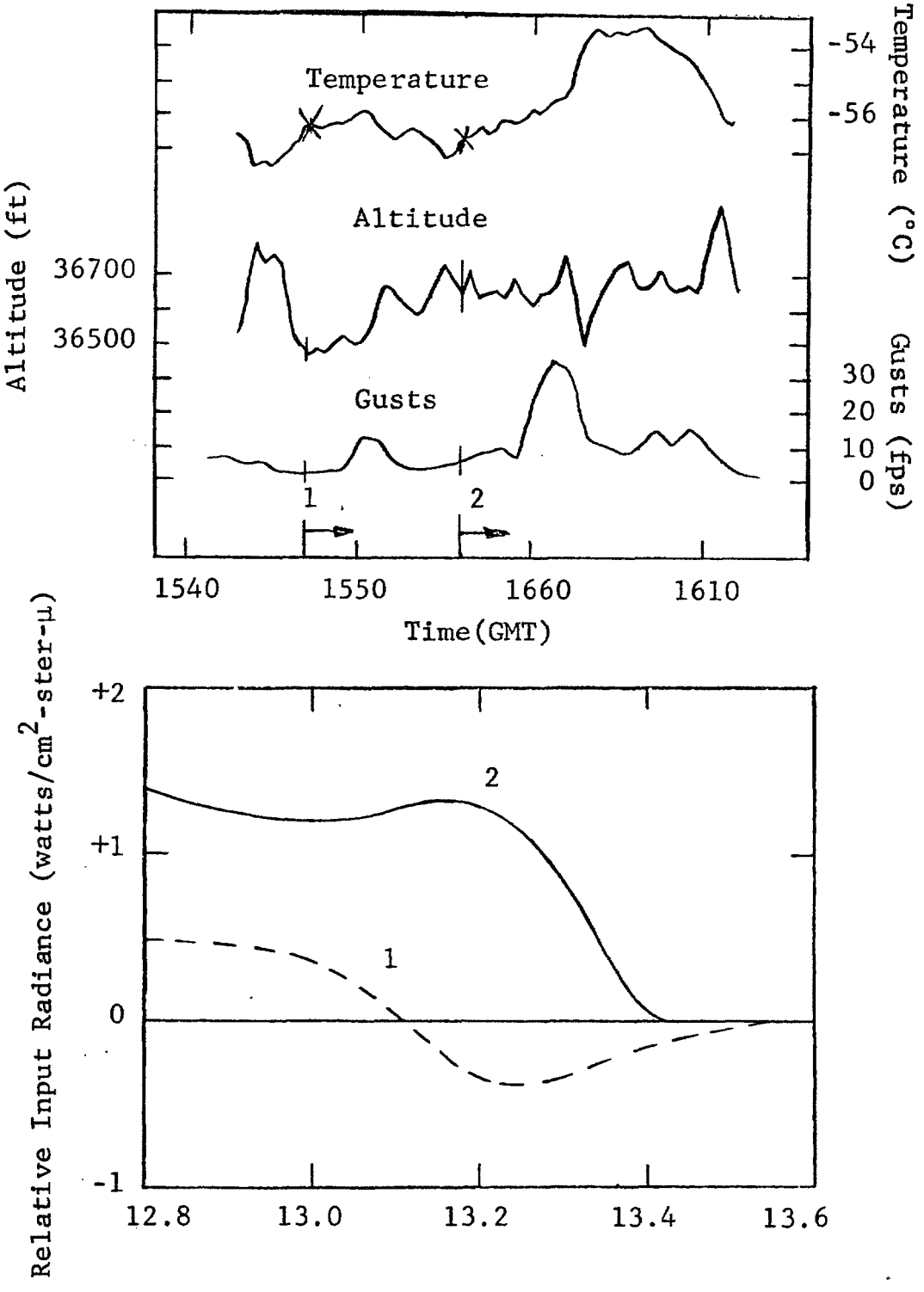

Figure 29 Temperature, Altitude, and Gust Records and Radiometric Instrument Output, Flight 27b

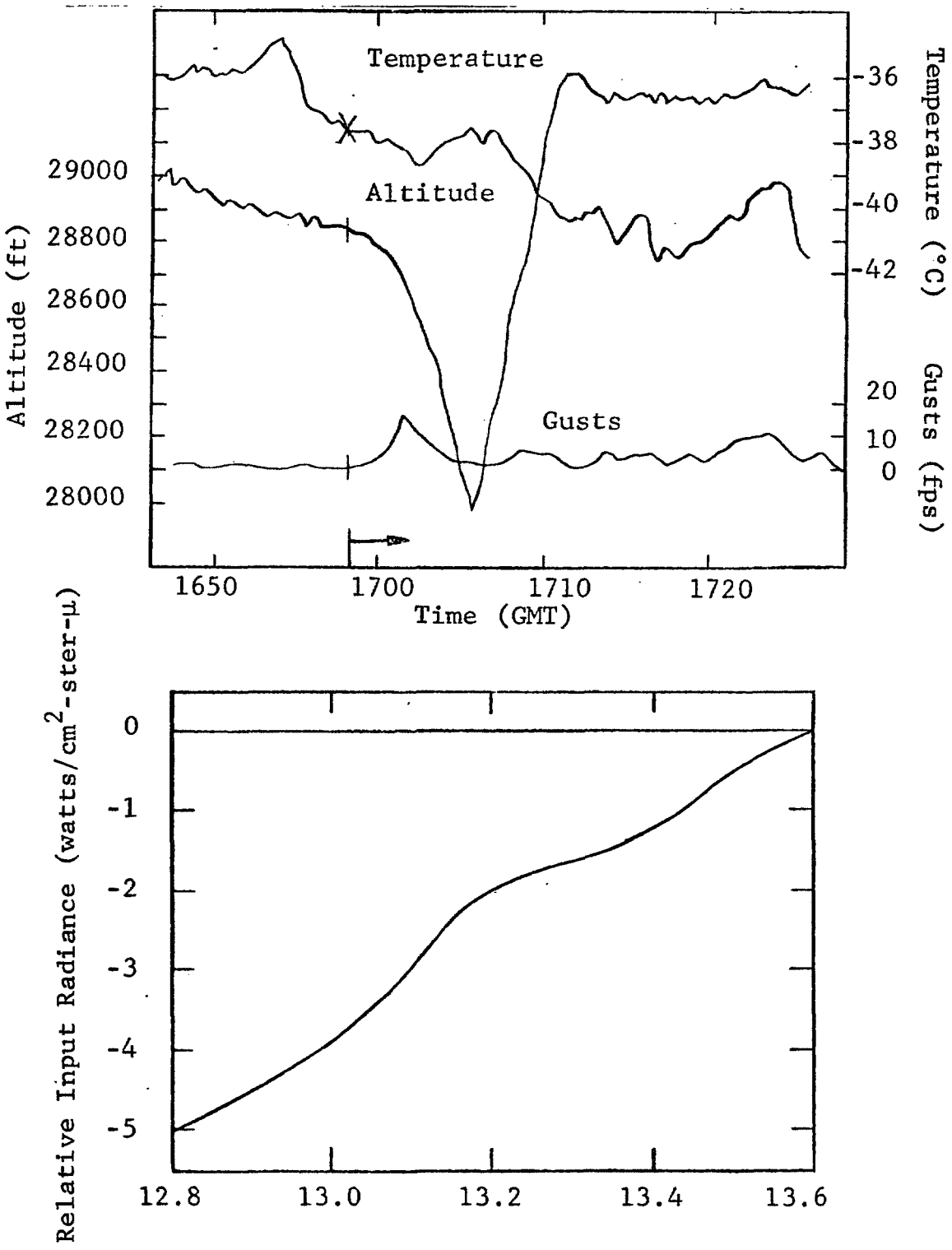

Figure 30 Temperature, Altitude, and Gust Records and Radiometric Instrument Output, Flight 26

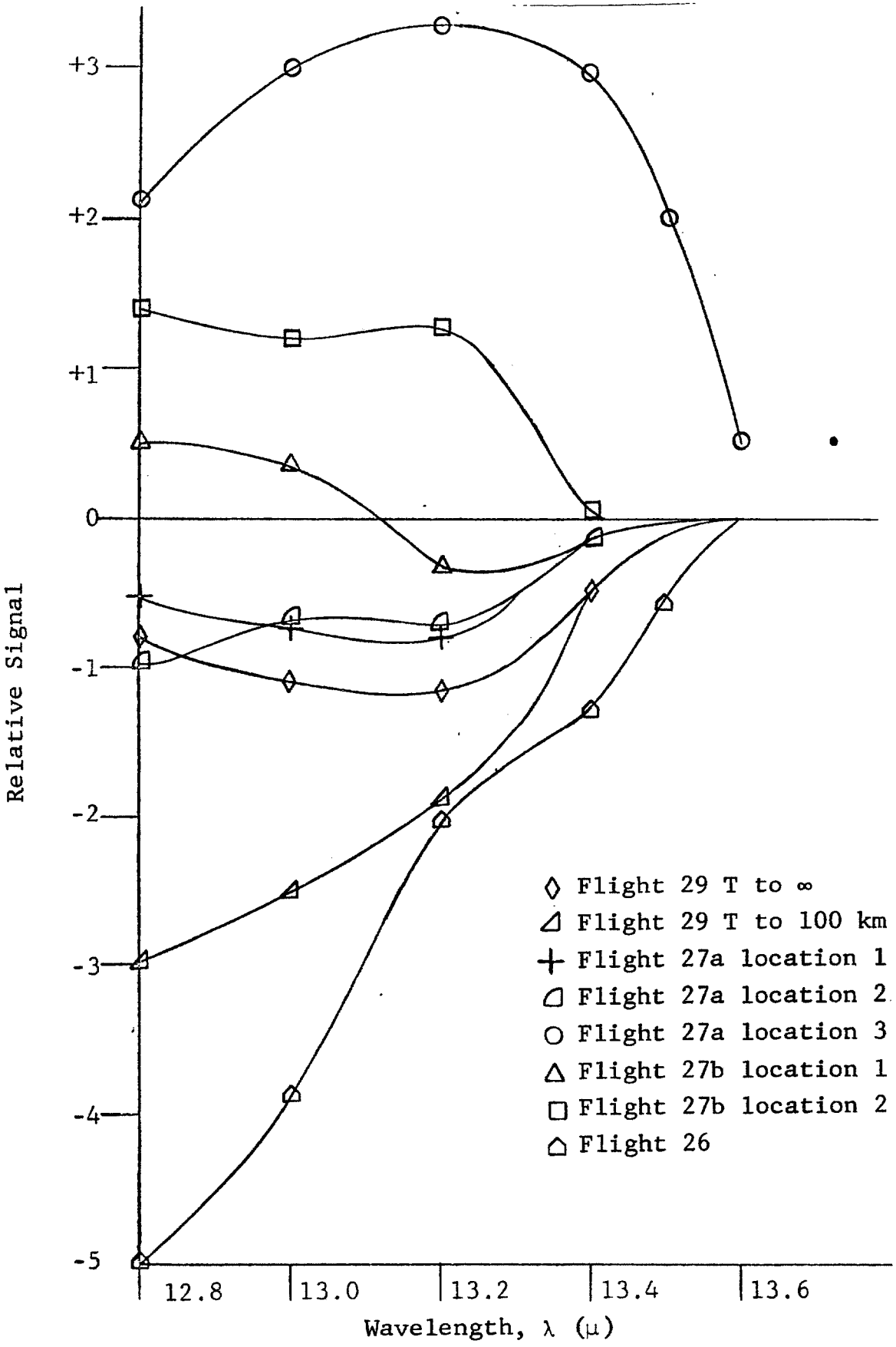

Figure 31 Comparison Signals

yet Figure 28 is the case of no turbulence ahead while Figure 29 represents a situation in which gusts up to 35 fps will be encountered along the flight path.

3.5.3 Evaluation. Although large scale temperature structure can be qualitatively inferred from the signal behavior the lack of correlation of that structure with turbulence is evident from the analysis of Project Jet Stream records. This was the contention of McLean (1965) in his analysis of the direct temperature-sensing technique used by Kadlec (1965) and we have here that the criticism applies to remote sensing as well. An examination of the data shown here does indicate a correlation between small-scale temperature structure (spikes), but no specific conclusions are possible because of the lack of information on the temperature structure in the adjacent nonturbulent air.

A recent series of flight tests conducted by the Canadian National Aeronautical establishment supports these reservations. A Fabry-Perot system similar to that described by Astheimar was flown on a T-33 aircraft. To ensure turbulence encounters, the flights were in areas of mountain wave activity. A number of problems with the airborne operation (lack of stabilization, radio frequency, interference) make it difficult to evaluate the results. The data presented by Mather (1967) are sufficient, however, to show that turbulence detection is sporadic. In addition, we must point out that our own examination of Mather's figures leads us to the conclusion that the instrument did not provide warning in several cases where detection was claimed by Mather. Possibly, this difference of opinion is due to our use of the figures in this report rather than the original data.

3.6 Infrared Schlieren System

Flow visualization techniques such as schlieren may be used to observe turbulence in fluid flows or over limited paths in the atmosphere. In a standard schlieren system the light from a small pinhole source is collimated by lens or mirror optics and this collimated beam passes through the flow region of interest. A second lens or mirror is then used to re-image the pinhole source in the plane of a knife edge, placed so as to block a large portion of the direct light from the source. Density gradients in the flow will produce ray deviations that will influence whether a particular ray passes or is blocked by the knife edge. An ancillary lens is usually used behind the knife edge to image a particular plane in the flow field. In many wind tunnel

pictures it is possible to observe the presence of turbulent boundary layers along the walls of the tunnel. Many other such schlieren-type systems have been used, and the brief description is given here to clarify the differences between standard schlieren techniques and the one we will now discuss.

The conditions of a conventional schlieren system cannot be found or generated in the context of CAT detection from aircraft but a related approach using an extended gradient source merits consideration (Figure 32). Because this has been referred to as a schlieren-type system, the differences between the two should be pointed out to avoid confusion. The source in the possible system is the earth's horizon. In spectral regions with small atmospheric absorption the radiance near the horizon will decrease rapidly with increasing angle from the tangent line to the earth. If this radiance gradient were sufficiently large, a knife edge could be used in the image plane of an airborne system to block direct radiation from the earth and the radiation reaching the detector after refraction by turbulence could then be detected. The most promising spectral region for such an approach is near 11μ where only weak continuum absorption by water vapor is present; this is also favorable on the basis of the earth's radiance. Working against these advantages is the small, but finite, radiance of the water vapor and the rather gradual fall-off in horizon radiance. From the data of Murcray and Brooks (Duncan, et al., 1965), we can see that an angle of several degrees from the horizon is required to reach the minimum background level (Figure 33).

To be able to detect and measure small angles (~10 arcseconds), a possible approach is to image the radiance gradient (or a portion thereof) and measure the redistribution of energy in the image due to turbulence.

To permit a qualitative assessment of this redistribution, a rather simplified horizon radiance function will be assumed initially and the conclusions from this analysis used to evaluate the more realistic case. The radiance near the horizon will be assumed to be of the form shown in Figure 34 with x the coordinate along the earth's radius perpendicular to the tangent and no variation along the y-direction perpendicular to both x and this tangent line.

We can see that a change in the radiance function will occur only for those regions where the radiance function is assymetrical over the effective angular width of the point-spread function (i.e., the second derivative of the radiance function must be different from zero). From the diagrams, we can see that only the earth-to-atmosphere and the tropopause transition regions have this required behavior. The horizon

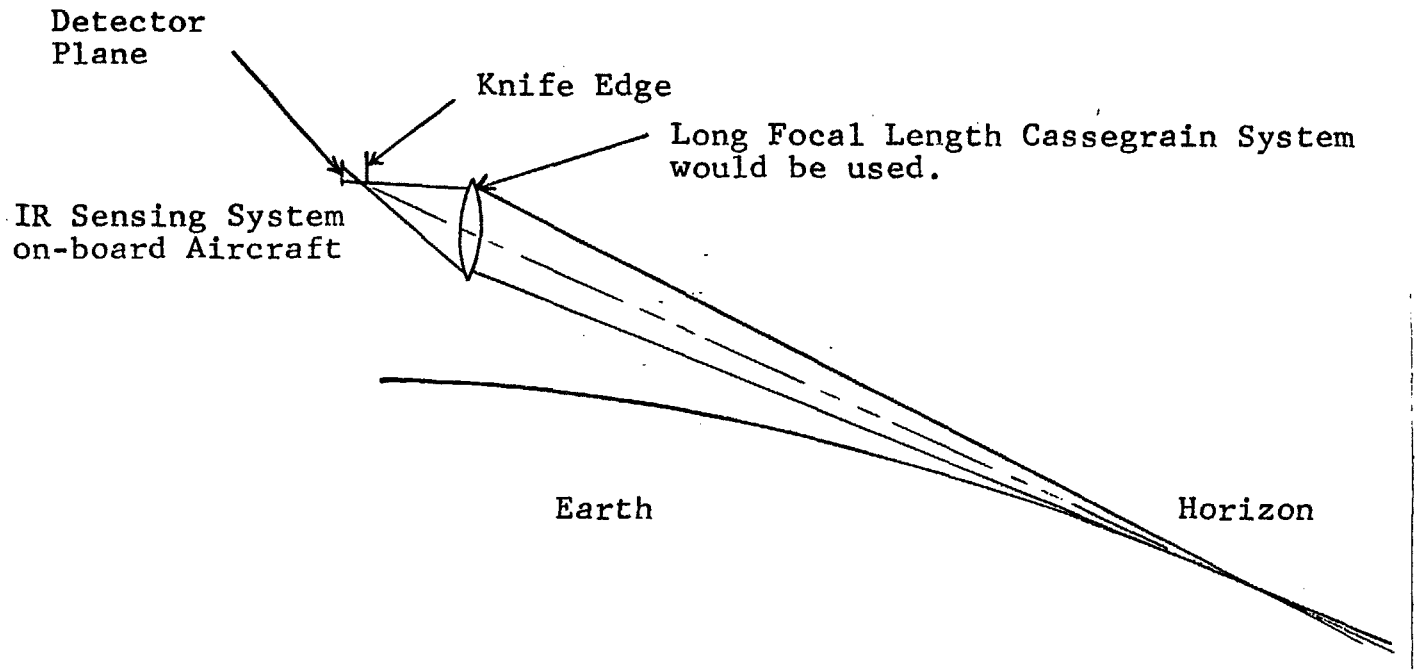

Figure 32 Schematic Diagram of Schlieren-Type System for CAT Detection

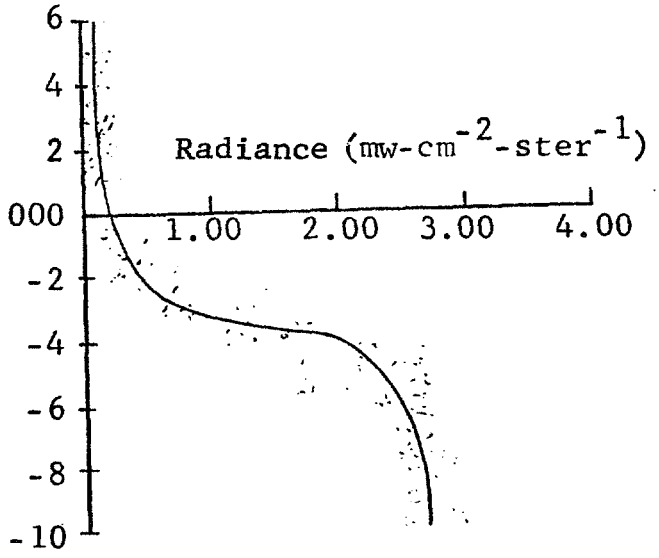

Radiance of the Earth's Horizon as Viewed from 27.1-km
Filter 5

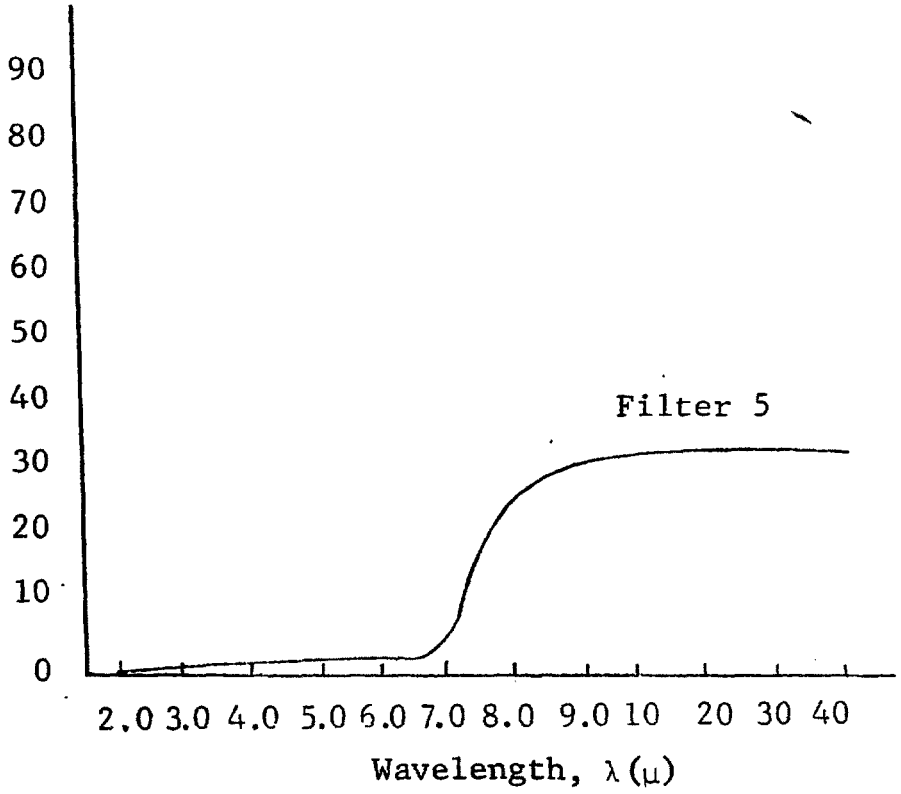

Figure 33 Filter Transmission Functions for the Radiometer of Murcray and Brooks (Duncan, et al., 1965)

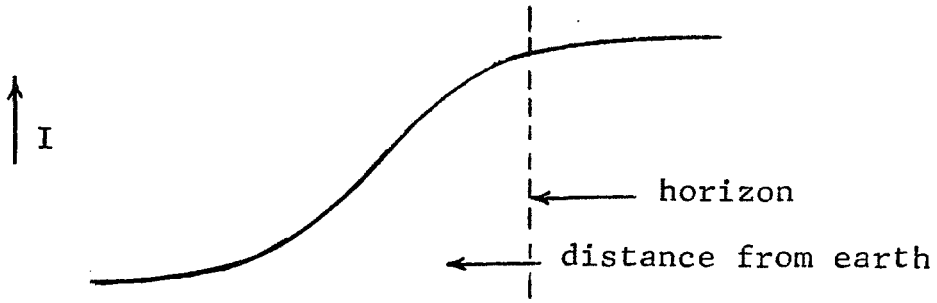

(a) Horizon Radiance Distribution

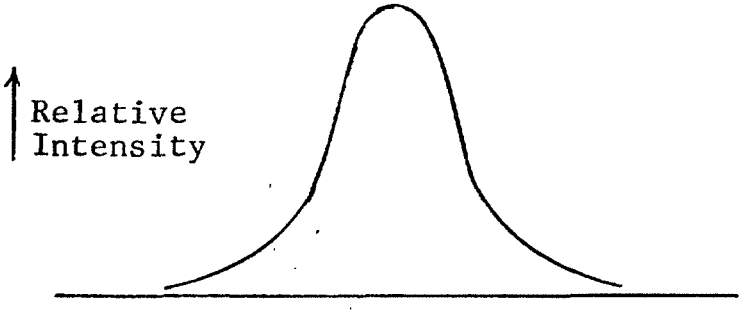

(b) Point Spread Function Due to Turbulence

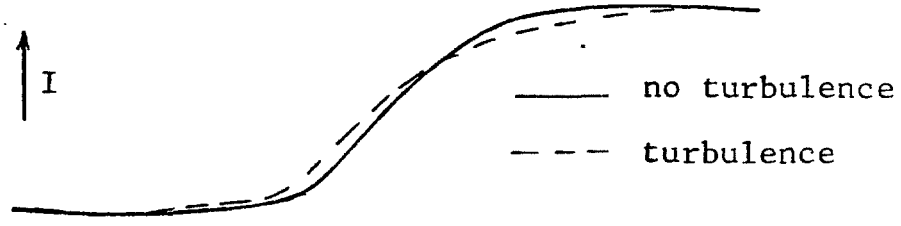

(c) Radiance Distribution in Image

Figure 34 Horizon Image Distribution

radiance calculated by Wark, et al. (1964), shown in Figure 35(a), has been partially replotted on an enlarged scale in Figure 35(b). From this we can see that, for angular regions exceeding the width of the turbulence point-spread function by a factor of three or more, the radiance function is so nearly linear that observable angular redistribution will not occur. The mean angular deviation due to turbulence would have to be about 10 to 20 arc-minutes for appreciable nonlinearities to exist. While the results for Murcray and Brooks were obtained at a higher altitude and with a broader spectral response than is the case for our approach, their curves also indicate the nonlinearities of the radiance function exist essentially only on a large angular scale. The rms deviation angle for a ray passing through a turbulent region can be estimated from the equation

$$\left[\overline{\Delta\alpha^2}\right]^{1/2} = \left[3b^{-1/3} \int_o^L C_n^2\,(x)dx\right]^{1/2}$$

given by Tatarski (1960). Here, b is the objective diameter and C_n is the refractive index structure constant. For a turbulent volume of length L and with constant C_n, the expression simplifies to

$$\left[\overline{\Delta\alpha^2}\right]^{1/2} = \left[3b^{-1/3}\, C_n^2\, L\right]^{1/2}.$$

Taking L equal to 50 km and C_n^2 equal to $10^{-16}\,\mathrm{cm}^{-2/3}$ gives a value for the deviation angle of (for 15-cm-diameter collector)

$$\left[\overline{\Delta\alpha^2}\right]^{1/2} = 2.5 \times 10^{-5} \text{ radian},$$

or ~5 arc-seconds. According to Atlas (1966), C_n ranges from 10^{-7} to 10^{-8} for CAT and the rms deviation should, therefore, fall in the range of 5 to 50 arc-seconds. With $C_n = 10^{-9}$ for the normal atmosphere, no appreciable contribution to this angle will come from the part of the path with no CAT. The total contribution should be of the same order as that from the CAT region and the rms angular deviation should, thus, be of the order of 5 to 50 arc-seconds.

To obtain an order of magnitude estimate of the redistribution, we can approximate the curve of Figure 35(b) by a gaussian. If we restrict ourselves to the portion between 2400 and 3600 arc-seconds, a reasonable fit is obtained with the equation

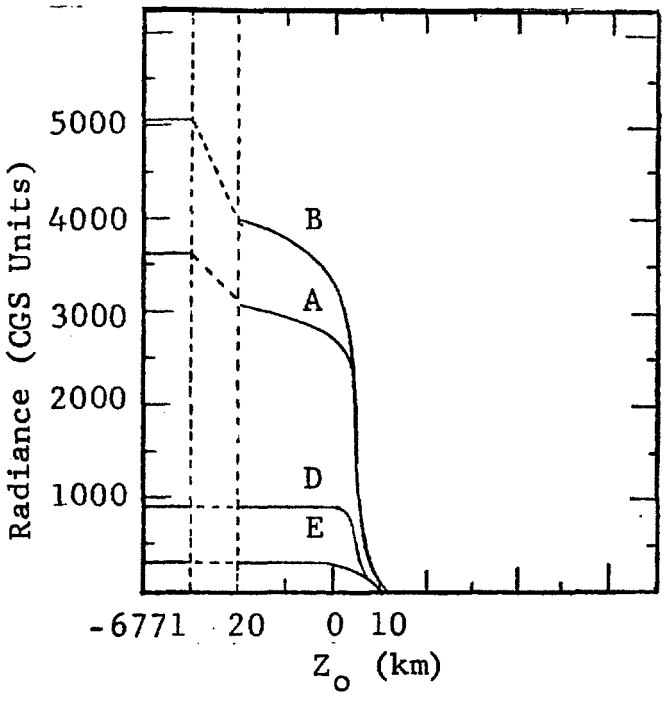

(a) Radiance Calculated by Wark, et al. (1964)

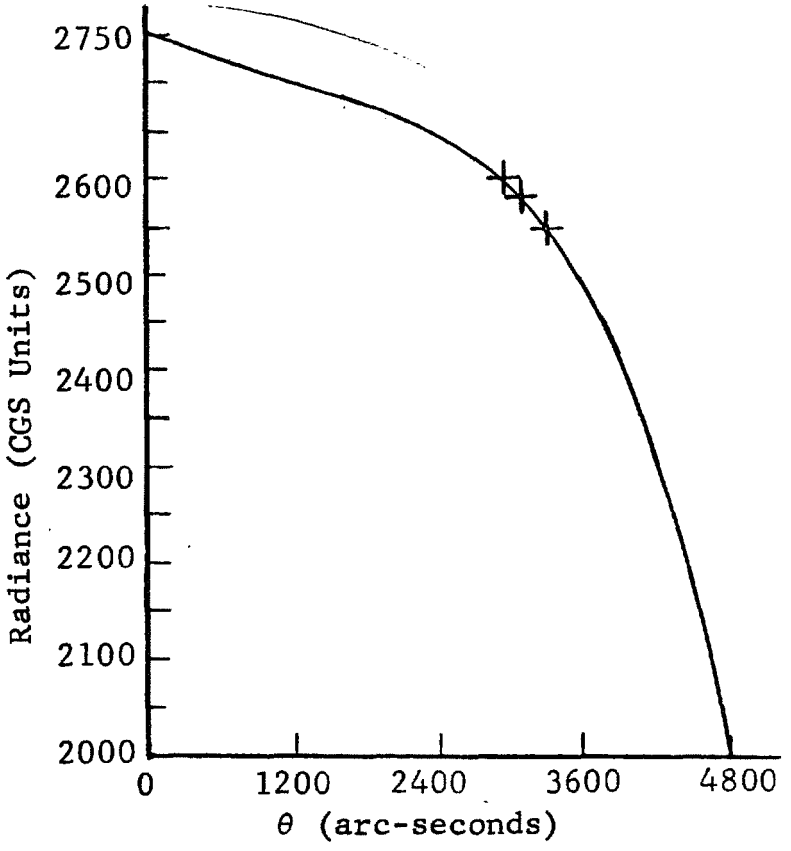

(b) Expanded Portion of a

Figure 35 Horizon Radiance

$$F(\theta) = 2790 \exp(-0.834 \times 10^{-8}\theta^2).$$

We are interested in the redistribution due to an rms angular deviation of 100 arc-seconds. Since no distribution occurs for a linear radiance function, we can estimate the observed change in the radiance function by calculating the departure of the function from a linear one over an angular distance of 200 arc-seconds. If values of 3000, 3100, and 3200 are used for θ, the calculated departure from linearity is about 0.1 percent; thus, we estimate the radiance change to be about

$$3 \times 10^{-7} \text{ watt/cm}^2 \text{ sterad}$$

for the example used. The curves for the other models used by Wark, et al., (1964) give a tenfold decrease in this and the atmosphere-space transition will give a value lower by two orders of magnitude.

From the point of view of the detectable power involved, we can use a collecting optics area of 200 cm^2 (15-cm collector) and a solid angle of 1×10^{-7} (to avoid spatial averaging) giving a change in the detected power of about 6×10^{-12} watt. As we have indicated, this value is about the maximum change we can expect, pointing out the impracticality of this technique in an operational system.

3.7 Measurement of Ozone Concentration

Redistribution of ozone by turbulence has been suggested as an indicator of CAT. Since ozone concentration does exhibit pronounced variation with altitude, such redistribution may well occur. A relationship between increased ozone concentration and is by no means clearly established, however. Some indications of a correlation have been found (Rosenberg, 1966) and we will, therefore, discuss the possibilities of using measurements of ozone concentration for CAT detection. Ozone has an absorption band at ~9.6μ, making thermal detection possible in view of the favorable Planck function for temperatures near 230°K. Before discussing the meteorological implications of ozone, it is instructive to estimate the kind of variation one might be able to detect.

The choice of system is between a radiometer responding to wavelengths in the entire absorption band and a narrow (0.1μ) band device either scanning the band or fixed at some point in the wings. This is a choice only in principle

because of the large amount of ozone along the path. This can be seen readily if we consider an aircraft altitude of 10 km; then the total path length through ozone is about 500 km. With a mean ozone mass of 0.01 cm NTP/km (Craig, 1965), this means that the absorption in all but the wings of the band is total. From the curves of Plass (1960), we can see that, for a total amount of ozone of 60 cm NTP and pressures of the order of 100 mm Hg any change in total ozone does not affect the band absorption noticeably unless the ozone change is very large. In other words, a radiometric system using the entire band will be completely insensitive to small changes occurring in a 30-km long volume. We can, therefore, use only wavelengths distant from the band center for our measurements.

Let us take a system with a 0.1μ bandpass, a collection angle of ω steradians, and also a volume of 30 km extent at 30-km range. We select a wavelength in the band such that the total absorption along the entire path is 50 percent. This is high enough to provide radiation, while still allowing us to approximate the atmosphere as optically thin in order to simplify calculation. If an appreciably greater absorption is chosen, then we are faced with the problem of insensitivity to ozone changes, (i.e., we can no longer use an average absorption coefficient even over the narrow region we are considering). If we choose a lower absorption then the radiance will be too small for detection. An assumption inherent in this approach is that a suitable averaged absorption coefficient can be used for the spectral bandwidth considered. We consider an isothermal path and neglect refraction. Assuming a temperature of 230°K and an absorptivity of 0.5 gives a total radiance of $R = 1 \times 10^{-4}$ watt/cm$^2\mu$ sterad near 9.6μ. With a spectral bandpass of 0.1μ and with $\omega = 2.5 \times 10^{-3}$ steradians, the irradiance at the detector will be $H = 2.5 \times 10^{-8}$ watt/cm^2. For the optically thin case we have assumed the 30-km long volume contributes 6 percent of the total irradiance. Calculations using Lambert's law yield a value of ~8 percent. The change in irradiance in response to a change in ozone concentration in the turbulent volume is thus given by $\Delta H = 0.06\ (\Delta n/n)\ H$. Substituting for the total irradiance, we get an irradiance change of $\Delta H = 1.5 \times 10^{-9}\ \delta n/n$ watt/cm^2. The noise-equivalent power density for an immersed thermistor bolometer can be taken as 1×10^{-9} watt/cm^2 for a 1-cps bandwidth. The minimum detectable ozone change that can be detected with a given S/N ratio is, therefore,

$$\frac{\Delta n}{n} = 0.67 \left(\frac{S}{N}\right).$$

With a cooled solid-state detector, an improvement of ~20 can possible be obtained, in which case $\Delta n/n = 0.03$ S/N. If a temperature difference is also associated with the turbulence volume, then the change in radiance due to a ΔT will be $\Delta H_T = (0.06\ \Delta\omega\lambda)(5.5R)(dT/T)$. With the previously used values for the instrumental constants, we obtain

$$\Delta H = 8 \times 10^{-9} \frac{dT}{T} \frac{watt}{cm^2} .$$

Since temperature fluctuations can be expected for turbulent volumes, the difficulty in making concentration measurements is apparent. This is one of the problems associated with all techniques using thermal radiation to measure gas concentration in the atmosphere.

The results of the calculations show that concentration differences would have to be of the order of 15 percent for detection with an acceptable S/N ratio. Any temperature changes occurring at the same time would either accentuate or mask this signal, depending on the sign of the temperature difference. It is thus apparent that measurement in the ozone band is not better than the thermal mapping approach. We must also consider that temperature gradients not associated with the turbulence are found many times (Endlich and Mancuso, 1964). In such cases, the possibility of obtaining ozone-concentration differences would be nonexistent.

The use of ozone as a tracer of atmospheric motions has been advocated for some time and correlations of vertical ozone distribution, total ozone, and large scale atmospheric motions have been established, at least qualitatively (Paetzold, 1953; 1955). The deposition of ozone in troughs of atmospheric waves has been predicted theoretically and agreement with measurements has been established (Bekoryukov 1965). The relationship between tropopause height and vertical ozone distribution has been under intensive investigation, with the results of Breiland (1964) being a good example. Breiland analyzed the soundings from 11 North American stations and obtained an excellent description of the behavior of ozone in relation to the temperature structure of the atmosphere. The results clearly show the influence of single and double tropopause on the vertical distribution of ozone.

Since the altitude of the tropopause depends on latitude and season, rather large variations of ozone can be expected for any fixed geometric altitude and geographic location. From the extensive measurements of vertical ozone,

we conclude that relatively small differences in altitude can give rise to relatively large differences in ozone concentrations. On the basis of Breiland's results, for example, the ozone concentration can increase by a factor or three or more in going from one kilometer below to one kilometer above the tropopause. From the extensive ozonesonde measurements we conclude that, at jet cruising altitude, small changes in relation to the tropopause can give rise to relatively large changes in ozone concentration. This is shown clearly in Figure 36, which is based on results presented by Brabets, et al., (1963), who measured the ozone concentration in the cabin of a commercial jet at cruising altitude of 35,000 ft. The cabin concentration has been shown to reflect the external ozone, and changes in a matter of 10 minutes can be rather large. We, therefore, conclude that the measurement of ozone variations is not attractive for CAT detection. Even if it can be demonstrated that there is a high correlation between increased ozone concentration and CAT, too many complicating phenomena will still exist for remote radiometric detection to comprise an operational system.

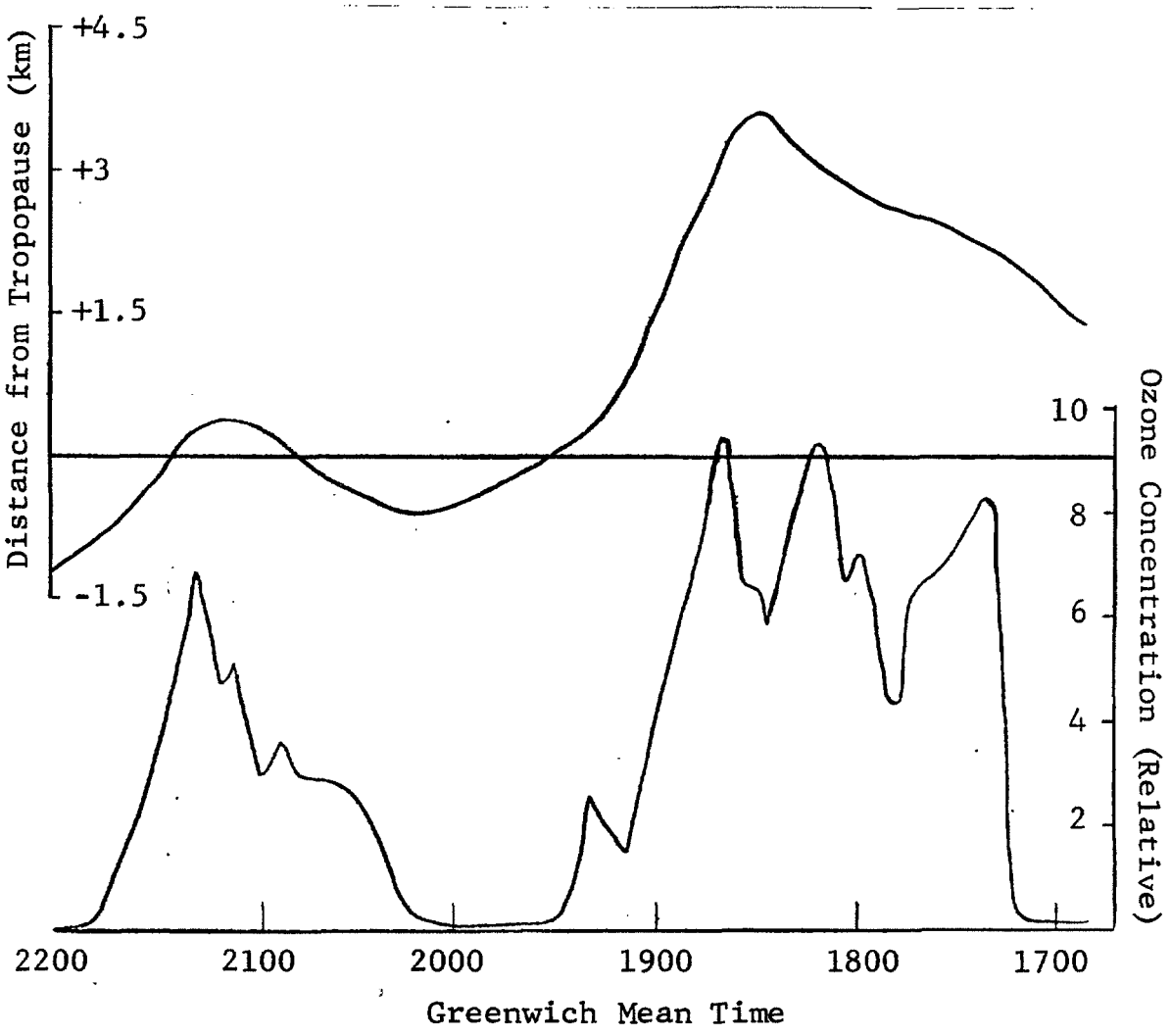

Figure 36 Ozone Concentration in Relation to Tropopause

4. CONCLUSIONS

The objective of this program was to find a way for providing an aircraft with advanced warning of CAT, using passive optical-detection techniques. These techniques were required to provided information to the direction, distance, size, and shape of the turbulent region.

Preparatory to the study of specific techniques it was necessary to analyze the optical characteristics of CAT, insofar as these could be determined, and the optical characteristics of the atmosphere itself. The optical characteristics of CAT are not well known, and experimental measurements and further theoretical work are urgently needed. A survey of the literature was conducted and calculations were made to determine the density, temperature, and refractive-index fluctuations that are associated with CAT. The evaluation of some of the detection techniques rests heavily on these estimates.

The techniques of passive optical detection that were evaluated were:

- Detection of spatial nonuniformities in Rayleigh scattered sunlight.
- Application of two detector systems with crossed fields-of-view to the detection of scattered sunlight. This system would permit distance information to be obtained.
- Relative movement of stellar images.
- Stellar scintillation.
- Detection of thermal emission from the atmosphere. Included here are consideration both of a temperature difference associated with a CAT region, temperature gradients, and/or increased ozone concentrations.
- Schlieren-type system using the earth's infrared horizon as the source.

Two of these techniques, the detection of density fluctuations by measurements of scattered sunlight and starlight scintillation, are sufficiently promising to warrant further experimental investigation. Although neither technique has 24-hour, all-weather capability, they are complementary in that measurements of scattered sunlight can obviously be made only during the day, while signal/noise requirements will, in general, limit the stellar

scintillation method to nighttime use. Similar collecting optics could be used for both systems as described in Appendix B, although different detectors are required because of the widely different signal levels involved.

A major problem in the application of the crossed-beam technique also using scattered sunlight is the shortness of the baseline that can be utilized. The maximum length of baseline for forward remote detection, necessary in a remote warning system, will be the wingspan of the aircraft. Differential twisting of the wings of the aircraft would also cause difficulties, which are difficult to estimate since information on this type of effect is not available. The crossed-beam technique could, however, be utilized to measure the optical characteristics of CAT.

Measurement of the relative motions of stellar images, discussed in Section 3.4, was eliminated from consideration because of the severe practical difficulties involved in acquiring and tracking at least two stars simultaneously with accuracies of a few seconds of arc.

The infrared Schlieren method utilizing the earth's horizon as a source, was found too insensitive to be practical. The second derivative of the function giving the horizon radiance as a function of altitude is too small for measureable changes in signal to be produced by refraction of radiation in turbulent regions.

Remote sensing of temperature ahead of an aircraft with an infrared radiometer or scanning spectrophotometer was evaluated in detail on the basis of temperature records obtained in Project Jet Stream Flights. This technique looks rather unpromising as does the remote detection of increased ozone concentrations which may be associated with CAT.

With regard to these last two techniques in particular, it is extremely doubtful that adequate correlation exists for reliable CAT detection. McLean (1965) has shown very clearly that temperature variations of the relatively large scale nature required for remote measurements to be possible are associated with jet fronts or other types of weather front rather than with clear air turbulence per se. This would lead to unacceptibly high false-alarm rates. Increase in ozone concentration has been frequently associated with changes in altitude of the tropopause rather than with CAT.

It has not been possible on this study contract to determine a passive optical technique for remote detection

of CAT, that needs only to be instrumented and installed on commercial aircraft as "the CAT detector."

We recommend that an airborne program be conducted to obtain more information on the characteristics of CAT as they relate to the techniques we have examined. This investigation should concern itself primarily with measurements relating to the most promising approaches: fluctuations in scattered sunlight and stellar scintillation. The preliminary design of an instrument to make such measurements is given in Appendix B. Remote detection of temperature gradients ahead of an aircraft by infrared radiometry should also be actively persued. Although it has been shown in this report that this techniques has many difficulties and uncertainties associated with both the measurements and in the interpretation of the results, it could, allied with other detection devices, become a part of a CAT warning system of the future.

The data needed to adequately evaluate these techniques would best be gathered in an experimental program. It has been established in experiments conducted by IIT Research Institute on NASA contract NAS8-20107 that fluctuations in scattered sunlight can be measured. Appendix A discusses these measurements and describes the way in which the cross-correlation of these fluctuations could be used to measure the characteristics of clear air turbulence which are presently rather badly defined.

Ground-based measurements of stellar scintillation are not adequate to determine the results that would be obtained in scintillation measurements from aircraft flying at high altitudes. Although saturation effects may occur which would limit the ability of the measurements to detect the presence of a region of CAT in the line of sight, this uncertainty can only be satisfactorily resolved by experimental measurements.

In conclusion it is very important to realize that the techniques described in this report are not capable of detecting CAT per se, but of detecting assumed characteristics of CAT. The relationship between these assumed characteristics and CAT as it interacts with an aircraft is not clearly determined. It is not sufficient in a CAT pilot warning system to have a device which indicates that a CAT region may be present in the vicinity of the aircraft flight path. To divert an aircraft from its planned flight path on the basis of remote CAT detection, the detector must be able to determine the intensity of the turbulence as it will affect the aircraft and, it must have a low false alarm rate.

Quite clearly the relationships between CAT and associated characteristics has to be further explored, but the cause is not advanced by the publicity releases that have occurred recently that implied that a infrared CAT pilot warning system is just around the corner.

REFERENCES

Astheimer, R. W. (1964), "An IR Technique for the Remote Detection of CAT," Proceeding Third Symposium on Remote Sensing of Environment, p. 105, U. Michigan Report #4864-9-X February 1965.

Atlas, D., Hardy, R., and Naito, K., (1966a), "Optimizing the Radar Detection of Clear Air Turbulence," J. App. Met. 5, 450-460.

Atlas, D., Hardy, K. R., Glover, K. M., Katz, I., and Konrad, T. G., (1966b), "Tropopause Detected by Radar," Science 153, Sept. 1966.

Bekoryukov, V. I., "Theory of Transport of Atmospheric Ozone in the Presence of Long Waves," Atmospheric and Oceanic Physics," (Izvestia Acad. Science USSR) 1, 521 (1965).

Brabets, R I. et al (1963), "Ozone Measurements in Current Jet Aircraft," Paper No. 63-235 presented at the AIAA Summer Meeting 1963.

Breiland, J G., "Vertical Distribution of Atmospheric Ozone and its Relation to Synoptic Meteorological Conditions," Jl. Geophys. Res. 69, 3801 (1964).

Bullrich, K., in Advances in Geophysics Vol. 10, New York; Academic Press, 1964, p. 99.

Burns, A., and Rider, C., Power Spectral Measurements of CAT Associated with Jet Streams, Project TOPCAT, Royal Aircraft Establishment, TR 65210, September 1965.

Clark, W. M., "High Altitude Daytime Sky Background Measurements Program," 1964, AFAL TDR 64-134, Part I.

Colson, De Ver (1966), "Nature and Intensity of Clear Air Turbulence," Proceeding ION/SAE Clear Air Turbulence Meeting 1966, p. 1.

Craig, R. A., The Upper Atmosphere: Meteorology and Physics, Academic Press, New York 1965, p. 187.

Duncan, J. C., Astronomy, (Harper & Bros. 1930), p. 412.

Duncan, J. et al (1965), "Infrared Horizon Sensors," U. of Michigan Report No. 2389-80-T, April 1965.

Endlich, R. M. and McLean, G. S. (1964), "Studies of the Climatology of Winds, Temperature and Turbulence in Jet Streams," AFCRL 64-834.

Fisher, M. J., and Krause, F. R., "The Crossed-Beam Correlation Technique," J. Fluid Mechanics, 1967, 28, 705.

Fusca, J. A. (1964), "Clear Air Turbulence," Space/Aeronautics August 1964, p. 60.

Gebel, R. K. H., in Advances in Electronics and Electron Physics, Vol. XVI (Academic Press 1962) p. 459.

Glagolev, Yu. A., "Experimental Data on the Microstructure of the Temperature Field at Heights of 20-30 Km", Bull. Academy of Sciences USSR, Geophysics Series No. 6, 1964, p. 579.

Gracheva, M. E., and Gurvich, A. S., Radiofizika (in press).

Greene, J., et al., "Early Warning of Clear Air Turbulence by Photometric Measurements", National Air Meeting on Clear Air Turbulence, p. 163.

Hardrath, H. F., "Some Factors Affecting Fatigue of Aircraft Structures", Proceedings of Conference on Aircraft Operating Problems, May 10-12, 1965, NASA SP-83, p. 37.

Hardy, K. R., Atlas, D. and Glover, K. M., (1966), "Multiwavelength Backscatter from the Clear Atmosphere," J. Geophys. Res. 71, 1537-1552.

Hufnagel, R. E. and Stanley, N. R. (1964), "Modulation Transfer Function Associated with Image Transmission through Turbulent Media," J. Opt. Soc. Am. 54, 52-61.

Hughes, J. V., "Sky Brightness as a Function of Altitude," Applied Optics, 3, 1964, 1135.

Johnson, G., and Montgomery, A. J., Survey of Detectors and Dynamic Calibration Methods for Remote Sensing Systems NASA Contractor Report, 1967, NASA CR-751.

Kadlec, P. W. (1965), "Flight Data Analysis of the Relationship Between Atmospheric Temperature Change and CAT," Eastern Airlines, Final Report Contract Cwb-10888, June 1965.

Keller, G., "Relation Between the Structure of Stellar Shadow Band Patterns and Stellar Scintillation," J. Opt. Soc. Am., 1955 45, 845.

Lloyd, J. W. F., et al., "Day Sky Intensity from 20 Km to 90 Km at 5500 A," Applied Optics, 1965, 4, 1602.

MacCready, Jr., P. B., et al., "Operational Application of a Universal Turbulence Measuring System," NASA CR-62025, November 1965, p. 10.

Mather, G K., Flight Evaluation of an IR Spectrometer as a CAT Detector, Aeronautical Rpt. No. LR-477, National Aeronautical Establishment (Canada), May 1967, AD 819 533.

McLean, G S (1965), "An Investigation into the Use of Temperature Gradients as an In-Flight Warning of Impending CAT," AFCRL 65-117.

Megaw, E. C. S., (1957), "Fundamental Radio Scatter Propagation Theory," Proc. IEE 104C, 441-455.

Merritt, E. S. and Wexler, R. (1964), "Radiometric Detection of CAT," Proceedings Third Symposium on Remote Sensing of Environment, p. 125, U. Michigan Report No. 4863-9-X, February 1965.

Mie, G., Ann der Physik, (4), 1908, 25, 377.

Montgomery, A. J., "Remote Sensing of Winds and Atmospheric Turbulence by Cross-Correlation of Passive Optical Signals," Proceedings of the Panel on Remote Atmospheric Probing of the National Academy of Sciences, Washington, D. C. (in press).

Munick, R. J. (1965), "Turbulent Backscatter of Light," J. Opt. Soc. Am. 55, 893 (1965).

Norman, S M. and Macoy, N. H., "Remote Detection of CAT by means of an Airborne Infrared System," AIAA Paper #65-459, presented at AIAA Meeting in San Francisco, July 1965.

Obukhov, A. M. (1959), "On the Influence of Buoyancy Forces on the Structure of the Temperature Field in a Turbulent Flow," Doklady Akad. Nauk, SSSR, 125, 1246.

Paetzold, H. K., "The Mean Vertical Ozone Distribution Resulting from the Photochemical Equilibrium, Turbulence and Currents of Air," Jl. Atm. and Terr. Physics 3, 125 (1953).

Paetzold, H. K. "New Experimental and Theoretical Investigations on the Atmospheric Ozone Layer," Jl. Atm. and Terr. Physics 7, 128 (1955).

Panofsky, H. A. (1965), "The Fine Scale Structure of the Atmosphere Above the Surface Layer in Clear Air," Paper presented at the URSI-UGGI Colloquium, Moscos 1965.

Plass, G. N., "Useful Presentations for Measurements of Spectral Band Absorption," Jl. Opt. Soc. Am. 50, 868 (1960).

Protheroe, W. M. (1955), "Stellar Shadow Patterns and Scintillation," J. Opt. Soc. Am. 45, 851-855.

Quasius, G. and McConless, F. (1966), "Star Trackers and Systems Design," Washington: Spartan Books.

Ragland, S. et al., "Simulation and Effects of Severe Turbulence on Jet Airline Pilots", NADCL-ML-6411, August 1964, p. 8.

Reiger, S. H., "Starlight Scintillation and Atmospheric Turbulence," Astron. Jl. 68, 395 (1963).

Reiter, E. R., "Clear Air Turbulence: Problems and Solutions," Proceedings National Air Meeting on Clear Air Turbulence, February 1966, (Society of Automotive Engineers, publ.) p. 5.

Reiter, E. R. and Burns, A. (1966), "The Structure of Clear Air Turbulence Derived from "TOPCAT" Aircraft Measurements," J. Atmos. Sci. 23 (2) 206-212.

Rosenberg, P., "CAT Detection and Warning", Proceedings National Air Meeting on CAT, February 1966 (Soc. of Automotive Engineers, publ.) p. 40.

Rytov, S. M. (1937), "Diffraction of Light by Ultrasonic Waves," Izv. Akad. Nauk SSSR, Ser. Fiz., No. 2, 223.

Sandomirskii, A B., et al., "Seasoned Brightness Variations at Altitudes up to 17.5 Km," Bull. Acad. Sciences USSR Geophysics Ser. No. 7, 1964, p. 679.

Stephens, J. J and Reiter, E. R. (1966), "Estimating Refractive Index Spectra in Regions of Clear Air Turbulence," U. of Texas Report No. P-12, NASA Grant NGR 44-012-048.

Tatarski, V. I. (1960), "Radiophysical Methods for the Investigation of Atmospheric Turbulence," Radiofizika 3 (4), 551-583.

Tatarski, V. I. (1961), "Wave Propagation in a Turbulent Medium," New York, McGraw-Hill Book Company.

Tatarski, V. I., "On Strong Fluctuations of Light Wave Parameters in a Turbulent Medium," Soviet Physics JETP, 1966, 22, 5.

Valley, S., ed., Handbook of Geophysics and Space Environments, New York: McGraw-Hill Co., 1965, p. 7-1.

Van de Hulst, H. C., Light Scattering by Small Particles, New York: Wiley & Sons, 1957, Chpt. 6.

Vinnichenko, N. K. et al., Some Data on Turbulence in the Upper Troposphere and Stratosphere Causing Airplane Buffeting, Meteorology and Hydrology, No. 11, November 1966, p. 35.

Volz, F. E., and Goody, R. M., J. Atm. Sciences, 1962, 19, 385.

Wark, D Q. et al (1964), "Variation of the IR Spectral Radiance Near the Limb of the Earth," Applied Optics 3, 221.

Wilkins, E. (1963), "Decay Rates for Turbulent Energy Through the Atmosphere " J. Atmos. Sci. 20, 473-476.

Willstrop, R. V., Absolute Measures of Stellar Radiation, Monthly Notices Royal Astronomical Soc. 121, 17 (1960).

APPENDIX A

Crossed-Beam Technique as a General Method of CAT Studies. The crossed-beam technique, which has been developed by IIT Research Institute and NASA Marshall Space Flight Center for the measurement of turbulence properties of air jets, rocket exhausts, and for atmospheric studies, has possible application to the detection of CAT. Mounting optical systems on the wing tip of an aircraft and crossing the fields-of-view some distance ahead of the aircraft has been previously considered in this report, but the short baseline and wing-tip torsional flexing pose some severe problems. Since, at the present time, direct measurements of CAT are lacking, application of the crossed-beam technique to study clear air turbulence generally would provide useful data. Such data would then permit better evaluations of proposed techniques for a CAT aircraft warning system. For this reason, we will consider how the crossed-beam technique could be used to measure the characteristics of clear air turbulence regions.

The validity of the crossed-beam techniques has been verified experimentally by measurements of turbulence properties of subsonic jets and by comparison of these results with hot-wire measurements. It is a powerful, remote sensing method provided that the experiment can be arranged in such a way that the fluctuations that are correlated between the two beams can be extracted from the uncorrelated portion of the signals within reasonable integration times. The ability to do this depends on the number of eddies along the fields-of-view, and also on the way in which the fluctuations along the fields-of-view contribute to the integrated signal. For example, with a ground-based system measuring scattered sunlight, the radiation scattered into the field-of-view of the detector will be weighted heavily toward the lower part of the troposphere because of the larger concentrations of both air molecules and aerosol particles. Similarly, for the same degree of turbulence the fluctuations would be greater at low altitudes in the same proportion as the mean signal contribution.

Before proceeding to discuss more details of methods suitable for CAT detection, we will define the turbulence properties of interest that may be measured using the crossed-beam technique. The mathematical basis of the method is given by Fisher and Krause (1967), who also describe some experimental results for the shear layer of a subsonic jet. The turbulent properties that can be

measured may be divided into two categories -- kinetic and dynamic properties. The kinetic properties are the convection speeds, eddy scales, eddy lifetimes, turbulent spectra, and so on. The dynamic properties relate to the magnitudes of the density, temperature, or pressure fluctuations in the fields-of-view of the detectors which produce the fluctuating signal. In the first case, it is largely immaterial what produces the fluctuations provided only that movements of the tracer follow the general movements of air that we are trying to measure. If, for example, a large contribution to the detected fluctuations is made by aerosol particles, then the distribution of eddy sizes will be different from that measured if the air molecules themselves were the major contributors. Owing to their mass and inertia, larger aerosol particles will be able to follow the movements associated with the larger eddies but not those of smaller eddies.

In the case of the atmosphere in general, and clear air turbulence in particular, there are no pressure variations associated with air turbulence. Air flow in the atmosphere is always highly subsonic, which means that density variations associated with turbulence are directly related to temperature variations. To measure directly the strength of the turbulence we need to be able to measure density variations directly or, if a tracer is used, the tracer concentration variations must be similar to the air density variations. Vertical winds could also be measured.

Experimental Measurements. The experimental configuration in the atmospheric crossed-beam experiments carried out to date is shown in Figure A1. The two photometers detect fluctuations in scattered sunlight caused by fluctuations in concentrations of aerosols and air molecules. Direct sunlight will be scattered by molecules and aerosols in the field-of-view of the detector so if there is a density increase or increase in concentration of aerosols in a volume element of the field-of-view, there will be an incremental increase in the direct scattered signal. However, light scattered into the field-of-view at higher altitudes may be scattered out of the beam and an increase in density or aerosol concentration in a volume element would therefore cause a decrease in detector signal. In addition there will be a contribution from multiple scattering into the 'beam'. The relative values of these different contributions will depend strongly on the atmospheric conditions and the angle of the sun with respect to the direction of view of the photometers.

APPENDIX A

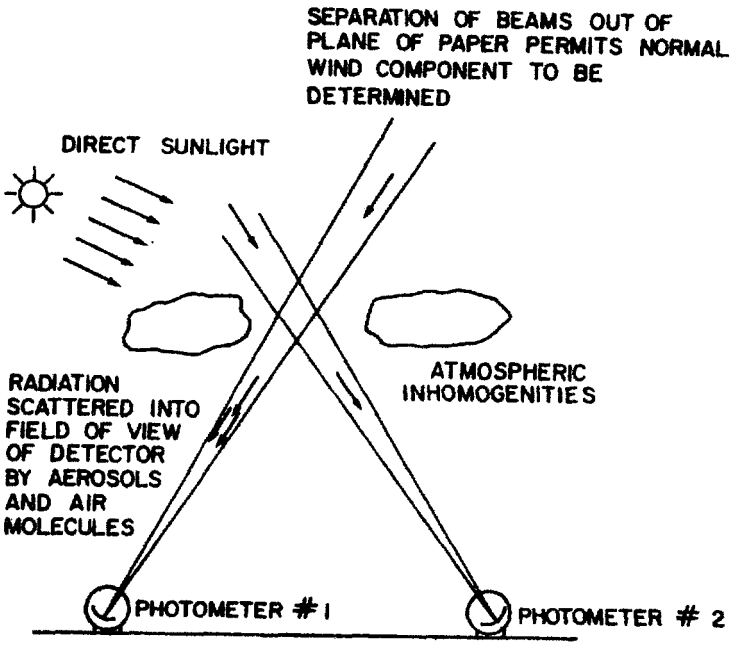

Figure A1 Application of Crossed Beam Technique to Measurement of Atmospheric Winds and Turbulence

If the direct scattered sunlight predominates it would be possible to obtain a positive correlation even in the complete absence of fluctuations in scatterer concentration in the region of the beam intersection point. The sunlight reaching this region has traversed a long path through the atmosphere and therefore there will be intensity fluctuations. Similar fluctuations will be present in the scattered sunlight which could result in a significant correlation between the two detected signals. However, when there is a lateral separation between the two beams as is necessary in wind measurement, this effect is minimized.

The photometer systems used in the atmospheric measurements of scattered sunlight have the following specifications:

APPENDIX A

Frequency Response	Variable within range 0.01 - 300 Hz
Mean Signal/Rms Noise	10^4
Field of View	5-30 minutes of arc
Spectral Response	0.7-1 micron
Spectral Bandpass	Variable (minimum 500 A)

Power spectral density measurements of the fluctuations under clear sky conditions are shown in Figures A2, and in Figure A3 these results are replotted with the ordinate - power spectral density x frequency. In this second plot the area underneath the curve in a particular frequency

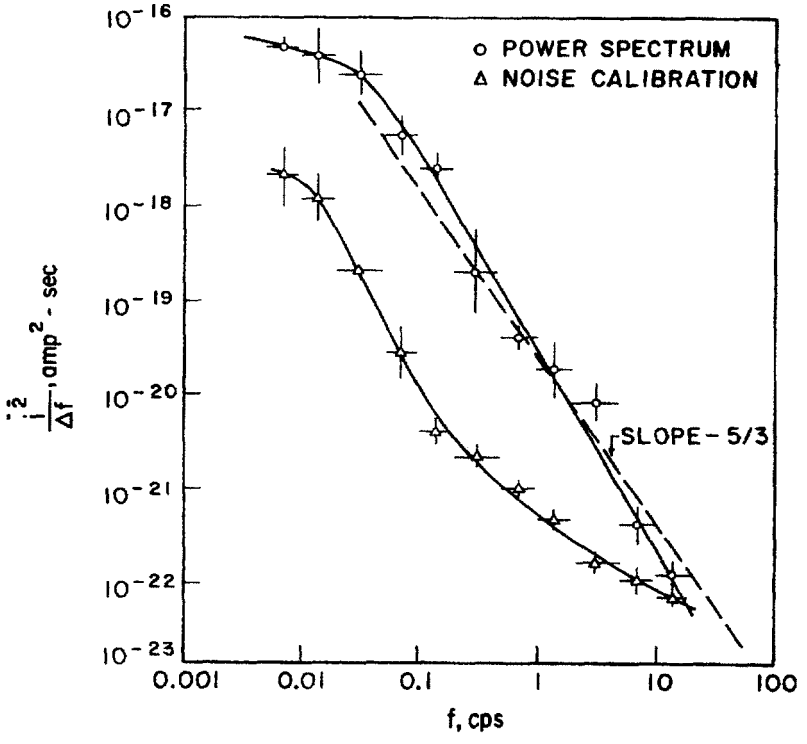

Figure A2 Single Beam Power Spectrum $\frac{i^2}{4f}$ vs f

interval, f, is directly proportional to the energy in this frequency interval. These results were obtained by playing back the recorded signals through a variable bandpass filter and measuring the output level with a RMS voltmeter. It can be seen that the fluctuations follow quite closely a -6.5 power law down to frequencies less than 0.1 cycles per second. The roll off beyond 0.01 cycles per second is due in part to the high pass filter which reduces the amplitude of the signal 3db at 0.01 cycles per second and winds down at the rate of 6db per octave.

A line of slope -5/3 is also shown in Figure A2 and it is evident that the results differ significantly from the -5/3 dependence that would be expected in point

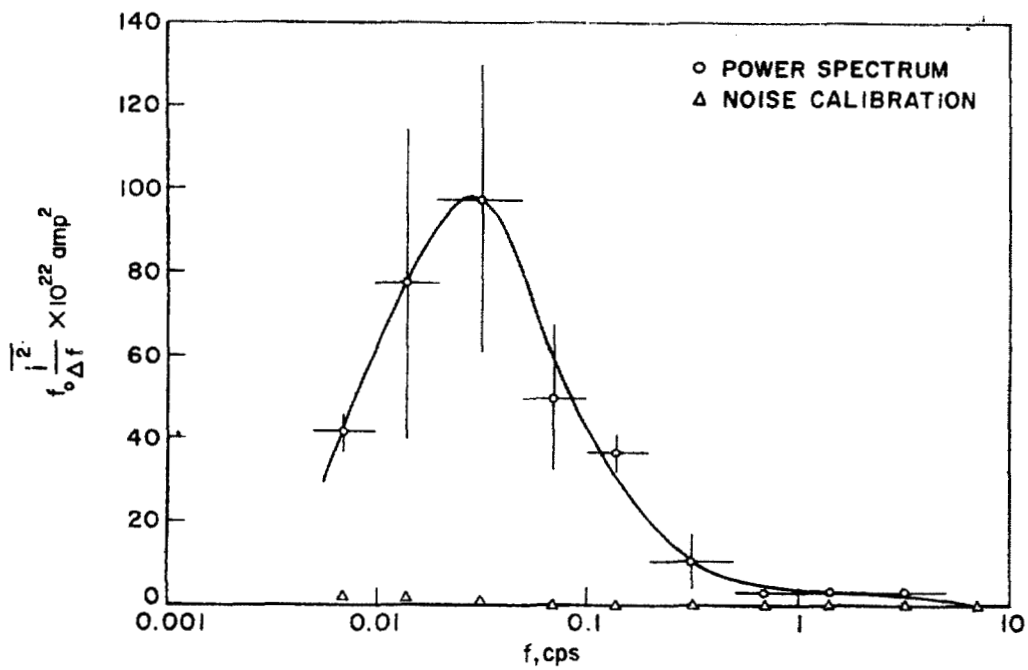

Figure A3 Single-Beam Power Spectrum, fo $\frac{\overline{i^2}}{4f}$ vs f

measurements. This is not an unexpected result because of the integration along the line of sight. The contribution of an eddy, being convected through the field-of-view of the photometer system, to the fluctuating signal will be proportional to both the variation in the number of scatterers associated with the eddy, and the size of the eddy measured along the field-of-view of the detecting system. Because the contributions from different eddies are uncorrelated then the resulting rms fluctuation from n eddies along the line of sight will only be $\sqrt{n}$ times the contribution of a single eddy. This intuitive argument would indicate that a -8/3 power law might be expected. At this time there is no proven explanation of the -6.5/3 power law that is actually measured, however, if the turbulent eddies were elongated in the flow direction, such a reduction in the power dependence could be observed. The effect of the increase in eddy scales and the decrease in the magnitude of the fluctuations with altitude would also be expected to change the power spectrum, but no attempt has yet been made to study the way in which these variables would effect it.

Crossed-Beam Measurements of Winds. Since atmospheric crossed-beam measurements detecting scattered sunlight are continuing at the present time this discussion is a status report of the results obtained to date. Successful wind measurements have been made, and this success has gone hand in hand with the development of suitable statistical methods to reduce the effects of non-stationarity in the data.

The geometry of the crossed-beam arrangement used in the atmospheric tests is shown in Figure A4. The location and viewing direction of the photometers are usually made to lie in two parallel vertical planes which are chosen to be approximately perpendicular to the wind direction. Most of the measurements to date have been made with the two beams crossed at an altitude corresponding to the top of the meteorological tower. Thus a direct comparison between the wind measured with an anemometer on top of the tower and that obtained from the crossed-beam measurements is possible. It should be noted that the altitude at which the wind is in fact measured depends on the wind direction. If the wind direction is perpendicular to the parallel vertical planes containing the lines of sight of the detector systems, then the altitude of measurement will be the height at which the beams would intersect if the two vertical planes were coincident. For all other wind directions an

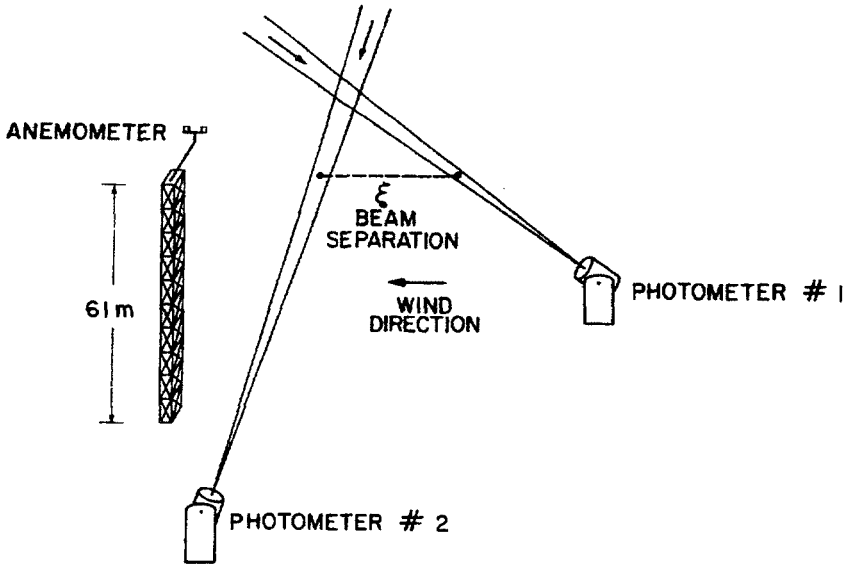

Figure A4 Geometry at Atmospheric Crossed Beam Arrangement

eddy can only traverse both 'beams' at a different altitude determined by the angle between the beams and the wind direction. Since in a practical case both the wind speed and the wind direction will be varying, the result obtained with the crossed-beam system represents a complex type of averaging over both altitude and time. If the wind direction is fairly constant within $\pm$ 20° of the plane of the beams then the altitude region over which the averaging will take place will be small, and the crossed-beam measurement can be considered to yield an average wind velocity at the crossing altitude.

Before describing some of the experimental results that have been obtained some comments about the fluctuation records, and the data processing are in order. Under clear skies the signal fluctuations with a bandpass from 0.01 - 10 Hz are typically of the order of 1% of the mean signal level. Although this fact is not completely established, the fluctuation levels appear to be less after a rain when the ground is still damp. This is not at all unlikely since the aerosol concentrations near the ground would be lower under these circumstances. In a 45 minute record it is

usually found that there are portions of the record in which the fluctuation level is considerably higher than the average. Sometimes there is an obvious cause for this, such as a car going by on a nearby dirt road raising a considerable dust cloud which drifts through the detector field-of-view. At other times there is no apparent reason for the increased activity. In any case, if a straight averaging procedure were used in the data processing, the portions of the record in which the fluctuations are large tend to dominate the correlation results.

To avoid this problem the data are processed in the computer in 6 minute segments, and the time averaged cross product is normalized with respect to the rms levels in that segment of the record before the pieces are averaged through the entire record. In other words, the correlation function is found for each segment and this procedure successfully prevents any particular piece from dominating the entire record.

Despite these precautions, spurious correlations are still sometimes obtained which make identification of the peak in the correlation function corresponding to the wind speed ambiguous. The so-called statistical error is utilized to help solve this problem. In simple terms a correlation function is found for each six minute piece of data throughout the record. These correlation functions are averaged and the rms variation in the value of the correlation function is found for each time delay. It is this rms variations, suitably weighted to obtain the desired statistical certainty in the result, which is called the statistical error.

Ideally, if a stationary situation existed, the statistical error would decrease as the square root of the number of pieces included; however, it is found in the atmospheric data that the error begins to decrease, but after some time period (usually between 30 minutes and one hour) the error either oscillates or starts to increase again. The integration time is therefore chosen as the time in which the statistical error reaches its minimum value.

Figure (A5-A8) shows some of the results obtained. Figure A5 is the result for a zero separation case with the fields-of-view of the two detectors intersecting at an altitude corresponding to the top of the meteorological

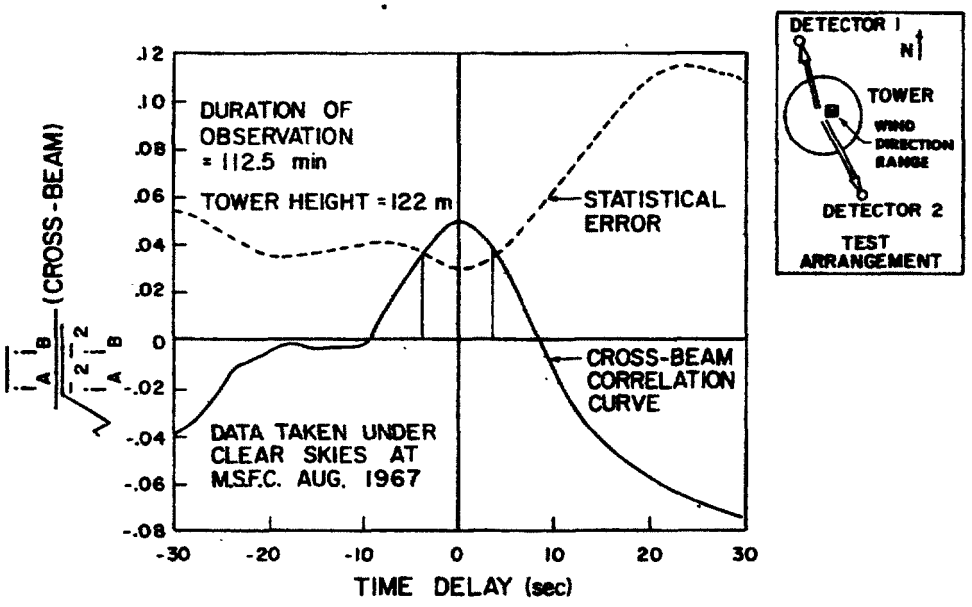

Figure A5 Cross Correlation Function - Zero Beam Separation

tower at MSFC. No wind information is of course available from this measurement. The correlation coefficient is quite small 0.05 and the peak only slightly exceeds the statistical error. However, the peak does occur accurately at t = 0 as would be expected in this measurement. The statistical error is associated, of course, with the value of the correlation function; hence with a 90% probability, the correlation function at zero time delay is 0.05 ± 0.03. This statistical probability results from the choice of weighing factor applied to the rms variations in the correlation function. Plotting the results in this manner is used for ease of presentation.

The remaining wind measurements were made at the Colorado State University meteorological test site in the North Platte River Valley, located in northeastern Colorado, approximately fifteen miles east of the first major pressure rise of the Rocky Mountains.

Figure A6 shows the anemometer data plotted as a first order probability density of velocity, and the correlation function plotted in terms of a wind velocity. Since the beam separation was 30 meters the long tail of the cross-correlation curve represents delay times from 2.5 to 5 seconds as compared with the 5-30 second time delay range covered by the peak. Thus this tail results from the method of presentation and is not significant. There is

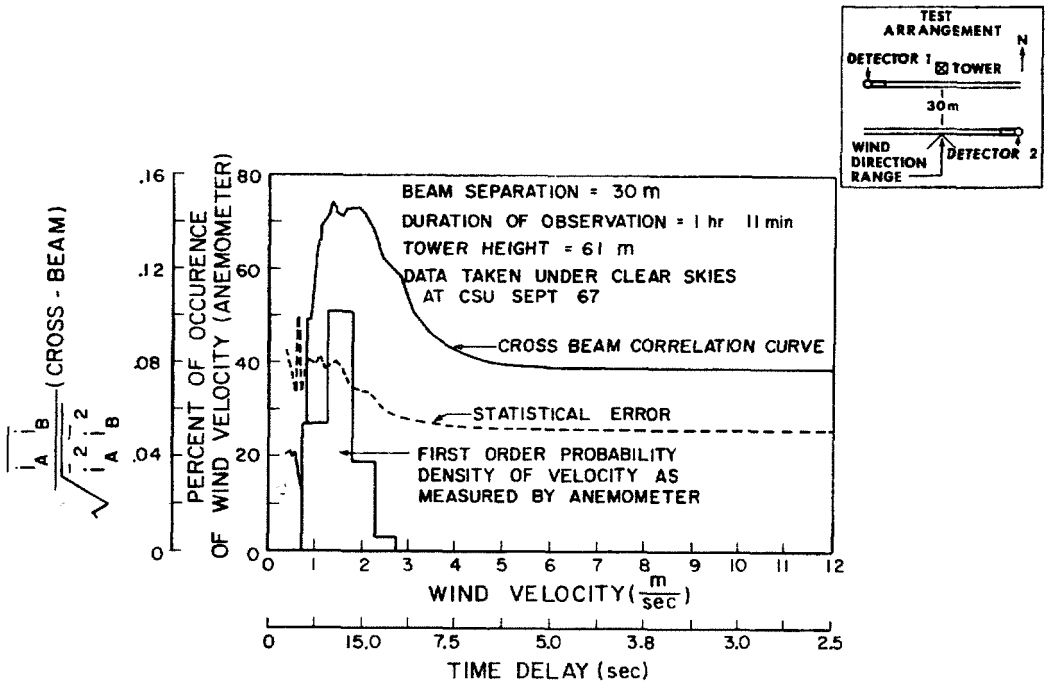

Figure A6 Light Wind Case 3 mph.

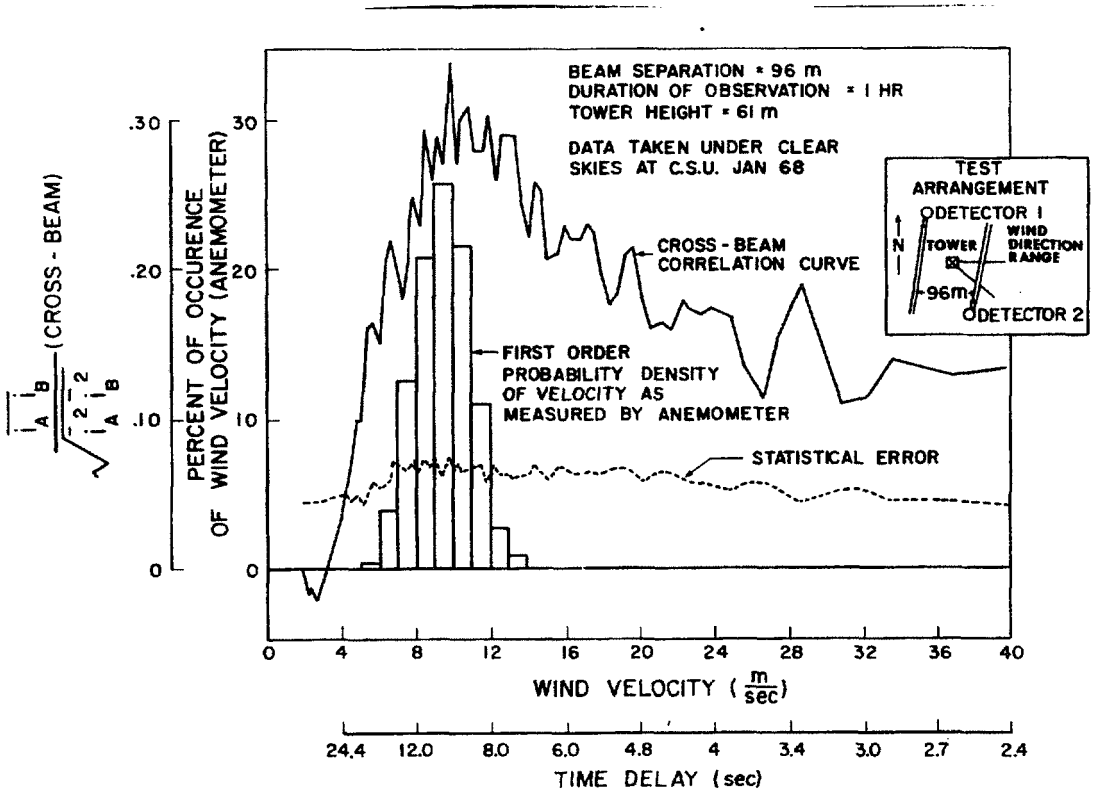

Figure A7 Medium Wind Case 20 mph.

quite good agreement between the anemometer and the crossed-beam results although the winds were light and variable.

Higher wind cases are shown in Figure A7 and A8 in which, once again, good agreement is shown between the anemometer and the crossed-beam results. In Figure A7 the statistical error is relatively small and the correlation coefficient at the peak is large. Under these windy conditions a greater concentration of aerosols might be expected to be present close to the ground, and this could weight the results by increasing the contribution to the fluctuating signal from low altitudes. This would have the effect of decreasing the number of eddies along the field-of-view of the photometers which contribute significantly to the fluctuation level, and therefore increase the correlation coefficient.

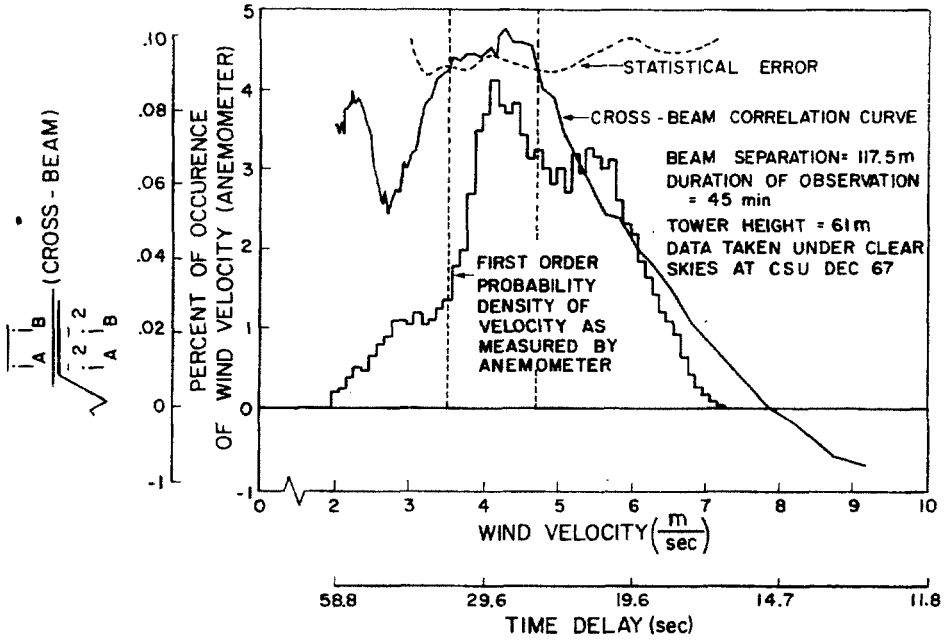

Figure A8 Low Wind - Large Beam Separation Case.

APPENDIX A

The results described above are summarized in the following table. There is encouragingly good agreement between the crossed-beam and the anemometer results. The field tests are continuing and it is hoped that results presently being analyzed will show the same promise of the results described here.

Future Development of the Crossed-Beam Technique. The immediate future developments of the crossed-beam technique have to be directed towards exploring the potential and the limitations of the method. For example, in order to remove some of the ambiguities which sometimes arise in determining the peak in the correlation function which corresponds to the wind speed, a multiple beam system is being developed. This will permit results for several beam separations to be obtained simultaneously, and in addition, because the beam will perforce be in a fan configuration, the wind direction can also be found if the correlation maxima are sufficiently well defined.

To avoid the limitations imposed on the present system under cloudy skies the potential of infrared measurements has to be explored. The physics of the problem in terms of trying to define the altitude contributions to the fluctuating signals in both the scattered sunlight and infrared cases has to be studied. This would permit estimates to be made of the altitude resolution and maximum altitudes for which useful wind data may be obtained.

Some new approaches in terms of the data reduction methods have to be developed. The use of the derivatives of the signals to effectively flatten the frequency spectra and narrow the correlation peak is presently being tried. Further examination of the statistical error, and the relative errors between correlations for different time delays obtained from the same data record have to be examined.

Conclusions. The potential future development of the crossed-beam technique once the feasibility of its application to atmospheric measurements has been demonstrated is very great. There are a large number of different types of measurements, some of which have been discussed above, that can usefully be made which will contribute to the understanding of atmospheric phenomena, and to improvement in weather forecasting.

X-BEAM AND ANEMOMETER COMPARISON

TEST CONDITIONS*							ANEMOMETER RESULTS			X-BEAM RESULTS		
RUN	DATE	T_{START} (hr)	T_{STOP} (hr)	WIND CONDITIONS	DIR. FLUCT. (deg)	BEAM SEP. (m)	(U_N) MIN. (m/s)	(U_N) MAX. (m/s)	(U_N) (m/s)	(U_N) (m/s)	B (cps)	$\frac{(U_N)_{XB}-(U_N)_{AN}}{(U_N)_{AN}}$ (%)
I	9/29/67	0905	1038	LIGHT WIND FROM SOUTH	±23	30	0.7	2.5	1.6	1.3	.45	17.65
II	1/03/68	1101	1203	LIGHT TO MODERATE WIND FROM EAST	±38	116	2.0	7.0	4.1	4.4	.50	6.82
III	1/03/68	1343	1445	MODERATE TO STRONG WIND FROM SE	±25	96	6.0	13.0	9.5	9.7	.63	2.11
IV	11/30/67	1235	1535	STRONG NW WIND	±30	71	8.0	20.0	14.6	13.6	.73	6.84

* ALL DATA TAKEN UNDER CLEAR SKIES IN ST. VRAIN RIVER VALLEY, COLORADO

APPENDIX A

Successful ground tests should be followed by measurements from aircraft. Clear air turbulence is of great importance as far as its effect on aircraft operations is concerned, and much could be learned of this phenomena by crossed-beam measurements from an aircraft. Of course in the aircraft case, instead of the fluctuations being produced by turbulence eddies being convected through stationary beams, the fluctuations will be largely produced by the movement of the "beams" or photometer fields-of-view through regions of atmospheric turbulence. The fluctuation frequencies will be considerably different. Also in the aircraft case, time delay tricks as illustrated in Figure A9 may remove the necessity of having two photometers separated in space.

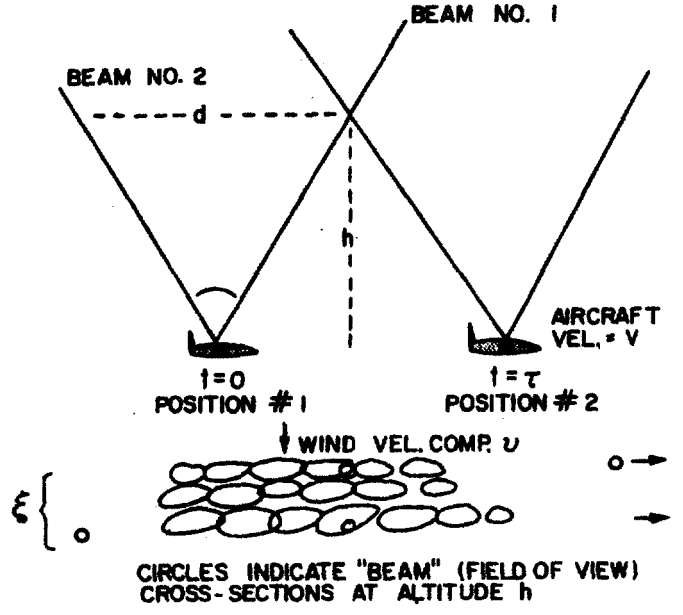

Figure A9 Scanning System Concept - For Particular Wind Speed u and Beam Separation ξ We have time τ for Line of Eddies Originally in Beam #1 to Reach Beam #2. At height, h . Beam Delay is τ , so a Maximum Correlation is Recorded for this Time Delay. With a Fan of Beam giving Number of Different ξ 's the Wind Component as a Function of Altitude may be Measured.

APPENDIX A

The two photometers are mounted on a stabilized platform and have an angle θ between their respective fields-of-view. If the turbulence structure is assumed to be frozen, then the fluctuations detected by photometer #1 originating from a height h above the aircraft will be repeated in signal from photometer #2 a time later, where is the distance d divided by the velocity of the aircraft. The altitude region of interest can therefore be studied by selecting the appropriate time interval To obtain wind speeds it is necessary to separate the photometer fields of view in a direction perpendicular to the plane of the paper. An ambiguity is introduced here which can only be resolved by use of a fan of "beams" from one of the photometer systems. This problem has been discussed by Krause et al (1966) and by Krause (1967) and will not therefore be considered further here.

The logical development of the technique through an aircraft operation phase together with the study of spectral regions in which signals are detected and which could be utilized by downward looking systems, would then enable the potential of satellite experiments to be accurately assessed.

APPENDIX B

Preliminary Design Considerations. A relatively simple instrument design is possible, if the objective is to measure fluctuations in scattered sunlight during the day and starlight scintillation at night. To utilize the short wavelength region below 4000 A in the scattered sunlight measurements, it is desirable to use mirror rather than lens collecting optics. A part of any experimental study of these techniques would determine the optimum wavelength range of operation, and a mirror system would permit considerable flexibility in this regard.

A schematic diagram of a possible system design is shown in Figure B1. It should be emphasized that this is not a CAT detector per se, but is an instrument by which the potentiality of two possible passive optical CAT detection techniques may be explored. The collecting system shown is of the Cassegrainian type with a 6-in. diameter primary mirror. Aperture A is the field stop and should be variable in size to cover a range of field angles from approximately 5 arc minutes to one degree. Typically, with a 6-in. primary mirror and an f/12 system this range of field angles would require field stop diameters from 0.05 to 1 in.

In the case of the measurements of scattered sunlight, the size of the field stop would affect resolution of eddy scales at different distances ahead of the aircraft. For stellar scintillation, it is necessary to limit the field-of-view so that there is only a single star in the field-of-view at one time. The measured fluctuations are then due solely to light from this one star. In fact, this is an idealistic situation since there will always be more than one star in the field-of-view so that we have the experimental requirement that the energy received from the star being observed has to be about an order of magnitude greater than the light from background stars. Since the average magnitude of background stars varies with position over the celestial sphere, the size of the field will depend on both the magnitude of the target star and its position in the celestial sphere. To study whether stellar scintillation measurements can provide a method of detecting CAT very bright stars can be used; however, an operational system will have to be able to operate with stars of the 7th magnitude. The maximum brightness of background stars is given by Quasius and McConless (1966) as approximately 700, 10th magnitude (visual) stars per square degree, and, therefore, for a 7th magnitude target star the field-of-view of the system would have to be less than 2.6 arc minutes

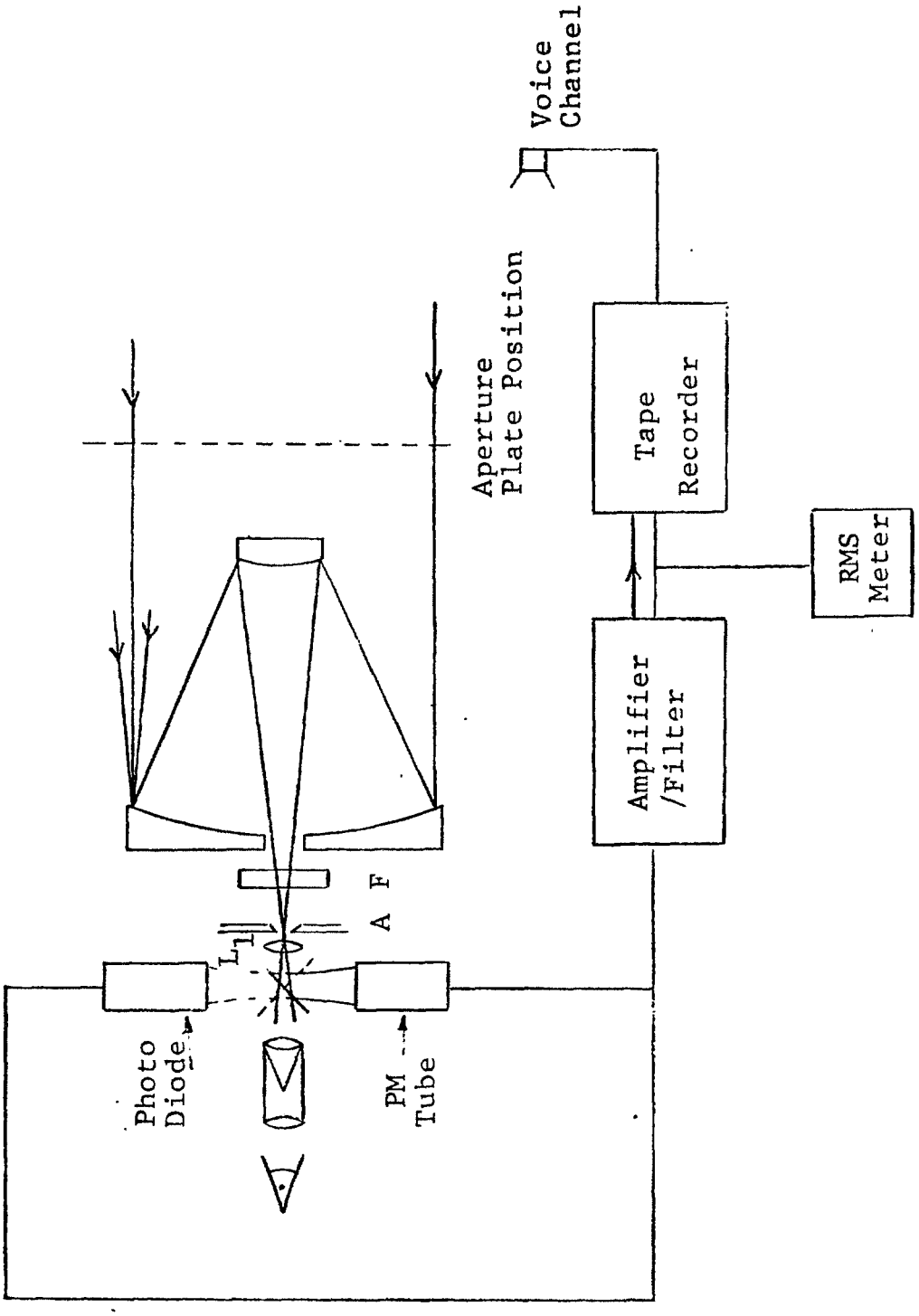

Figure B.1 Schematic Design of an Airborne Optical System

for the radiation from background stars to be one tenth of the radiation from the target star. With this small field-of-view an operational system would clearly have to be mounted on a stabilized platform; however, for initial experiments to check out the method, very bright stars could be used, and hence a much larger field, which would relax the pointing accuracy requirement.

The filter, F, would be used to limit the spectral bandpass of the system. This is another variable which should be explored both for the scattered sunlight and stellar scintillation techniques. Field lens L_1 images the entrance aperture of the system on to the detector. In this way any movement of a star image within the field stop will not cause a variation in the light distribution over the detector. Photodetectors do not have uniform response over the sensitive areas and, therefore, if the detector was phased directly behind the field stop, any movement of the star image within the field stop could produce quite large fluctuations.

Two detectors are shown with a mirror that can be rotated through 90° to direct the input radiation to either the photomultiplier tube or to the photodiode. The signal levels will be such that the photomultiplier would be much too sensitive for detection of scattered sunlight. Finally, for initial acquisition of a star, it should be possible to move the mirror out of the way and view by eye.

Signals would be recorded on magnetic tape through an amplifier and filter. Mean levels should also be recorded and an rms meter with variable time constant included for real time monitoring of the signal levels.

Provision could very easily be made in this design for measurement of the correlation function for stellar scintillation in the plane of the entrance aperture. Aperture plates containing two small circular holes of various spacings could be placed in the position shown and a second photomultiplier included to enable the light coming through the two apertures to be measured at the same time. The correlation function discussed in section 3.1 is related to the characteristics of the turbulent region through which the light has passed. Tatarski (1961) has shown that the correlation goes to zero for two points separated by a distance where is of the order of L. We may treat L, here, as the range to the CAT zone; however, this technique rests on the presence of a CAT

region producing a significant increase in the scintillation levels. Since the theoretical approach has not lead to reliable results this will have to be proven experimentally.